



HAL
open science

Förster Resonance Energy Transfer Immunoassays Using Engineered Proteins for Breast Cancer Biomarker Detection

Yu-Tang Wu

► **To cite this version:**

Yu-Tang Wu. Förster Resonance Energy Transfer Immunoassays Using Engineered Proteins for Breast Cancer Biomarker Detection. Biological Physics [physics.bio-ph]. Université Paris Saclay (COMUE), 2018. English. NNT : 2018SACLS340 . tel-01909324

HAL Id: tel-01909324

<https://theses.hal.science/tel-01909324v1>

Submitted on 31 Oct 2018

HAL is a multi-disciplinary open access archive for the deposit and dissemination of scientific research documents, whether they are published or not. The documents may come from teaching and research institutions in France or abroad, or from public or private research centers.

L'archive ouverte pluridisciplinaire **HAL**, est destinée au dépôt et à la diffusion de documents scientifiques de niveau recherche, publiés ou non, émanant des établissements d'enseignement et de recherche français ou étrangers, des laboratoires publics ou privés.

Förster Resonance Energy Transfer Immunoassays Using Engineered Proteins for Breast Cancer Biomarker Detection

Thèse de doctorat de l'Université Paris-Saclay
Préparée à Université Paris-Sud

École doctorale n°575 :
electrical, optical, bio- physics and engineering (EOBE)
Spécialité de doctorat : Physique

Thèse présentée et soutenue à Orsay, le 24 Sep 2018, par

Mme Wu Yu-Tang

Composition du Jury :

M. Karsten Haupt Professeur, Université de Technologie de Compiègne Laboratoire Génie Enzymatique et Cellulaire (GEC)	Président
M. Hans-Gerd Löhmannsröben Professeur, Université de Potsdam Institut de Chimie	Rapporteur
Mme. Simona Mura Maître de Conférences, Université Paris-Sud Institut Galien Paris Sud (IGPS)	Examineur
Mme. Marie-Béatrice Valerio-Lepiniec Maître de Conférences, Université Paris-Sud Institut de Biologie Intégrative de la Cellule (I2BC)	Examineur
Mme. Gaëlle Charron Maître de Conférences, Université Paris Diderot Laboratoire Matière et Systèmes Complexes (MSC)	Examineur
M. Niko Hildebrandt Professeur, Université Paris-Sud Institut de Biologie Intégrative de la Cellule (I2BC)	Directeur de thèse

“Brothers, I do not account of myself to have laid hold; but one thing I do: Forgetting the things which are behind and stretching forward to the things which are before, pursue toward the goal for the prize to which God in Christ Jesus has called me upward.....”

Philippians 3:14-15

Titre : Tests immunologiques par transfert d'énergie par résonance de Förster en utilisant des protéines modifiées pour la détection de biomarqueurs du cancer du sein

Mots clés FRET, boîtes quantiques, complexe de lanthanides, bioconjugaison, spectroscopie résolue en temps

Les protéines modifiées ont suscité un grand intérêt en raison de leur taille extrêmement petite par rapport à l'anticorps entier. Ces petites protéines de liaison ont démontré de nombreux avantages tels qu'une biodistribution rapide, une bonne pénétration dans le tissu tumoral et une élimination rapide du sérum et des tissus non-infectés. Ainsi, ces protéines devraient être d'excellentes alternatives aux anticorps pour les applications cliniques. Cette thèse présente le développement de biocapteurs basés sur des anticorps synthétiques et le transfert d'énergie par résonance de type Förster (FRET) résolu en temps par la détection de biomarqueurs.

Les tests immunologiques à base de FRET sont établis en utilisant des complexes de terbium (Tb) comme donneurs de FRET et des boîtes quantiques semi-conducteurs (QDs) comme accepteurs de FRET. Les propriétés photophysiques exceptionnelles de ce couple de FRET Tb-QD permettent une détection quantitative ultrasensible. Des anticorps monocaténaire (single-domain antibody, sdAb) et des petites protéines d'affinité synthétiques (albumin-binding domain-derived affinity protein, ADAPT) sont utilisées pour étudier différentes stratégies de conjugaison d'anticorps, et quantifier des biomarqueurs cliniques (EGFR, HER2). Ce travail peut être considéré comme une condition préalable à l'utilisation des QDs en diagnostic clinique.

Title : Förster resonance energy transfer immunoassays using engineered proteins for breast cancer biomarker detection

Keywords : FRET, quantum dots, lanthanide complex, bioconjugation, time-resolved spectroscopy

Abstract : Engineered affinity proteins have raised great interest due to their extremely small size compared to full length antibodies. Such small binding proteins have demonstrated many advantages such as quick biodistribution, good penetration into tumor tissue, and fast elimination from serum and nondiseased tissues. Thus, they are expected to be excellent alternatives to antibodies for clinical applications. This thesis focuses on the development of biosensors based on engineered antibodies and time-resolved Förster resonance energy transfer (FRET) through biological recognition of biomarkers.

FRET-based immunoassays are established using terbium complexes (Tb) as FRET donors and semiconductor quantum dots (QDs) as FRET acceptors. The exceptional photophysical properties of the Tb-QD FRET pair allow for ultrasensitive quantitative biosensing. Single-domain antibodies (sdAb) and small engineered scaffold antibodies (ADAPT) are used to investigate different antibody-conjugation strategies for quantifying human epidermal growth factor receptors (EGFR, HER2) as clinical biomarkers. This work can be considered as a prerequisite to implementing QDs into applied clinical diagnostics.



Acknowledgements

First and foremost, I would like to express my deepest gratitude to my supervisor Prof. Niko Hildebrandt, our "captain FRET", who offered me the opportunity to join this big family, to be a member of FRET and gave me lots of freedom to choose the project. Although I met so many difficulties in my research, he gave his constant support and guidance throughout my PhD.

I thank Prof. Hans-Gerd Löhmansröben and Prof. Karsten Haupt, who dedicated their time for being reviewers for my PhD thesis.

I also want to thank our collaborators for their kindness, availability and scientific advice they have given me in this work.

I would like to thank to all past and current members in the NanoBioPhotonics group for creating a nice atmosphere to discuss freely about our own research, and give their valuable advices with their profession.

Special thanks to Dr. Shashi Bhuckory and Dr. Xue Qiu for their patience and guidance for technical tuitions especially in the FRET immunoassay; to Chi Chen for answering me all my scientific questions with his knowledge; to Jiajia Guo for assisting me with data analysis; and to Tudor Haruta for his help with the translation of my abstract and summary.

I would like to thank Ministry of Education in Taiwan and University Paris-Sud for financial support during my PhD.

The past four years have gone by so fast. Thanks to the never-ending support of my family and friends, especially to my husband Yong Fern and my daughter Sarah always be with me through the ups and downs and encourage me to carry on. Without them this work would have never been possible.

Contents

Acknowledgements	v
List of Publications	viii
1 Introduction	1
2 Background	6
2.1 Förster resonance energy transfer	6
2.1.1 Introduction	6
2.1.2 Theory and Formalism	7
2.2 FRET-based application	10
2.2.1 Immunoassays	11
FRET-based Immunoassay	12
2.2.2 Cellular-based imaging	14
2.3 Luminescent lanthanides	15
2.3.1 Introduction	15
2.3.2 Lanthanide complexes	17
2.3.3 Lanthanide Tb complexes as FRET donors	18
2.4 Quantum Dots	20
2.4.1 Introduction	20
2.4.2 Photophysical properties of QDs	20
2.4.3 Surface functionalization	22
2.4.4 Quantum dots as FRET donors and acceptors	24
2.5 Bioconjugation	26
2.5.1 Introduction	26
2.5.2 Streptavidin-Biotin interaction	27
2.5.3 Polyhistidine-metal affinity	29
2.5.4 Covalent attachment	29
2.6 Instrumentation	32
2.6.1 Characterization	32
2.6.2 Time-resolved immunoassays	32

3	ADAPT for HER2 detection	35
3.1	Introduction	35
3.2	Materials and Methods	37
3.3	QD-antibody conjugation	37
3.4	LTC-antibody conjugation	38
3.5	Characterization of FRET pairs	39
3.6	Homogeneous FRET immunoassays	40
3.7	Results and discussion	40
3.7.1	Antibody conjugates	40
3.7.2	HER2 sensor development	42
4	Nanobodies for EGFR detection	46
4.1	Introduction	46
4.2	Materials and Methods	47
4.3	QD-antibody conjugation	47
4.4	LTC-antibody conjugation	48
4.5	Characterization of FRET pairs	49
4.6	Homogeneous FRET immunoassay	50
4.7	Results and discussion	50
5	Summary and outlook	57
6	Appendix	58
	Bibliography	65

List of Publications

Original publications

1. Y.-T. Wu, X. Qiu, P.M.P. van Bergen en Henegouwen, K. Susumu, Igor L. Medintz and N. Hildebrandt. Competitive Tb-to-quantum dot FRET immunoassay for EGFR using a single anti-EGFR nanobody. (in preparation)
2. C. Chen, L. Ao, Y.-T. Wu, V. Cifliku, M. Cardoso Dos Santos, E. Bourrier, M. Delbianco, D. Parker, J. M. Zwier, L. Huang, N. Hildebrandt, Single-nanoparticle cell barcoding by tunable FRET from lanthanides to quantum dots. *Angewandte Chemie International Edition* **2018**, published online : DOI : 10.1002/anie.201807585.
3. Y.-T. Wu, X. Qiu, S. Lindbo, K. Susumu, Igor L. Medintz, S. Hober, N. Hildebrandt, Quantum dot based FRET immunoassay for HER2 using ultrasmall affinity proteins. *Small* **2018**, 14, 1802266.
4. S. Bhuckory, E. Hemmer, Y.-T. Wu, A. Yahia-Ammar, F. Vetrone, N. Hildebrandt, Core or shell? Er³⁺ FRET donors in upconversion nanoparticles. *European Journal of Inorganic Chemistry* **2017**, 5186–5195.
5. S. Bhuckory, L. Mattera, K. D. Wegner, X. Qiu, Y.-T. Wu, L. J. Charbonnière, P. Reiss, and N. Hildebrandt. Direct conjugation of antibodies to the ZnS shell of quantum dots for FRET immunoassays with low picomolar detection limits. *Chemical Communications* **2016**, 52, 14423-14425.
6. X. Qiu, K. D. Wegner, Y.-T. Wu, P.M.P. van Bergen en Henegouwen, T. L. Jennings, and N. Hildebrandt. Nanobodies and antibodies for duplexed EGFR/HER2 immunoassays using terbium-to-quantum dot FRET. *Chemistry of Materials* **2016**, 28, 8256-8267.

Poster presentation

1. Y.-T. Wu, X. Qiu, S. Lindbo, K. Susumu, Igor L. Medintz, S. Hober, N. Hildebrandt, Ultrasmall Scaffold proteins (ADAPT) for terbium-to-quantum dot FRET immunoassays against HER2. *Fluorescent Biomolecules and their Building Blocks (FB³)*, Glasgow, UK, 2018

List of Abbreviations

BSA	bovine serum albumin
cDNA	complementary DNA
ChA	acceptor channel
ChD	donor channel
Cys	cysteine
DNA	deoxyribonucleic acid
EGFR	epidermal growth factor receptor
ELISA	enzyme-linked immunosorbent assay
FLIM	fluorescence-lifetime imaging microscopy
FP	fluorescent protein
FRET	Förster resonance energy transfer
FWHM	full width at half maximum
HER2	human epidermal growth factor receptor 2
His₆	hexahistidine
IR	infrared
LLC	luminescent lanthanide complex
Ln	lanthanide
LOD	limit of detection
LTC	lanthanide terbium complex
MCS	multichannel scaling
MWCO	molecular weight cut-off
NHS	N-Hydroxysuccinimide
NIR	near infrared
NP	nanoparticle
PEG	polyethylene glycol
PL	photoluminescence
PMT	photomultiplier tubes
QD	quantum dot
R₀	Förster radius (the distance at which energy transfer efficiency is 50%)
RNA	ribonucleic acid
SD	standard deviation
sdAb	single domain antibody

ssDNA	single strand DNA
sulfo-EMCS	N- ϵ -maleimidocaproyl-oxysulfosuccinimide ester
TCSPC	time-correlated single photon counting
TG	time-gated
TR-FRET	time-resolved FRET
UCNP	upconversion nanoparticle
UV	ultraviolet
V_HH	single-domain antibody
Vis	visible

Dedicated to my family...

Chapter 1

Introduction

Early diagnosis of cancer is crucial for a successful treatment. As normal diagnostics analysis in the laboratory can be a time-consuming and complicated process, rapid, sensitive and specific immunoassays for protein biomarkers in serum, whole blood or plasma have the potential to largely improve early diagnosis and follow-up treatment [Rusling et al., 2010]. Therefore, there is an increasing demand of biosensors development for detecting cancer biomarkers at ultralow concentrations during early stages of the disease and disease progression-monitoring for the benefit of patients. Biosensors based on Förster resonance energy transfer (FRET) have demonstrated many advantages for simple, fast, sensitive and multiplexed diagnostics. Due to the r^{-6} distance dependency for the transfer efficiency, also called FRET efficiency, FRET is versatile and sensitive for qualitative and quantitative analysis of biological interactions and processes in a nanoscale range of *ca.* 1-20 nm. FRET is a non-radiative energy transfer between an excited donor molecule (FRET donor) and a ground state acceptor molecule (FRET acceptor), which must be in close proximity and energetic resonance as expressed by spectral overlap integral [Förster, 1948]. For detecting the target of interest, there are many signal transduction strategies according to the signal increases or decreases in the response of the target, which is mediated by the biomolecules to which donor and acceptor are conjugated. For FRET-based sandwich immunoassays, both donor and acceptor are conjugated with two different target recognition biomolecules. The presence of the target results in binding and a close proximity of FRET donor and acceptor to provide a measurable change of FRET signals. The unique ability of FRET to probe target biomolecule concentrations and inter- and intramolecular separation distances has led to a rapidly growing amount of FRET studies concerning biomolecules and biological complexes [Clegg, 1995, Selvin, 1995].

Various materials that are utilized in FRET now encompass organic dyes, fluorescent proteins, semiconductor quantum dots, metal chelates, noble metals and other nanoparticles. Among all of them, the combination of luminescent lanthanide complexes (LLCs) as donors and quantum dots (QDs) as acceptors are one of the most particular FRET pairs [Hildebrandt, Wegner, and Algar, 2014, Geißler et al., 2010]. Their

photophysical properties enable exceptionally large Förster distances (R_0 , distance for which FRET is 50 % efficient) up to 11 nm beyond the usual FRET distance of *ca.* 1 - 10 nm. LLCs are composed of a lanthanide cation coordinated by a ligand that serves as a light-harvesting antenna. Due to the forbidden f-f transitions of the lanthanide ions, LLCs show multiple, narrow and well-separated emission bands that are very well suited for spectral-multiplexing. Moreover, LLCs possess long excited-state lifetimes up to a few milliseconds, which allows for time-resolved measurements and provides a great potential for temporal-multiplexing [Bünzli and Piguet, 2005, Geißler et al., 2013]. QDs are semiconductor nanocrystals that display several advantages over conventional organic dyes including high molar extinction coefficients, broad absorption and narrow and symmetric emission bands with full width at half maximum (FWHM) \sim 25-40 nm spanning from UV to near-infrared, large effective Stokes shift and remarkable photostability. In particular, a very unique feature is their size-tunable emission as a result of quantum confinement effects. As the semiconductor material is reduced to nanoscale, the continuous energy bands split into discrete excitonic (hole-electron interaction) states. As a result of excitons that are confined to smaller dimensions than the Bohr radius (assumed as hole-electron distance), the band gap energy increases with decreasing QD size, which effects the absorption and emission wavelengths of QDs shift to the blue spectral region. The well-established synthesis and surface functionalization strategies render QDs biocompatible and enable conjugation with biomolecules in aqueous solution [Medintz et al., 2005]. In most of FRET-based application, QDs are usually used as FRET donors [Willard et al., 2001]. The main problems of accessing QDs as acceptors is their broad absorption and high extinction coefficient, which will easily lead to efficient direct excitation of QDs at almost any wavelength used for donor excitation due to the broad absorption spectrum of QDs. Therefore only a minor fraction of QDs in the ground state participate in FRET. The solution to this problem is the use of materials with long excited-state lifetimes as FRET donor such as LLCs (lifetimes up to several milliseconds) and pulsed excitation. The combination of LLCs and QDs permits spectral multiplexing of different QD colors for the same donor with facile separation of the different emission bands due to greatly reduced optical crosstalk. Also, their large and broad molar absorptivities (extinction coefficients) result in large spectral overlap integrals and therefore long Förster distances [Morgner et al., 2010].

As a result of the aforementioned advantages of LLCs and QDs as FRET pairs, FRET becomes a very promising technique for time-resolved (TR) photoluminescence (PL) measurements that allow for efficient suppression of PL intensity due to directly excited acceptors and sample autofluorescence. Therefore, such FRET pairs have been used in clinical diagnostics for the detection of different biomarkers [Kupstat, Kumke,

and Hildebrandt, 2011, Wegner et al., 2013]. The most popular approach to target those biomarkers is to use antibodies within homogeneous immunoassay, which simplifies the sample preparation procedure without several incubation, washing, and separation steps but only a very simple mix and measure procedure. The distance inside the immunoassays can be adapted by the size of photoluminescent materials and the antibodies. That is, by alternating smaller size of antibodies with the same specificity or more compact luminescent materials, FRET can be further improved.

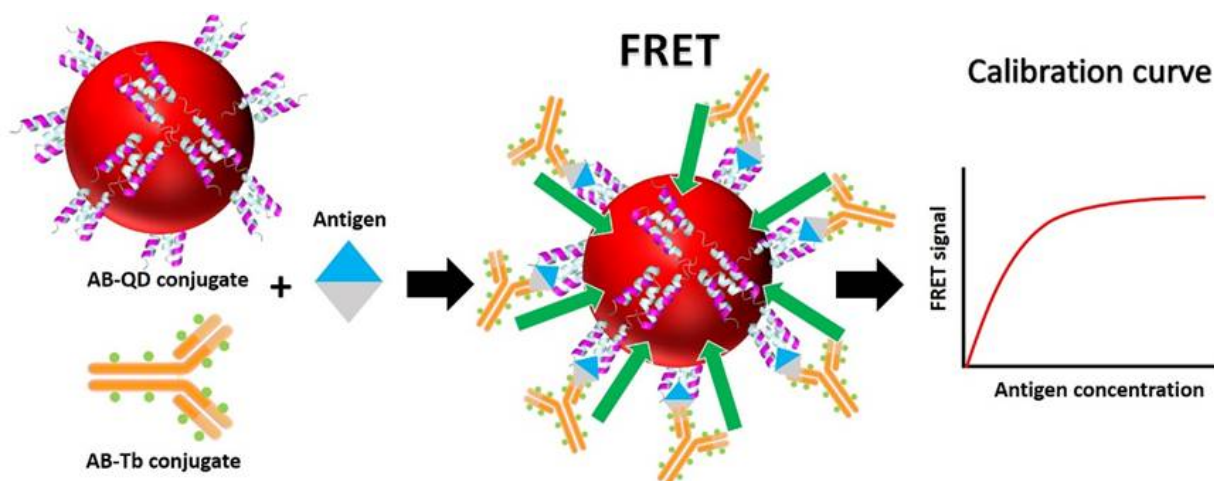


FIGURE 1.1: Principle of the homogeneous immunoassay. The combination of Tb- and QD-antibody (AB) conjugates allows for the formation of Tb-AB-antigen-AB-QD sandwich complexes upon addition of antigen, which results in FRET from several Tb to the central QD. Time-gated detection of FRET-sensitized QD photoluminescence is used for a sensitive quantification of the antigen concentration. The assay leads to a typical immunoassay calibration curve, for which the FRET signal increases with increasing antigen concentration until a saturation is reached when the antigen concentration equals the Tb-AB or QD-AB concentration.

The aim of this work is to utilize the exceptional photophysical properties of Lumi4-Tb complexes (LTC) and QDs for TR-FRET and investigate the influence of antibody sizes on the sensitivity of the immunoassay for the detection of cancer protein biomarkers. For TR-FRET sandwich immunoassays (Figure 1.1), two antibodies that bind to different epitopes of the antigen (biomarker) are labeled to LTC and different emitting QDs, respectively. A detailed photophysical characterization of FRET pairs (LTC and QD conjugates) was performed and the labeling ratios were estimated using UV/Vis absorption spectroscopy. The formation of antibody-antigen-antibody complexes conjugated with LTC donors and QD acceptors gives rise to FRET. The first study (**Chapter3**) presents ultrasmall (~ 6.5 kDa, $\sim 1.0 \times 1.5 \times 2.5$ nm³) albumin-binding domain-derived

affinity proteins (ADAPTs) for the quantification of the human epidermal growth factor receptor 2 (HER2) [Lindbo et al., 2016, Nilvebrant et al., 2014]. These small affinity proteins are beneficial for multivalent nanoparticle conjugation and efficient FRET. ADAPT variants against HER2 containing the histidine tag (ADAPT-His₆) and a cysteine (ADAPT-Cys) either at the N terminus or the C terminus were produced by our collaborators from KTH - Royal Institute of Technology (Stockholm, Sweden) [Lindbo et al., 2016, Nilvebrant et al., 2014]. Anti-HER2 pertuzumab antibody (Roche Genentech) was used for LTC-NHS labeling through the primary amines of lysine residues. Two different QD conjugation methods were applied for comparison. ADAPT-His₆ can efficiently self-assemble by metal affinity coordination to the Zn-rich surfaces of QDs emitting at 625nm (QD625, Thermo Fisher) coated with zwitterionic ligands. This direct assembly on the QD surface provides efficient FRET. Another way is to use ADAPT-Cys, which can label to ITK QDs with amino-PEG emitting at 705 nm (QD705, Thermo Fisher) through sulfhydryl chemistry. The amine-reactive QDs were converted to maleimide-reactive QDs by using the heterobifunctional crosslinker sulfo-EMCS, which has NHS ester and maleimide reactive groups. The maleimide activated QDs were then conjugated to the ADAPT-Cys via free sulfhydryl groups, which were reduced by TCEP. The labeling ratios of QD and ADAPTs is very difficult to quantify due to the large difference of extinction coefficients of the QDs and ADAPTs at 280 nm but the large excess of ADAPTs per QD and the functionality of the FRET assays provided very good evidence for a successful ADAPT-QD conjugation. Homogeneous TR-FRET immunoassays could quantify HER2 both in 50 uL buffer and serum-containing samples with sub-nanomolar detection limits using a clinical benchtop immunoassay analyzer (KRYPTOR compact plus). The limit of detection (LOD) was acquired from the linear part of the calibration curve. The LOD of QD625 conjugate outperformed previously tested assays with antibodies, antibody fragments, and nanobodies. Although the QD705 conjugate showed higher detection limits than the QD625 conjugate, the results provided important information concerning the possibility of color multiplexing and versatility of ADAPT-conjugation to other nanoparticles.

The second study (**Chapter 4**) focuses on single-domain antibodies (sdAb), which are antibody fragments consisting of a single monomeric variable domain with a molecular weight of only 15 kDa and are used in many different antibody based applications [Schumacher et al., 2018]. For the realization of the sandwich immunoassays two kinds sdAb were provided by our collaborators at Utrecht University (Netherlands). These nanobodies bind to non-overlapping epitopes of the human epidermal growth factor receptor 1 (EGFR), noted as EgA1 and EgB4, with three separation tags (histidine, biotin, cysteine) and without tag (no tag) for several conjugating strategies with FRET pairs. EgA1-no tag and EgA1-His₆ were used for LTC labeling. EgB4-His₆, EgB4-biotin

and EgB4-Cys were used for three different conjugation strategies. The QDs applied in these systems were the same QD625 and QD705 that were used in the previous study. Additionally, another commercial QD emitting at 705 nm (sAvQD705, 705 ITK Streptavidin Conjugate Kits) is introduced here for biotin-streptavidin recognition, where the streptavidin covalently attached to the inner amphiphilic coating without a PEG linker, and therefore provided more freedom for the co-assembly of other biomolecules to the QD. Thus, the detection limit of EgB4-biotin-sAvQD705 conjugate is lower than EgB4-Cys-QD705 conjugate. Interestingly, another FRET pair EgA1-His₆-LTC and EgB4-His₆-QD625 showed slightly reduced FRET with increasing EGFR concentrations due to the LTC-conjugate self-assembled on the QD625 by metal polyhistidine affinity. The addition of EGFR replaces some of the LTC-conjugates resulting in a competitive displacement immunoassay. The concept was confirmed by another experiment, in which the QD FRET acceptor without conjugated sdAb, that is EgA1-His₆-LTC and QD625, still showed the same competitive result, which was applicable to detect EGFR at sub-nanomolar concentrations. This competitive assay is highly interesting because it requires only one single type of EGFR-specific sdAb, which strongly reduces the antibody development and reagent costs.

In summary, the results from this PhD thesis demonstrate that small affinity proteins can be very advantageous for QD-based immunoassays. Such small proteins (e.g., ADAPT, sdAb) allow for multivalent QD conjugation, which can increase QD FRET-sensitization. ADAPTs were shown to outperform any other types of antibodies for HER2 immunoassays. SdAbs were used to develop a competitive homogeneous immunoassay that requires only one antibody (instead of two), which can be considered as a useful alternative strategy for EGFR detection. Both strategies for QD-based homogeneous FRET-immunoassays with small affinity proteins provide a large potential for advanced in vitro diagnostics and other FRET-based biosensing applications, e.g., for imaging analysis of epidermal growth factor receptor dimerization.

Chapter 2

Background

2.1 Förster resonance energy transfer

2.1.1 Introduction

Energy transfer can be divided to four mechanisms, that is Förster resonance energy transfer (FRET), reabsorption, complex formation and collision quenching where excitation energy can be transferred from donor to acceptor. These mechanisms can take place by either radiative or non-radiative pathways. Radiative energy transfer, also known as reabsorption that requires emission of a photon by donor with subsequent absorption of that photon by acceptor, occurs from 1 μm to infinity. In contrast to radiative energy transfer, non-radiative energy transfer occurs without absorption and emission of a photon. There are two energy transfer mechanisms. 1) Dexter energy transfer mechanism happens when donor and acceptor in short distance (0-1 nm) accompanied with electron exchange; 2) The FRET mechanism takes effect at longer distances (1-20 nm) through coupling of the transition dipole moments of donor acceptor pairs. Among all of them, FRET appears to be the most popular and important tool in biology and biochemistry [Meer, 2013].

To explore the discovery, the biological mechanism in the human body is always a goal for the scientist. Due to its extremely sensitive distance (1-20 nm) dependence under physiological condition, the energy transfer between donor and acceptor fluorophores at nanometric distances can be obtained from the luminescence measurement, which will occur but not be significantly affected by the biomolecules in the sample. It can provide the information for cellular signaling, receptor-ligand binding, protein-protein interaction, DNA/RNA analysis and enzymatic reaction [Hildebrandt, Wegner, and Algar, 2014]. These favorable properties allow this technique to be widely used in the biochemistry, structural biology and polymer chemistry to investigate the mechanism of biological process [Lakowicz, 2006]. This chapter will cover a basic introduction of theoretical background, how to choose adequate pairs to perform successful FRET experiments and related applications.

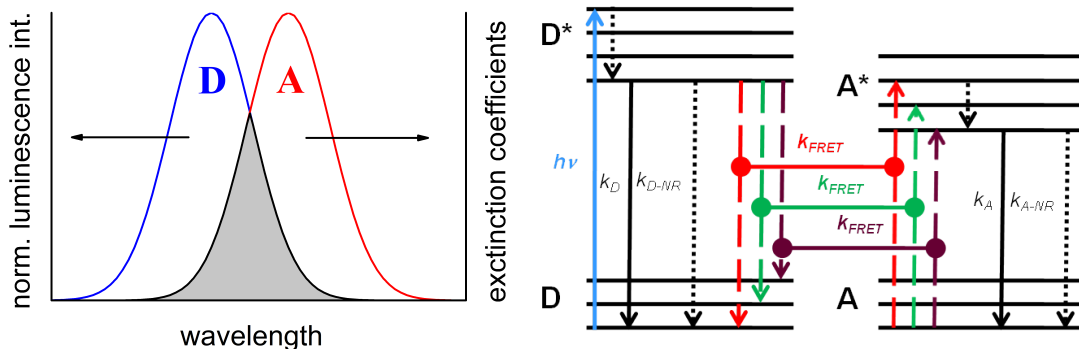


FIGURE 2.1: Left. The overlap (gray area) between donor emission(D) and acceptor absorption(A) defines overlap integral (J) to calculate Förster distance (R_0). Right. The simplified Jablonski diagram shows that FRET happens upon resonance of electronic transitions between excited state of donor (D^*) and acceptor (A^*) then followed by radiative and nonradiative decay to the ground state (A). (Reprinted from [Hildebrandt, 2013])

2.1.2 Theory and Formalism

Resonance energy transfer was proposed in theory and successfully elucidated with experimental data using spectral overlap, quantum yields and lifetimes by a German scientist Theodor Förster in the late 1940s. In honor of his work, FRET is named as Förster resonance energy transfer. In a verbal definition, FRET is a non-radiative energy transfer from an excited-state donor molecule (D^*) to a ground state acceptor molecule (A), where the donor-acceptor distance is between 1-20 nm. In this close proximity, FRET is based on the approximation that dipole-dipole coupling can be represented by Coulombic coupling. The basic principle of FRET is shown in the Jablonski diagram (Figure 2.1 Right), the transitions are in energetic resonance. The FRET process can be considered one of deactivation pathways for an excited donor. The rate of energy transfer k_{FRET} is given by Equation 2.1 and the inverse sixth power distance dependency (r^{-6}) can be observed here [Förster, 1948, Clegg, 1995].

$$k_{FRET} = \tau_D^{-1} \left(\frac{R_0}{r} \right)^6 \quad (2.1)$$

τ_D is the luminescence lifetime of donor (in the absence of acceptor), r is the separation distance between donor and acceptor, where the FRET rate (k_{FRET}) and all other decay rate for radiative and non-radiative (k_R and k_{NR}) are in equilibrium $k_{FRET} = k_R + k_{NR} = \tau_D^{-1}$, the FRET efficiency is 50 %. This distance is commonly referred to as Förster distance R_0 , giving rise to Equation 2.2 which includes several crucial variables.

$$R_0 = \left(\frac{9(\ln 10)\kappa^2\Phi_D J(\lambda)}{128\pi^5 N_A n^4} \right)^{1/6} \quad (2.2)$$

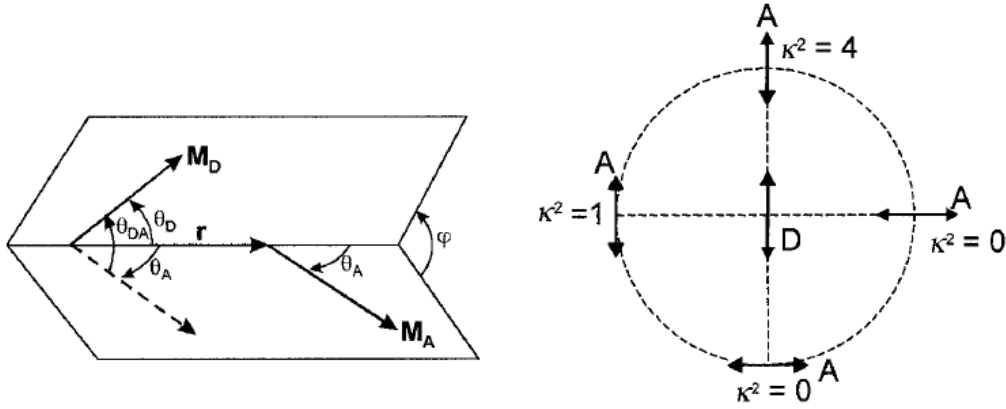


FIGURE 2.2: Left. Angles used in the equation 2.5 and 2.6. Right. Values of κ^2 depends on the orientation of donor and acceptor transition dipole moment. (Reprinted from [Valeur, 2001])

where κ^2 is the orientation factor between D and A, Φ_D is the quantum yield of the donor, N_A is Avagadro's constant, n is the refractive index of the medium, and $J(\lambda)$ is the spectral overlap between donor emission and acceptor absorption. The spectral overlap J is defined as:

$$J = \int \bar{I}_D(\lambda) \varepsilon_A(\lambda) \lambda^4 d\lambda \quad (2.3)$$

where \bar{I}_D is the area-normalized donor emission and $\varepsilon_A(\lambda)$ is the extinction coefficient (molar absorption) of the acceptor (Figure 2.1 Left.). Using $N_A = 6.023 \times 10^{23} \text{ mol}^{-1}$, nm units for λ , and $\text{M}^{-1}\text{cm}^{-1}$ for the extinction coefficient leads to

$$R_0 = 0.02108(\kappa^2 \Phi_D n^{-4} J)^{1/6} (nm) \quad (2.4)$$

One of the important variable called orientation factor, κ^2 describes the orientation of the transition dipole moments of donor and acceptor and can be calculated with the following equation:

$$\kappa^2 = (\cos \theta_{DA} - 3 \cos \theta_D \cos \theta_A)^2 \quad (2.5)$$

$$\cos \theta_{DA} = \sin \theta_D \sin \theta_A \cos \phi + \cos \theta_D \cos \theta_A \quad (2.6)$$

where $\cos \theta_{DA}$ is the angle between donor and acceptor transition dipole moments, and θ_D and θ_A are the angles between donor and acceptor transition dipole moments and the vector \vec{r} connecting donor and acceptor. κ^2 can range from 0 (perpendicular transition moments) to 4 (collinear transition moments), when transition moments are parallel $\kappa^2 = 1$ (Figure 2.2 Right). In most FRET experiments we consider $\kappa^2 = 2/3$, means that during FRET the donor and acceptor are able to rotate in all the orientation at a rate that is much faster than the excited state lifetime of donor (isotropic dynamic averaging, sphere). But not all the FRET system are applicable in the assumption. For

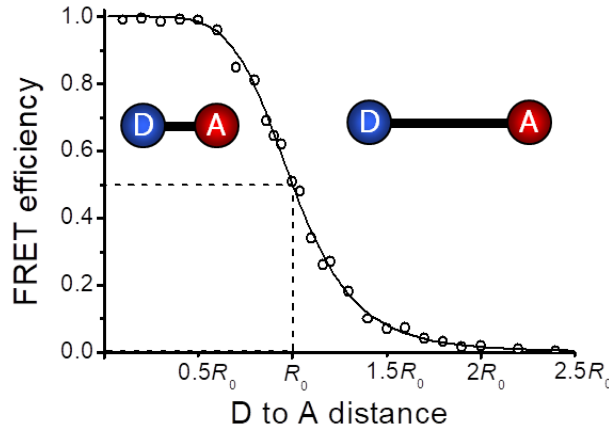


FIGURE 2.3: FRET efficiency as a function of D-A distance

example, if using fluorescent proteins as donor and acceptor, or attach the fluorophore to the double-helical DNA in the rigid structure, they may have a fixed orientation (static isotropic averaging, line) then this assumption is no longer valid. The κ^2 can take values between $1/3$ and $4/3$ (from sphere to line, or line to sphere), or range from 0 to 4 (line to line). Hence, it is important to take into account the orientation of donor and acceptor transition dipole moments, otherwise it will cause a serious error in the calculations.

The efficiency of energy transfer (FRET efficiency, η_{FRET}) is the quantum yield of energy transfer, can be calculated by using the FRET rate and the decay rate of the donor in the first part of Equation 2.7, combining Equation 2.1 to the Equation 2.7 leads to the relationship of Förster distance R_0 and the distance between donor and acceptor r . As shown in the Figure 2.3 due to the r^{-6} distance dependency, FRET efficiency is mostly sensitive in the region of $0.5R_0$ to $2.0R_0$, beyond this range FRET is either too efficient for shorter distances or negligible for longer distances.

$$\begin{aligned} \eta_{FRET} &= \frac{k_{FRET}}{k_{FRET} + k_D + k_D} = \frac{k_{FRET}}{k_{FRET} + \tau_D^{-1}} \\ &= \frac{1}{1 + (r/R_0)^6} = \frac{R_0^6}{R_0^6 + r^6} \end{aligned} \quad (2.7)$$

FRET efficiency can also be determined by measurable photophysical properties such as intensity (I), lifetime (τ) and quantum yield (Φ). In Equation 2.8, the spectroscopic data of D in the absence (subscript D) and presence of A (subscript DA) are used to calculate FRET efficiency. Combining Equation 2.8 with Equation 2.7 enables to estimate the donor and acceptor distance r , which allows to use FRET as a spectroscopic molecular ruler.

$$\eta_{FRET} = 1 - \frac{I_{DA}}{I_D} = 1 - \frac{\tau_{DA}}{\tau_D} = 1 - \frac{\Phi_{DA}}{\Phi_D} \quad (2.8)$$

In most biosensing applications, the main interest is to quantitatively detect the analytes. Using the ratiometric approach to calculate FRET ratio (F_R) by measuring donor (I_D) and acceptor (I_A) intensity simultaneously, we can know the analyte concentration. This method can be very advantageous for analytical application as it can intrinsically correct for medium interferences and excitation energy fluctuation. More details will be discussed in Section 2.7.2.

$$F_R = \frac{I_A}{I_D} \quad (2.9)$$

2.2 FRET-based application

FRET-based application can be divided into two categories, that is target sensing and structural analysis. The intrinsic distance dependence of FRET makes it ideal for monitoring a wide range of molecular recognition events, and detecting many types of target analytes. There are a number of potential in vitro target analytes of interest, including proteins, metabolites, drugs, toxins, nucleic acids, human cells, microbes and other pathogens [Gubala et al., 2011]. Biomarkers are of particular interest in the clinical diagnostics because they act as an indicator to measure and evaluate the normal biological process, pathogenic process or pharmacologic responses to a therapeutic intervention [Group et al., 2001]. Especially it can identify the type and stage of diseases, determine disease prognosis, and monitor the treatment outcomes [Sapsford et al., 2010]. The recognition molecules can interact with the target of interest through various mechanisms, including cleavage, binding or structural rearrangement resulting in measurable change of FRET signal. These recognition molecules can take various forms such as antibodies, aptamers, oligonucleotides (DNA, RNA), peptides, and small organic molecules. FRET assays by nucleic acid and protein-based are the main types of FRET-based sensors currently being used. The implementation of FRET and microscopy techniques are used to study the folding and conformational changes of biological structures and provide an inside view in inter- and intra-cellular processes [Schuler and Eaton, 2008, Prevo and Peterman, 2014]. In the following section mainly focus on the FRET-based immunoassay, it is also the main part within the work and a short summary of FRET-based sensing in the cellular environment.

2.2.1 Immunoassays

Immunoassays can be considered one of the most widespread use analytical tools in medicine and fundamental life-science research which are used to detect an analyte based on binding reaction between an antibody and an analyte. The special properties of antibodies concerning specificity, sensitivity and flexibility are i) an extremely wide range of binding targets, e.g. natural and synthetic chemical, biomolecules, cells and viruses; ii) the high specificity of each antibody to its target; and iii) the strong binding affinity between an antibody and its target. In general, immunoassays can be classified into two groups, heterogeneous and homogeneous assays, which depend on a separation of unbound labeled analyte before bound signal is measured. Heterogeneous assays require several washing steps to separate the unbound components due to the immobilization of the antibody or analyte on a solid phase. For homogeneous assays no washing and separation steps are required, as it generates signal only when the binding reaction happens [Wild, 2013].

Heterogeneous and homogeneous assays can be performed either in competitive or immunometric (non-competitive) design. Non-competitive immunoassay is also known as two-site or sandwich immunoassay, consists of two antibodies bind to the different epitopes of analyte to form a sandwich complex. One antibody is used to capture the analyte and another antibody is labeled with fluorophore, chromophore or radioactive isotope for signal generation to detect upon biological reaction. The signal intensity is directly proportional to the analyte concentration (Figure 2.4 Left). The competitive immunoassay is mainly used for the detection the small analyte which can only bind to one antibody, the analyte compete with labeled analyte to the limited amount of capture antibody, hence the detected signal is indirectly proportional to the analyte concentration of the sample (Figure 2.4 Right).

The accuracy of an immunoassay may be influenced by sources of interference, which decrease the accuracy. The most predominant is the hook effect, which can be directly seen in the calibration curve (Figure 2.5). Low-dose hook effects appear occasionally in competitive assays. At low concentration of analyte, in particular those radioactive assays where the antigen is labeled to a very high specific activity and result in higher signal than in the absence of analyte. The high-dose hook effect mostly occurs in the immunometric (sandwich) immunoassay due to the excess analyte saturates both capture and detection antibody simultaneously and result in falsely decreased results that prevents the formation of capture antibody-antigen-detection antibody complex. Therefore, it is necessary to ensure the concentration of capture and detection antibodies are enough to cope with the levels of analytes. This effect can be avoided by increasing the amount of antibody and reducing the amount of analyte or by sample dilution [Davies, 2013].

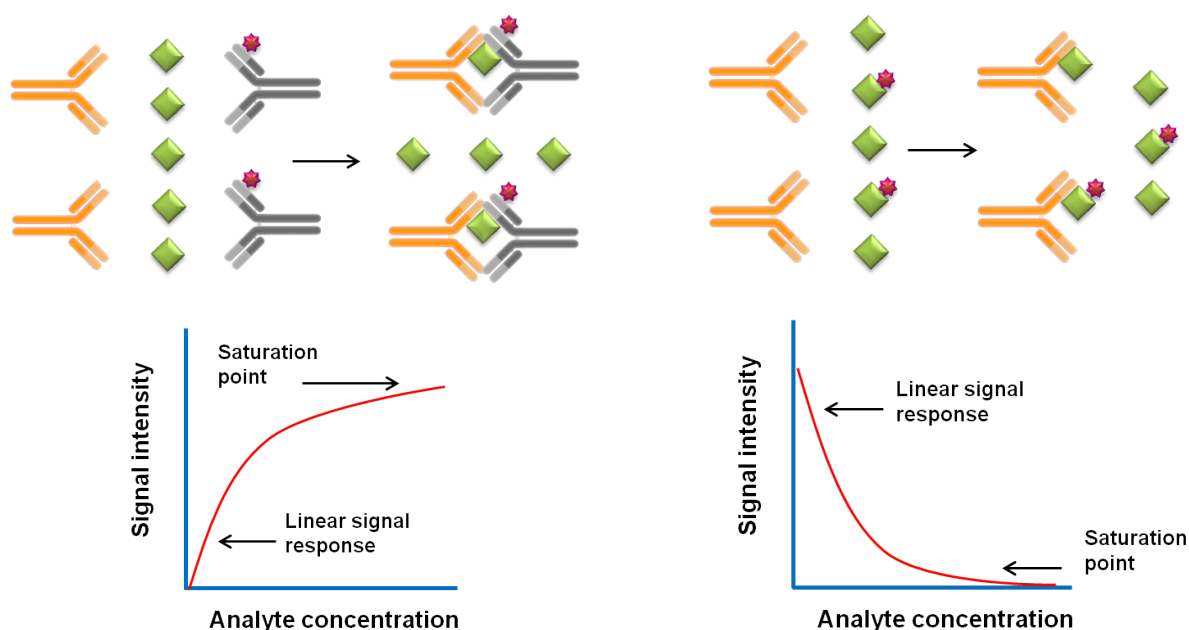


FIGURE 2.4: Left. Non-competitive immunoassay (sandwich format)
 Right. Competitive immunoassay (orange:capture antibody, gray with red star:labeled detection antibody, green:antigen)

FRET-based Immunoassay

The conventional enzyme-linked immunosorbent assay (ELISA) is commonly used method in medical research laboratories for detecting and quantifying analytes indicated by a color change brought by an enzymatic reaction in a complex mixture [Van Weemen and Schuurs, 1971, Engvall and Perlmann, 1971]. This method requires careful surface immobilization of capture antibodies, antigens and detection antibodies with crucial washing to remove unbound species. In comparison, to perform FRET-based immunoassay, homogeneous sandwich immunoassay is more advantageous. A competitive homogeneous energy transfer-based immunoassay was first demonstrated by Ullman et al. in 1976, since then, FRET-based immunoassays have been greatly improved [Ullman, Schwarzberg, and Rubenstein, 1976]. It can directly detect the analyte in the solution, overcoming limitations such as long incubation times, multiple washing steps, nonspecific adsorption on surface upon immobilization. Besides, different FRET pairs enable FRET in the 1-20 nm range to detect small and large analyte, thereby in the presence of the analyte brought the donor and acceptor together into the close proximity at which FRET can occur. FRET signal can be monitored by the extent of donor quenching and acceptor sensitization to estimate the analyte concentration. The amino acid within antibodies provide a wide range of functional groups, thus can use various labeling strategies for bioconjugation.

Even though the sandwich assay represents the mainstream immunoassay format

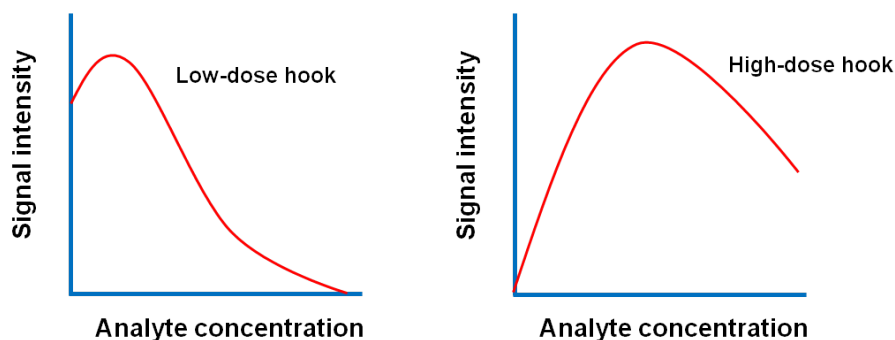


FIGURE 2.5: Left. Low-dose effect Right. High-dose effect

using FRET-based biosensing, the relatively large dimensions of antibody-antigen-antibody complex can decrease the energy transfer efficiency. To overcome this limitations, new FRET materials such as lanthanide complexes and QDs or fragmented antibodies have reported to improve FRET efficiency. The high quantum yields of QDs have been used to extend the Förster distance (R_0) for sensitive detection of estrogen receptor β -antigen using IgGs in a sandwich assay format [Wei et al., 2006]. QDs and lanthanide complex as FRET pairs have been developed to detect prostate-specific antigen [Kupstat, Kumke, and Hildebrandt, 2011] and alpha-fetoprotein [Chen et al., 2012] in homogeneous sandwich immunoassay format. The narrow emission bands of QDs to avoid spectral crosstalk and the use of long-lifetime lanthanide complexes allowed time-resolved measurement to decrease background signal and increase the sensitivity. These advantages allowed to perform multiplexing detection in the diagnostics. QDs and terbium-complex has been recently designed for multiplexing detection of EGFR/HER2 in a single sample using antibodies and nanobodies systems [Qiu et al., 2016]. There also has been increasing interest in using near-infrared (NIR) emitting lanthanides and upconversion nanoparticles (UCNPs) because of anti-Stokes energy transfer that eliminates the background signal from the direct excited acceptors [Laitala and Hemmilä, 2005].

In addition to the direct labeling of antibodies, attaching either donor or the acceptor fluorescent probe with complementary single-strand deoxyribonucleic acid (ss-DNA) can resulting efficient FRET between the donor and acceptor fluorophores upon target hybridization [Heyduk and Heyduk, 2010, Wang, Tian, and Chang, 2012]. An alternative approach to improving FRET efficiency is to decrease the distance between donor and acceptor through fragmented antibodies [Ohiro et al., 2007, Sasajima et al., 2006] and small-size engineered antibodies [Wegner et al., 2014].

2.2.2 Cellular-based imaging

FRET-based imaging techniques are more advantageous for understanding molecular mechanisms within a living cell or tissue using microscopy. In fluorescence microscopy, colocalization refers to the observation of the spatial overlap between two fluorophores. Due to the resolution limit of classical microscope (diffraction limit), this method can only detect in 200-500 nm range, therefore the colocalisation between two proteins does not provide the evidence about their interaction degree. Since FRET occurs over distances of 1-10 nm, FRET-based microscopy has been considered as an ideal technique to study protein-protein interactions in the close proximity, which provides the additional magnification surpassing the optical resolution of the light microscope. There are several intensity-based imaging techniques that apply the method of FRET to conventional wide-field, confocal and multi-photon microscopes. However, quantitative intensity-based FRET methods are problematic for some situations, such as donor bleedthrough (saturation) or directly excited acceptor fluorescence. On the other hand, fluorescence lifetime imaging microscopy (FLIM) is the most rigorous method for determining FRET. The lifetime of fluorophores can be measured directly by time-correlated single-photon counting (TCSPC), in which fluorescence decay histograms are compiled from fluorescence photon arrival times after pulsed excitation on a nanosecond timescale. It is more sensitive than intensity-based method as the fluorescence lifetime does not depend on concentration, photobleaching, excitation intensity to avoid less crosstalk artifacts [Sekar and Periasamy, 2003, Zeug et al., 2012, Becker, 2012].

However, the assemble FRET experiment provide only the average observation based on an ensemble, it is hard to explain the intrinsic phenomena in many physical, chemical and biological process. Recently the major progress in the fluorescence microscopy instrumentation, raising its detection sensitivity to the single-molecule level. The single-molecule FRET (smFRET), which involves labeling biomolecules of interest with FRET pairs, ables to identify subpopulations that would be indistinguishable in ensemble FRET measurement. This allows to study the dynamics of conformational fluctuation, for example protein folding and DNA/RNA folding dynamics. One of the most promising challenges is to translate smFRET measurement from *in vitro* to the intracellular environment, and coupled with single-molecule tracking to fully characterize single-molecule conformation, dynamics and interaction with the complex medium [Schuler and Eaton, 2008, Ha, 2001].

2.3 Luminescent lanthanides

2.3.1 Introduction

The lanthanides series comprises 15 elements (from lanthanum to lutetium), which are located at the sixth period and Group IIIB of the periodic table. Lanthanides including scandium and yttrium are called rare earth metals instead of the scarcity on earth but the difficulty to find them in larger amounts of pure element [Tyler, 2004]. The first rare earth metals were discovered in 1787 with the mineral Ytterbite, which found nearby the village of Ytterby (Sweden). The mineral was studied by a Finnish chemist John Gadolin and found an unknown oxide, which he named yttria. Later on the pure element yttrium was obtained then more lanthanides were revealed until the last one promethium (Pr) to be discovered in 1938. The discovery of lanthanides took more than 100 years, due to the similarity in their chemical properties, and found as oxides which have proved to be particularly difficult to separate from each other [Werts, 2005].

The similarity can be explained by the electronic configuration of the lanthanide atoms and their corresponding ions. Lanthanides from cerium (Ce) to lutetium (Lu) are progressive filled valence electrons in 4f orbitals and share the electronic configuration of xenon. The general electronic configuration is usually donated as $[\text{Xe}]4f^n5d^16s^2$ ($n = 0-14$). Particularly, the oxidation state of lanthanides Ln^{3+} ($[\text{Xe}]4f^n$, $n = 0-14$) is the most stable for all lanthanide in the aqueous solutions and only show small difference in complex formation and solubility. These small differences are due to their decrease in ionic radii of ions with increasing nuclear charge. This consequence is so called lanthanide contraction, which caused by the large size and diffuse localization of electrons in f orbitals providing the poor shielding of the outer electrons from the increasing nuclear charge. Furthermore, the electrons in the 4f orbitals are shielded by the filled 5s and 5p orbitals, thus the 4f orbitals do not directly participate in chemical bonding. The emission wavelengths of lanthanide are minimally perturbed by the surrounding environment, resulting in sharp and narrow-line emission bands. The f-f transition are parity forbidden by the spin and Laporte rule leading to very low extinction coefficient and long excited-state lifetime to several millisecond [Bünzli and Piguet, 2005].

Most of lanthanide ions are luminescent, this property can be explained by a vast number of energy levels involving a redistribution of electrons in 4f orbitals. Here we use Eu^{3+} as example (Figure 2.6 Right.). The energy levels of free Eu^{3+} ions in 4f orbitals are determined by the Coulombic interaction and the spin-orbit coupling between f electrons. The Coulombic interaction, which represents the electron-electron repulsion within the 4f orbitals, generates total orbital angular momentum (L) and total spin angular momentum (S) with a separation in the order of 10^4 cm^{-1} . Each of these terms is split into several J-levels by spin-orbit coupling to an extent of 10^3

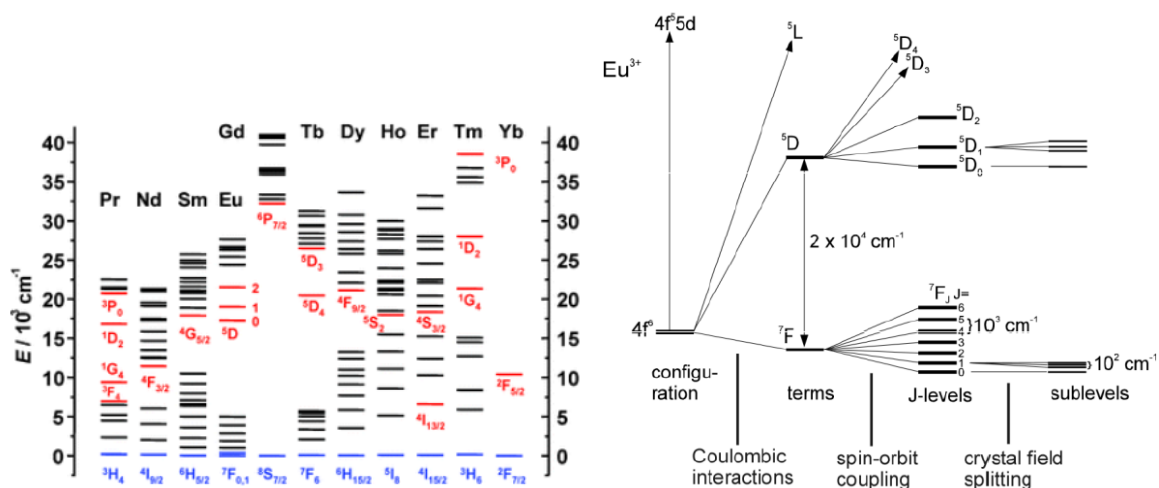


FIGURE 2.6: Left. A summary of ground and excited-state energy levels for the Ln^{3+} series. The main luminescent excited state are highlighted in red, while the ground state term is indicated in blue (Reprinted from [Bünzli and Piguet, 2005]) Right. Diagram represents the interaction leading to the splitting of electronic energy level of Eu^{3+} . (Reprinted from [Werts, 2005])

cm^{-1} , which makes the total angular momentum (J) of the f electrons. When present in a complex environment, where the Eu^{3+} is coordinated with ligands, the individual J -levels are split up further to sublevels by the electric field of the ligand, which is usually referred to as the crystal field. These splittings are usually small (10^2 cm^{-1}) and, depending on the spectral resolution of the spectrometer, appear as fine structure on the individual bands. Therefore, each set of L , S , and J corresponds to a specific distribution of electrons within the 4 f -shell and defines a particular energy level. Thus, the free ion levels can be described by the term symbols $(2S+1)L_J$ with $(2S+1)$ the total spin multiplicity. The ground state and excited state energy level of Ln^{3+} ions are shown in Figure 2.6 Left, where radiative transition between the energy levels occurs to give rise the luminescent lanthanide ions. With respect to the energy gap requirement, Eu^{3+} , Gd^{3+} and Tb^{3+} seems to be the best ions in terms of their emission properties. However, Gd^{3+} emits in the UV region due to the large energy gap between $8S_{7/2}$ and $6P_{7/2}$, whereas Eu^{3+} and Tb^{3+} have their emission in the visible range and are highly suited for application in bioanalysis. Several other ions (Pr^{3+} , Nd^{3+} , Er^{3+} , Yb^{3+}) emit weak luminescence in the NIR region, which have gained in popularity with efficient sensitizing groups. With NIR excitation, light scattering and autofluorescence by biological tissues is substantially reduced, results in a depth of penetration in tissue much larger than UV/Vis excitation. Based on these properties, lanthanide containing luminescent probes are now increasingly being used for cancer detection by time-resolved imaging and in many biological applications [Werts, 2005, Han et al., 2014].

2.3.2 Lanthanide complexes

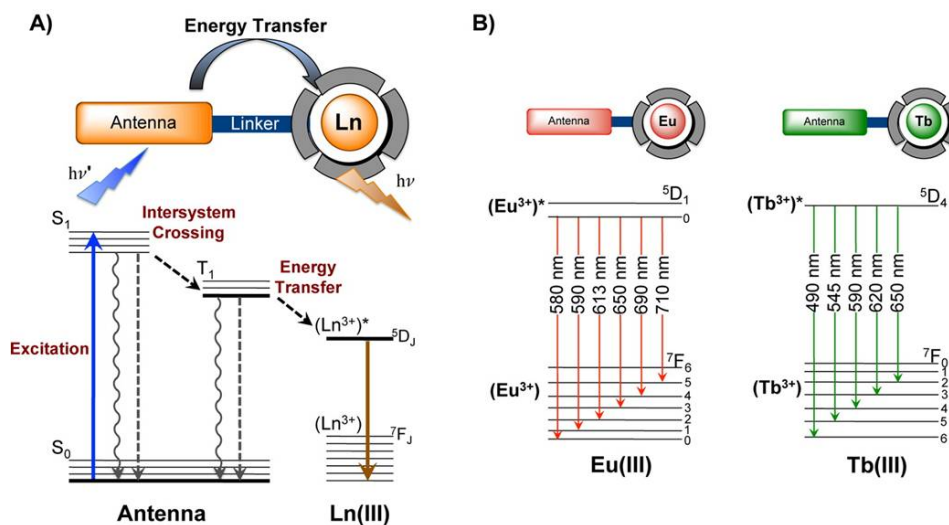


FIGURE 2.7: A) The simplified Jablonski diagram of antenna effect. B) Luminescent 4f-4f transitions of Eu(red) and Tb(green) complex and commonly observed emission wavelength from ⁵D_J excited state to the ⁷F_J ground states. (Reprinted from [Heffern, Matosziuk, and Meade, 2013])

Since the parity (Laporte) forbidden nature of 4f transitions, the direct absorption of Ln³⁺ is very weak hence suffer the consequence of weak luminescence of Ln³⁺ due to low molar extinction coefficient ($< 1 \text{ M}^{-1} \text{ cm}^{-1}$) [Gschneidner, Eyring, and Lander, 2002] and their luminescence is efficiently quenched by coordination of water molecules [Horrocks Jr and Sudnick, 1979]. In order to overcome these low extinction coefficient, an alternative path has been worked out which is called antenna effect, that is luminescent metal ions can be chelated to a chromophore ligand that acts as an "antenna" [Weissman, 1942]. The mechanism is shown in a simplified Jablonski diagram (Figure 2.7A), the antenna ligand absorbs a photon (hν*) to the singlet excited state (S₀ → S₁) then undergoing intersystem crossing to the longer-lived triplet state (S₁ → T₁) and populates the Ln³⁺ excited states through intramolecular energy transfer (T₁ → ⁵D_J). In some cases, the singlet state may directly transfer energy to the central ion, but it is not common, due to short-lived singlet state the process is not efficient. Finally, characteristic radiative emission from ⁵D_J excited state to the ⁷F_J ground state via internal conversion. This is so called luminescent lanthanide complex (LLC). In addition to transferring energy to the metal, the ligand also serves as a shield against solvent molecules from the first coordination sphere, which is essential to avoid quenching of the lanthanide luminescence through non-radiative deactivation process based on vibration of O-H and N-H bonds, and provide stable metal complexes. Furthermore, the antenna effect results in large "Stokes shift" between ligand absorption and lanthanide

emission which makes it easily detected without inner filter effect from LLC absorption. The overall quantum yield (Φ_{Ln}^L) of a lanthanide complex is given by Equation 2.10:

$$\Phi_{Ln}^L = \eta_{ET} \cdot \Phi_{Ln}^{Ln} \quad (2.10)$$

where Φ_{Ln}^L is the quantum yields from the indirect excitation upon ligand to the centered metal ion, Φ_{Ln}^{Ln} is the intrinsic quantum yields of the lanthanide metal ions when direct excitation on the 4f excited state and η_{ET} represents the sensitization efficiency from ligand to the lanthanide ions. The intrinsic quantum yield Φ_{Ln}^{Ln} essentially depends on the energy gap between the lowest lying excited state of the metal ion and highest sublevel of its ground multiplet. The smaller this gap will lead to depopulation by nonradiative processes. Even if the intrinsic quantum yield is large, high excitation energy is required to get the sharpness of the absorption bands ([Bünzli and Piguet, 2005]). The best way to improve the overall quantum yield (Φ_{Ln}^L) is use antenna with high energy gap between the triplet excited state of the ligand and the lowest emitting levels of the Ln^{3+} ions, at least $2,500 \text{ cm}^{-1}$ to $3,000 \text{ cm}^{-1}$ difference. A low energy gap will limit quantum yield due to the thermal deactivation caused by back-energy transfer. The ligand must form stable complexes over a wide pH range and resist aqueous hydrolysis at subnanomolar concentrations. Furthermore, the ligand also should be multidentate (common coordination number is 8 to 9) that able to saturate the Ln^{3+} coordination sphere to prevent water act as quencher to reduce the luminescence due to the enhanced non-radiative deactivation process based on high energy vibration of the O-H bond. And the ligand should have high absorption coefficient. The lanthanide terbium complex (LTCs) used in this thesis is octadentate, macrocyclic ligand of the Lumi4-Tb complex developed by Raymond and co-workers (Figure 2.8 middle) which contains 2-hydroxyisophthalamide moieties with maximum absorption at ca. 340 nm and a noticeable extinction coefficient of $26,000 \text{ M}^{-1}\text{cm}^{-1}$ in a buffered aqueous solution [Xu et al., 2011]. This LTCs can be conjugated to the biomolecules via maleimide or -NHS functional group and has been demonstrated to be very efficient donor in the time-resolved FRET experiments [Geißler et al., 2013].

2.3.3 Lanthanide Tb complexes as FRET donors

Tb and Eu ions are the most often used lanthanides as FRET donors, in the following mainly focus on discussion concerning the characterization of LTCs as FRET donors. LTCs shows several promising properties for using as FRET donor especially combined with QD as FRET acceptors (i) unpolarized emission, Tb possess multiple emission transition dipole moments and therefore a dynamic averaging can be applied that

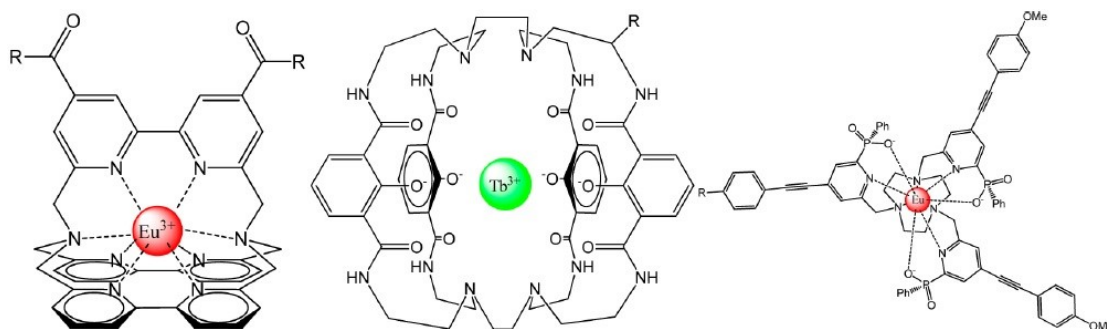


FIGURE 2.8: Representative examples of LLC (R stands for the place of introduction of the activated function). (Reprinted from [Geißler et al., 2013])

limits the orientation factor κ^2 to values between $1/3$ and $4/3$ (average $\kappa^2 = 2/3$); (ii) long-lived excited states up to millisecond lifetimes which can easily avoid autofluorescence background in the time-gated measurements, which can be used for temporal multiplexing. The PL lifetime of the LTC donors ($\tau_D > 2$ ms) is much longer than the PL lifetime of dye or QD acceptor ($\tau_A < 100$ ns), this fast acceptor decay can be neglected against the long FRET-quenched donor lifetime (τ_{DA}), and thus the lifetime of the donor in the presence of acceptor (τ_{DA}) is equal to the lifetime of FRET-sensitized acceptor (τ_{AD}), which leads to the equation 2.12

$$\eta_{FRET} = \frac{R_0^6}{R_0^6 + r^6} = 1 - \frac{\tau_{DA}}{\tau_D} \quad (2.11)$$

If $\tau_D \gg \tau_A$:

$$\eta_{FRET} = \frac{R_0^6}{R_0^6 + r^6} = 1 - \frac{\tau_{DA}}{\tau_D} = 1 - \frac{\tau_{AD}}{\tau_D} \quad (2.12)$$

(iii) large Stokes shift (usually more than 150 nm), due to the separation of excitation by the antenna effect and emission from chelated lanthanide ions, which is suitable for time-gated detection; (iv) well-separated emission bands; the possibility of energy transfer over large distance and combine several acceptors with emission maximum between or beyond the emission bands of LTC to perform spectral multiplexing. All these advantages of lanthanide complexes in the application of FRET-based biosensing are used in homogeneous assays and also can be found in many commercially available bioassays with time-resolved FRET (TR-FRET). Such detection technologies are for example homogeneous time-resolved fluorescence (HTRF) [Mathis, 1999], time-resolved amplified cryptate emission (TRACE) [Bazin, Trinquet, and Mathis, 2002], lanthanide

chelate excitation (LANCE) [Hemmila, 1999], or LanthaScreen [Roberts et al., 2008].

2.4 Quantum Dots

2.4.1 Introduction

Quantum dots (QDs) are nanometer-sized semiconductor nanocrystals which are synthesized from mixture of II-VI, III-V, and IV-VI groups of the periodic table, such as ZnS, ZnSe, CdS, CdSe, CdTe, InP and etc. While many early studies mainly focused on their size-dependent optical properties, now has merged as an important class of material extending from biomedical, electronics and energy applications. Due to their small nanometric sizes, quantum mechanical behavior can be observed from their tunable PL emission color by varying the core size of QDs (Figure 2.9) [Alivisatos, 1996]. The initiation of using QDs for biological applications was reported by two publication of articles in 1998, showing the potential of water-soluble QDs for cellular imaging [Chan and Nie, 1998, Bruchez et al., 1998]. The most popular QD fluorophores for biological applications are made of CdS, CdSe and CdTe cores overcoated with a layer of ZnS because this chemistry and conjugation strategies are the most defined. The ZnS layer in the shell is to protect the core from oxidation and exposure to the surrounding environment also greatly improves the PL yield [Dabbousi et al., 1997, Hines and Guyot-Sionnest, 1996]. III/V group or ternary semiconductors such as InP and InGaP are possible alternatives which lack of cytotoxic cadmium ions [Li and Reiss, 2008]. Although, the usage of QDs in the biological application is controversial due to its toxicity of heavy metals, so that this question is under debate. Their unique photophysical properties still allow them to have great potential in biological application and regard as alternatives to complement the deficiencies of conventional organic dyes [Medintz et al., 2005].

2.4.2 Photophysical properties of QDs

QDs properties show high interest to biologists include (i) brightness: arises from high quantum yield (QY \approx 0.2-0.9) and high molar extinction coefficient ($\epsilon \approx 10^4$ - 10^6 M⁻¹ cm⁻¹, that \sim 10-100 times more than organic dyes); (ii) broad absorption with narrow, size-dependent, symmetric photoluminescence (PL) spectra (full-width at half-maximum \sim 25-40 nm) range from UV to NIR that are more suitable for spectral multiplexing; (iii) large effective stokes shifts allows efficient separation the excitation and emission light to avoid spectral crosstalk; (iv) remarkable photostability have high resistance to photobleaching and photo-chemical degradation to the environment; (v)

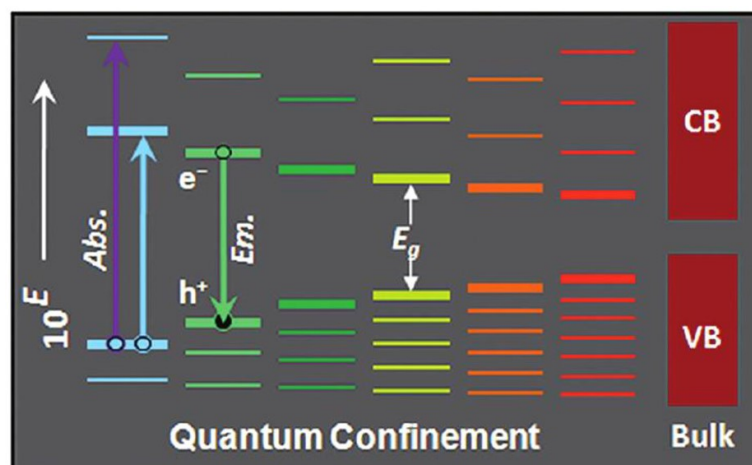


FIGURE 2.9: Quantum confinement effect results in size-tunable QD PL. Quantization of the energy level as a result of the quantum confinement effect in a QD. E_g represent the bandgaps energies, E_m the radiative emission of a photon upon recombination of electron (e^-) and hole (h^+). Energy levels are color coded: The smaller the QD the more blue shifted will be its photoluminescence. Continuous conduction band (CB) and valence band (VB) of bulk semiconductor shown as comparison. (Reprinted from [Algar et al., 2011a])

some QDs provide high two-photon absorption cross sections, which can excite at NIR to have deeper tissue penetration and decrease the autofluorescence from biological matrix [Resch-Genger et al., 2008, Rosenthal et al., 2011].

The unique properties of QDs are based on their size-dependent optical and electronic properties, which are intermediate between those of bulk semiconductors and discrete molecules. In a bulk semiconductor, the valence band is occupied with electrons and the conduction band is empty separated by an energy bandgap of 0.5-3.5 eV (Figure 2.9). When it is excited by a photon of energy, a promoted electron into the quasi-continuum conduction band and left a positive hole in the valence band. The Coulomb interaction between the electron and the hole leads to a quasi-particle, which is called an exciton. The average distance between electron and hole is referred as the Bohr radius. In the case of QDs, the density of electronic states is not sufficient to form complete band structures and discrete energy levels exist at the band edge. As the QDs material is reduced to nanoscale, the continuous energy bands split into discrete excitonic states. As a result of excitons that are confined to smaller dimensions than the Bohr radius, the band gap energy increases with decreasing QD size, which effects the absorption and emission wavelengths of QDs shift to the blue spectral region. This phenomenon is known as quantum confinement effect. It should be noted that large surface-to-volume ratio of QDs is also an important aspect, which effect their photophysical properties due to large fraction of atoms on the surface. For example, a 5 nm CdS QD has approximately 15% of its 3300 atoms on the nanocrystal surface

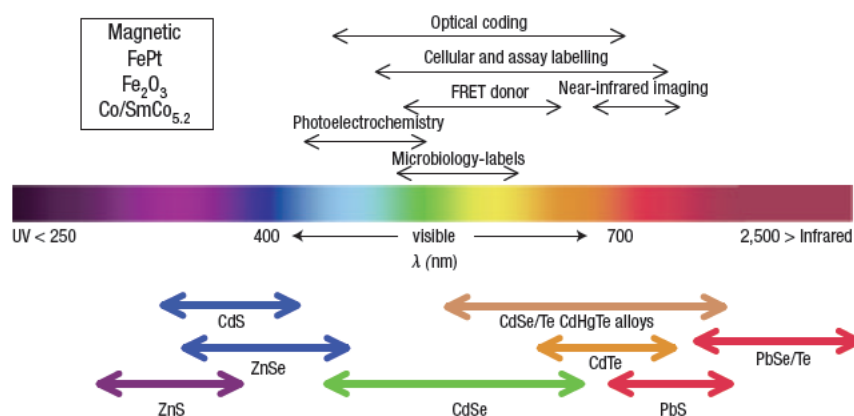


FIGURE 2.10: Representative QD core materials and their emission ranges for the most studied types in the biological application. (Reprinted from [Medintz et al., 2005])

and a 4 nm CdSe QD has approximately 33 % of its 1500 atoms at the surface. The impurities, dangling bonds, vacancies on the surface of QDs, which are referred as trap state, can greatly reduce quantum yield by non-radiative recombination of the exciton. In order to minimize trap state and confine the core excitons, the core QD is usually coated by one or more shells with suitable lattice parameter and a higher band-gap energy semiconductor material. Such core/shell or core/shell/shell QD structure can effectively increase fluorescence quantum yield, photochemical stability and minimize blinking. By controlling their core sizes, the shell thickness and the composition of the semiconductor materials of cores and shells. Thus, the final absorption and emission of QDs can be tuned to PL colors emitting across the near-ultraviolet, visible, and near-infrared spectrum, making them ideally suited for all kinds of spectroscopic applications (Figure 2.10) [Algar, Massey, and Krull, 2013].

2.4.3 Surface functionalization

The preparation of water-soluble, biocompatible, highly luminescent and monodisperse QD is extremely important for use in biological application. The big milestone of synthesizing high-quality QDs is reported by Bawendi group, that QDs are synthesized at high temperature by pyrolysis of organometallic precursors in the presence of hydrophobic coordinating ligands (mixture of trioctyl phosphine/trioctyl phosphine oxide, TOP/TOPO) in organic solvents which passivate the surface and permit slow steady crystallite growth [Murray, Norris, and Bawendi, 1993]. In order to make it soluble, phase transfer to the aqueous solution is required by surface functionalization with hydrophilic ligands either through ligand exchange, encapsulation or silica coating [Medintz et al., 2005]. Figure 2.11 shows a schematic overview of how these chemical strategies are implemented with QDs.

Ligand exchange is the method to replace QDs native hydrophobic ligand TOP/TOPO with bifunctional ligands that contain a surface anchoring moiety to bind to the inorganic QD surface and an opposite hydrophilic end group to achieve water solubility. Surface anchoring moiety can be thiol (-SH), amine (-NH₂), or phosphine (-PH₂) functionality. Hydrophilic functionality groups such as hydroxyl (-OH), carboxyl (-COOH), methoxy (-OCH₃) and poly(ethylene glycol) (PEG) [(-OCH₂CH₂)_n] are for aqueous dispersion [Bergman and McHale, 2011]. Thiol groups have been the most popular utilized as anchors due to the strong affinity with QD surface metal atoms (Cd and Zn). The simplest embodiment of a coating is mercaptoacetic acid (MAA), a monothiolate ligand bind the QD surface and the other end a carboxylate group provide aqueous colloidal stability [Chan and Nie, 1998]. However, deprotonation of the carboxyl groups limiting the QD utility in basic pHs and low ionic strength. To overcome these problems, Mattoussi et al. first developed the use of PEGylated- dihydrolipoic acid (DHHLA), a bidentate, dithiol ligand that binds the QD more tightly to enhance colloidal stability over a large pH range and ionic strength [Mattoussi et al., 2000]. Poly(ethylene glycol) (PEG) also improves biocompatibility and reduce nonspecific binding and successfully incorporate a variety of functional groups for bioconjugation [Susumu et al., 2007]. Another important goal is to develop coating that can minimize the QDs hydrodynamic size while still retaining stability and biocompatibility, because thin coatings are crucial for cellular uptake and biosensing application based on FRET where the efficiency is directly related to the distance between donor and acceptor molecules. Thus, zwitterionic ligands are explored as alternatives to larger PEG ligands. Susumu et al. developed a series of DHHLA-based zwitterionic ligand allowing high affinity with QD attachment and showing rapid and efficient cellular uptake [Susumu et al., 2011]. These zwitterionic ligand resulted in compact QDs with small hydrodynamic diameters, colloidal stability under wide pH range and high salt concentration, low cellular toxicity and directly conjugate with His-tagged biomolecules onto QD surface in a close proximity also could be functionalized with other reactive groups for biomolecule attachment. Ligand exchange can provide water-soluble QDs with small hydrodynamic diameter but sometimes it suffer from a decrease of quantum yield as surface state is modified. The other strategy for preparing aqueous QDs with a minimal decrease in quantum yield is by encapsulation of the native QD inside an amphiphilic ligand [Algar et al., 2011a].

Encapsulation is a method by overcoating the QDs that still retaining their original synthesized hydrophobic ligands with amphiphilic ligands through hydrophobic interaction. Phospholipids and amphiphilic polymers are the most common used amphiphilic ligands. Although the encapsulation method with polymer coating keep the original hydrophobic ligand of QDs and prevent water from interacting with surface

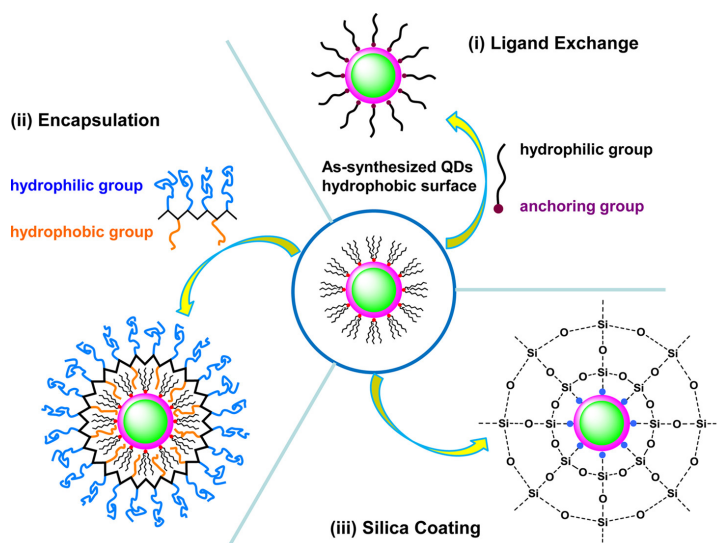


FIGURE 2.11: Three are three chemistry approaches to make QDs colloidally stable in aqueous solution (i) ligand exchange (ii) encapsulation (iii) silica coating. (Reprinted from [Hildebrandt et al., 2016])

to preserve their original quantum yields. However, it often results in large hydrodynamic diameter, which is not favorable for FRET applications. Silica coating consists of a siloxane network formation on the QD surface through hydrolysis of silane molecules and subsequent cross-linking [Bruchez et al., 1998]. Compared to the ligand exchange method, the silica layer is still relatively thick resulting in large hydrodynamic diameter, so not too many biosensing studies using silica-coated QD [Hildebrandt et al., 2016].

These surface preparations not only change the QDs photophysical properties, but also directly influence subsequent bioconjugation. The different strategies can contribute to the size, surface charge and hydrodynamic diameter of the final hydrophilic QD. When designing QD-based biosensing assays, it is important to take into accounts all the factors because they can impact the intended utility, such as FRET interactions, cellular delivery, and in vivo circulation, distribution. Therefore, many researches are dedicated to develop new hydrophilic compact ligand to minimize the thickness of QD surface ligand layer and improve synthesis methods for biological applications.

2.4.4 Quantum dots as FRET donors and acceptors

QDs can be used as both FRET donors and acceptors, which have been published many studies in literatures. In the most of applications, QDs are used as FRET donors in bioassays with various organic dye acceptors [Clapp, Medintz, and Mattoussi, 2006], due to its photophysical properties which are (i) size tunability, which allows for an ideal spectral overlap with other acceptors; (ii) broad absorbance band, which enables

for excitation at any wavelength to avoid acceptor absorption; (iii) large QD surface, which allows to attach many acceptors to QDs therefore increase the FRET efficiency with increase numbers of acceptors (n):

$$\eta_{FRET} = \frac{nR_0^6}{nR_0^6 + r^6} \quad (2.13)$$

where n is the number of acceptors surrounding a single donor [Clapp et al., 2004]. The major limitation for using them as FRET acceptors is their wide excitation spectra, which will easily lead to spectral crosstalk from the direct excitation when using common organic fluorophores as FRET donors. The problems arises from the lifetime of a QD (>10 ns) compared to the typical organic dye (<5 ns). When both QDs and dyes are excited, dye will decay back to its ground state while many QDs acceptors in the excited states, which strongly limits the possibility for FRET [Clapp et al., 2005]. FRET is a non-radiative energy transfer from the excited state donor to the ground state acceptor, therefore the acceptor must be in the ground state [Algar et al., 2014]. To overcome this limitation, the best way is to use lanthanide complex as FRET donors based on their extremely long lifetimes (millisecond). Here we use LTCs as FRET donor as example. After excitation, both LTCs and QD are in the excited states, after several nanoseconds the main fraction of QDs have decayed back to their ground states when most of the LTCs are still in the excited states, which allows for efficient FRET. We have mentioned in Section 2.3.3 the unique PL properties of LTCs as FRET donor. Another alternatives to avoid light excitation is the use of bioluminescent, chemiluminescent as donors, or UCNPs due to their ability to excite at NIR region. The main advantages of using QDs as FRET acceptors are (i) narrow, symmetric and tunable emission bands, which allows to use several QD acceptors with the same donor without spectral crosstalk and provide a great potential for spectral multiplexing (Figure 2.12); (ii) high extinction coefficient, which can cover most of LTCs emission peaks resulting in large spectral overlap integral and long Förster distance (up to 11 nm) (Figure 2.12); (iii) large QD surface, which allows conjugation of several donors to increase the possibility of QD FRET sensitization with the number of donors (m), but not increase FRET efficiency [Geißler et al., 2013, Geißler et al., 2010]. The probability of QD FRET sensitization by LTC donors (m) can be approximated as:

$$P = 1 - (1 - \eta_{FRET})^m = 1 - \left(\frac{r^6}{R_0^6 + r^6}\right)^m \quad (2.14)$$

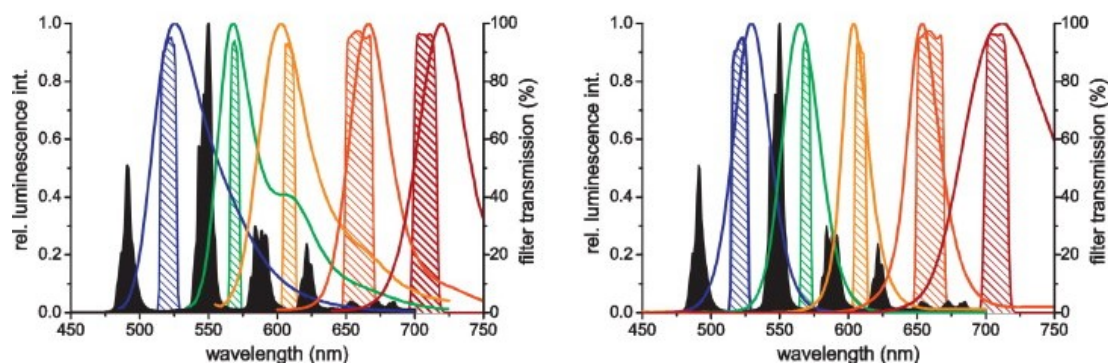


FIGURE 2.12: LTC-donor-based multiplexed FRET using different organic dyes (Left) and QDs (Right). LTC-PL spectra in black. Left: organic dyes OregonGreen (blue), AlexaFluor555 (green), AlexaFluor568 (orange), Cy5 (red) and AlexaFluor700 (brown); Right: Qdot525 (blue), Qdot565 (green), Qdot605 (orange), Qdot655 (red) and Qdot705 (brown). It clearly show that several QD acceptors are suitable for the spectral multiplexing, but several dye emission spectra with a shoulder, which leads to spectral crosstalk of various dyes to different detection channel. (Reprinted from [Hildebrandt, Wegner, and Algar, 2014])

2.5 Bioconjugation

2.5.1 Introduction

Bioconjugation is a crucial strategy that can label biomolecules with different substrates for further sensing application. Conjugation techniques are dependent on two interrelated parts; reactive groups and the functional groups. The functional groups can be found in biomolecules (proteins, DNA, carbohydrates, lipids, etc.). The amino acid residues within the proteins and peptides are often targeted for conjugation. The major functional groups including primary amines ($-NH_2$), carboxyls ($-COOH$), sulfhydryls ($-SH$) and carbonyls ($-CHO$) can be targeted by a number of chemical reactive groups. Reactive groups such as crosslinker, tags and probes, provide the means to specially label on the functional groups of biomolecules [Hermanson, 2013, Sapsford et al., 2010]. The initial choice of bioconjugation chemistry can play an important role in the subsequent applications. There are several important criteria to be satisfied that allow controlled attachment of protein or other biomolecules to any NP (e.g. QD), including the ratio of biomolecule per QD, the biomolecule orientation on the QD, the relative separation distance from the QD, the attachment affinity, and it should always maintain the optimal function and activity after conjugation (Figure 2.13). Although in practice it is not easy to achieve all these criteria, keep these in mind will provide us a capability to design and optimize of such QD-based FRET sensors [Hildebrandt et al., 2016].

In general, five bioconjugation methods are used as highlighted by the use of a

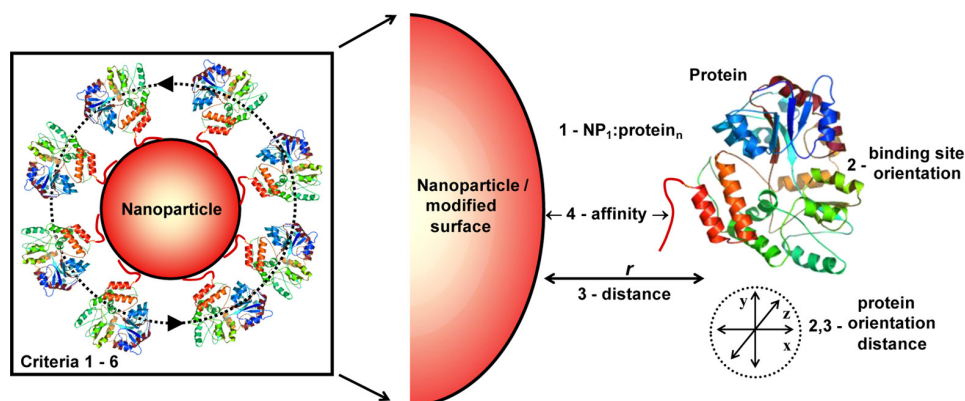


FIGURE 2.13: Schematic representation of principle criteria for controlled attachment of a protein or biomolecule to the NP. (Reprinted from [Medintz, 2006])

peptide and NP as example, it is the same principle of protein and QD (Figure 2.14). (i) Electrostatic interaction: the opposite charge on the surface of NP and the peptide, by charge-charge interaction create a NP-peptide assembly; (ii) Direct attachment: the functional groups of biomolecules can directly coordinate on the surface of NP, e.g. a thiol from the cysteine residue of peptide coordinate to the Zn on the QD surface, or biomolecules with polyhistidine (His_n) can directly attach to Zn rich surface QDs through metal-affinity coordination. His_n also has affinity for other metals (Ni, Cu, Co, Fe, Mn) which would be applicable to other material NPs; (iii) Secondary interaction: use ligand-receptor interaction such as biotin-streptavidin recognition, e.g. biotinylated peptide can bind to the NP-streptavidin conjugate; (iv) Covalent attachment: use classical bioconjugation chemistry by crosslinkers such as the ligand with carboxyl group can conjugate to the aminated peptide through carbodiimide (EDC) chemistry using sulfo-NHS (N-hydroxysulfosuccinimide) or amino (PEG) NPs can join to the thiol from biomolecules through sulfhydryl-reactive chemistry using sulfo-EMCS (N- ϵ -maleimidocaproyl-oxysulfosuccinimide ester). The converse use of the above mentioned methods are equally the same; (v) Encapsulation: the peptide is within the matrix during or after NP synthesis, which is a very common method for designing drug delivery (Sapsford et al., 2013, Hildebrandt et al., 2016). Three different conjugation methods and materials are introduced which are related to this work.

2.5.2 Streptavidin-Biotin interaction

Streptavidin-biotin binding interaction perhaps is the most well-known method used for preparing QD-bioconjugate. Such high affinity binding is the strongest noncovalent protein-ligand interaction in nature currently known with a dissociation constant of 10^{-15}M . Native Streptavidin (sAv) is a tetrameric glycoprotein which has the ability to

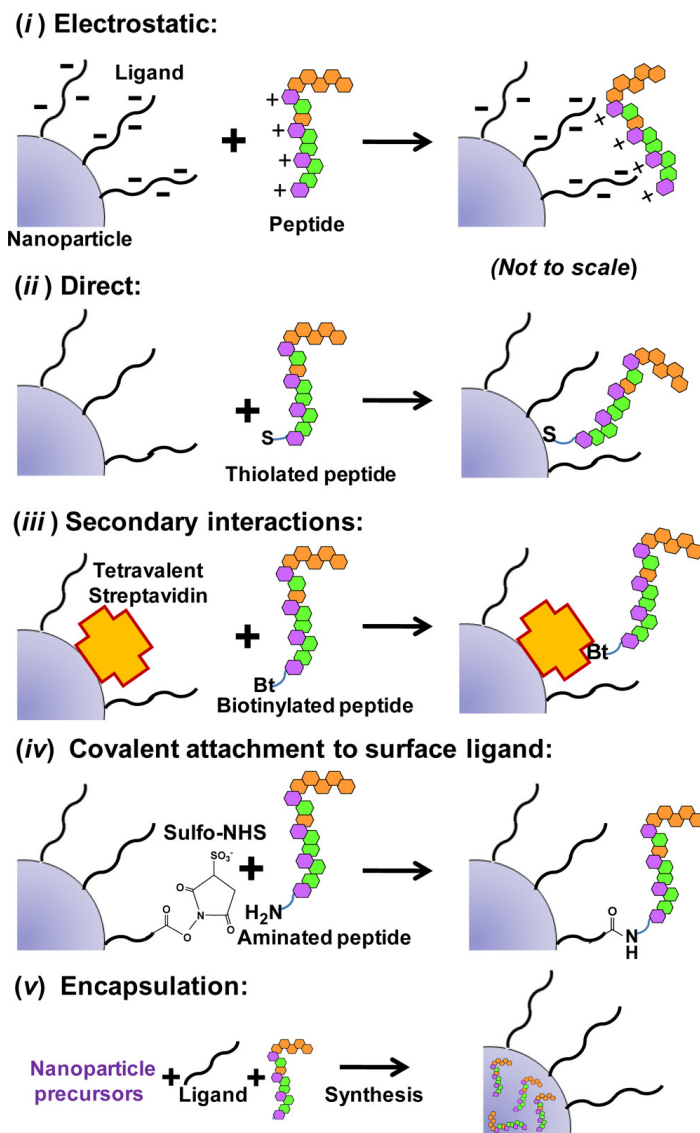


FIGURE 2.14: Five general attachment schemes used for bioconjugation biomolecules to the NPs. (Reprinted from [Sapsford et al., 2013, Aubin-Tam and Hamad-Schifferli, 2008])

bind up to four biotin molecules. This strong binding between biotin and sAv is due to the hydrogen bonding from the heteroatoms of biotin and amino acids residues of sAv. Moreover, there are numerous van der Waals force-mediated contacts and hydrophobic interactions between biotin and tryptophane residues in the binding site. This superior property is ideal for purification and detection strategies in developing biological applications. Many Streptavidin-coated QDs are commercially available. Biotinylated proteins or other biomolecules can be obtained by using enzymes through monophosphorylation and transfers the biotinyl moiety to the target protein during expression or reacting with biotin crosslinkers such as succinimidyl and maleimide derivatives.

2.5.3 Polyhistidine-metal affinity

One of direct attachment used in this work was based on metal coordination by histidine residues. The imidazole side chains on the polyhistidine residues can coordinate directly to the transition metals such as Co^{2+} , Cu^{2+} , Ni^{2+} , and Zn^{2+} . This strong affinity between the polyhistidine residues and the metal ions, which is also utilized in immobilized metal ion affinity chromatography (IMAC) for protein purification. Moreover, the small size of histidine tags shows no significant effect on the protein function. These properties of polyhistidine can be used to bioconjugate with different kinds of inorganic NPs. For QD bioconjugation, three ways are shown in Figure 2.15, A) self-assembly of polyhistidine to ZnS surface of QD through imidazole moieties; B) self-assembly of polyhistidine to the Ni^{2+} supplemented carboxyl polymer-coated QDs; C) self-assembly of polyhistidine through nickel(II)-nitrilotriacetic acid (Ni^{2+} -NTA) coated NP [Algar et al., 2011b].

Imidazole side chain of His_n -tagged biomolecules directly coordinate to the Zn^{2+} at the surface of the ZnS shell that commonly surrounds the core CdSe nanocrystals. This strong interaction has a dissociation constant (K_D) in nanomolar range (10^{-7} - 10^{-10} M). The self-assembly in bulk solution is very fast, reaching equilibrium within minutes (~ 100 - 200 s) at room temperature with dissociation constant $K_D \approx 10^{-9}$ M [Sapsford et al., 2007]. However, it is still stronger than most antibody bindings (10^{-6} - 10^{-9} M). The dissociation constant may vary depending on the number of histidine monomer. Histidine tags shorter than four monomers providing lower binding affinity and larger dissociation constant, whereas more than six monomers does not improve both properties. Therefore, the most common polyhistidine tags are formed of six histidine residues (His_6). This strong affinity is due to the linear arrangement of histidine residues that provide polyvalency and cooperative interactions with the nanoparticle surface [Hainfeld et al., 1999]. Due to this reason polyhistidine self-assembly can control the ratio of biomolecule per QD simply through one-to-one stoichiometry and provides effectively zero-length conjugation between the QD and biomolecule [Sapsford et al., 2007]. This cause His_n conjugation advantageous in FRET applications that shorter the distance between donor and acceptor in comparison to the biotin-streptavidin system and is considered the closest approach to meet all the criteria for ideal bioconjugation [Blanco-Canosa et al., 2014].

2.5.4 Covalent attachment

Crosslinking is the process of chemically joining two or more molecules by a covalent bond. Most frequent way is to use commercial crosslinking reagents that possess reactive ends to specific functional groups such as primary amines or sulfhydryls on

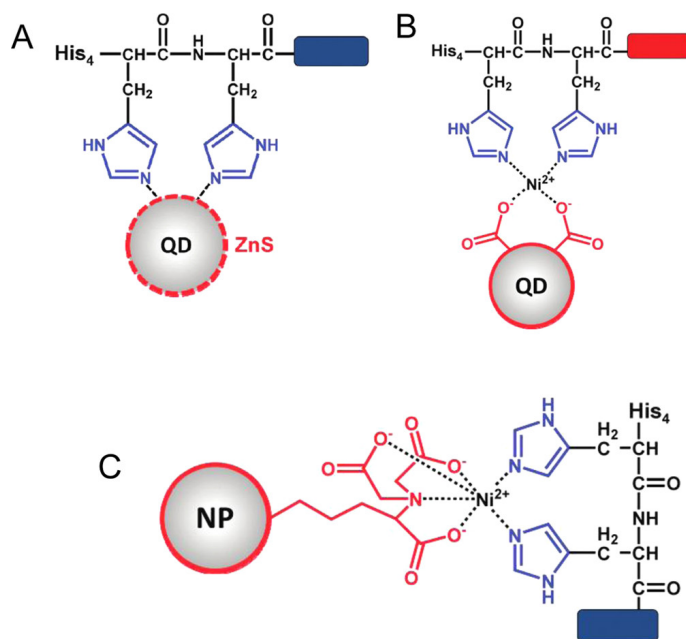


FIGURE 2.15: (A) Zn^{2+} -polyhistidine self-assembly. (B) Carboxylate- Ni^{2+} -polyhistidine self-assembly. (C) Nitrilotriacetic acid- Ni^{2+} -polyhistidine self-assembly. (Reprinted from [Hildebrandt et al., 2016, Algar et al., 2011b])

proteins, peptide, oligonucleotides or other biomolecules. There are various bioconjugation strategies for attaching fluorophores or nanoparticles to biomolecules. The most common chemistries targeting these groups are illustrated in Figure 2.16. Among them amine-reactive chemistry using succinimidyl (NHS) ester, carboxyl-reactive chemistry using carbodiimides (EDC crosslinking for coupling with an amine containing compound), and sulfhydryl-reactive chemistry using maleic acid imides are very frequently used strategies. In this work, we mainly targeted primary amines to react with NHS for LTC conjugation, and free thiol groups to react with maleimide reactive groups for QD conjugation. In order to transform the amino-reactive QDs into maleimide-reactive QDs, we use sulfo-EMCS, a water soluble heterobifunctional crosslinker that contains NHS ester on one end and a maleimide reactive group on the other end. Recently, a system study using commercial 605, 650, 705 nm Qdot ITK amino PEG QDs (Thermo Fisher) showed the standard conjugation procedure of these QDs via sulfo-EMCS crosslinkers [Bhuckory et al., 2016]. When applying different materials, this method requires optimization and several purification steps to get fine-tune conjugate activity. Therefore it is relatively difficult to control the labeling ratio compared to the streptavidin-biotin and polyhistidine-metal systems. Figure 2.17 gives an overview of bioconjugation and surface coating strategies that can be performed on a QD.

Target	Reactive Group	Product	Example Mechanism ⁴
Free Thiol	Maleimide ¹ Haloacetyl/Alkyl Halide Arylating agents Aziridine Acryloyl derivatives Disulfide Exchange ¹ – pyridyl disulfides, 5-thio-2-nitrobenzoic acid (TNB)	Thioether Thioether Thioether Thioether Mixed disulfides	
Aldehyde/ Ketone	Hydrazine ¹ Amines	Hydrazone Schiff's base (imine) ²	
Free Amine	<i>N</i> -hydroxysuccinimide ester (NHS) ⁴ Acyl azides Isocyanates, Isothiocyanates Sulfonyl chlorides Aldehydes, Gltoxals Epoxides, Oxiranes Carbonates Arylating agents Imidoesters Carbodiimides, anhydrides	Amide Amide Urea, thiourea Sulfonamide Imine, secondary amine ³ Secondary amine Carbamate Arylamine Amidine Amine ⁴	
Carboxylate	Carbodiimides ¹ , Carbonyl/diimidazole Diazoalkanes, Diazoacetyl	Amides ⁴ Ester	
Hydroxyl	Epoxides, Alkyl halogens Periodate Isocyanates ¹ , Carbonyl/diimidazole, <i>N,N'</i> -disuccinimidy carbonate, <i>N</i> -hydroxysuccinimidy chloroformate	Ether Aldehyde Carbamate or urethane ⁴	
Reactive Carbon (On a phenol <i>e.g.</i> tyrosine)	Diazonium ¹	Diazo bond	

FIGURE 2.16: Selected biological functional groups and representative reaction mechanisms. (Reprinted from [Sapsford et al., 2013])

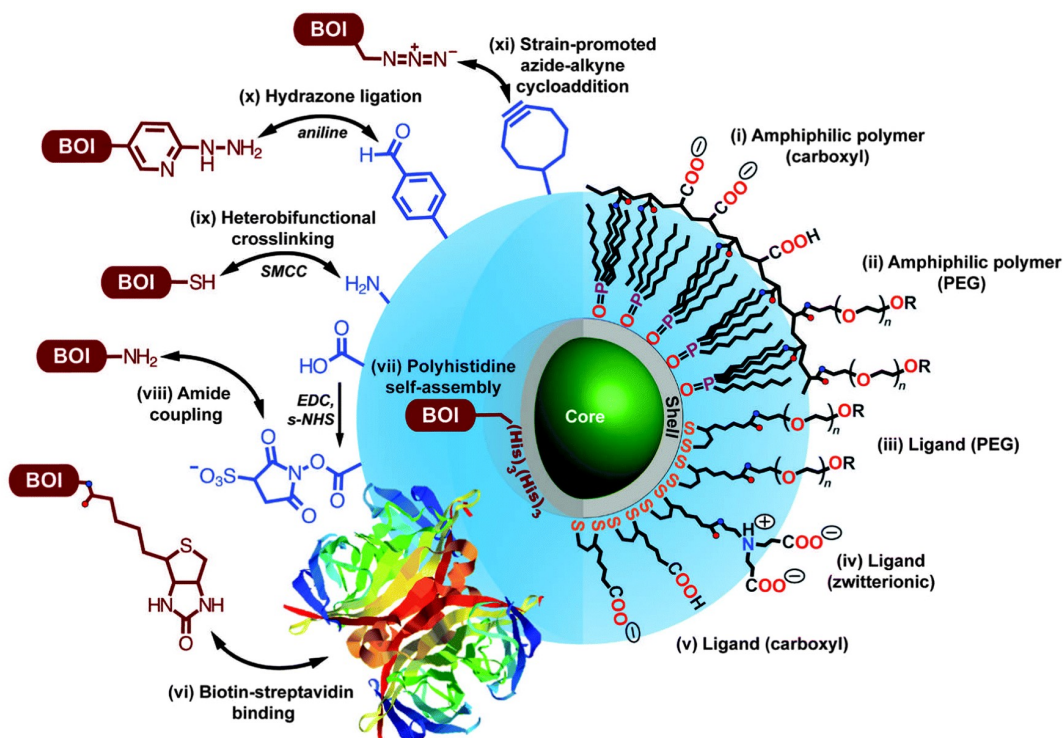


FIGURE 2.17: Overview of different bioconjugation (left side, BOI = biomolecule of interest) and surface coating (right side) strategies for QDs. (Reprinted from [Wegner and Hildebrandt, 2015])

2.6 Instrumentation

2.6.1 Characterization

Absorption spectra were acquired using a Lambda 35 UV/Vis spectrometer from Perkin Elmer (Waltham, MA, USA) or SPECTROstar Nano (BMG-Labtech, Germany) in combination with LVis plate. Emission spectra of LTC and QD were recorded on FluoTime 300 fluorescence spectrometer from PicoQuant (Berlin, Germany) using a continuous-wave Xe lamp as excitation source or a spectrophotometer (Xenius, SAFAS, Monaco).

2.6.2 Time-resolved immunoassays

FRET immunoassay with time-resolved measurement provided highly sensitive detection compared to traditional fluorescence immunoassays. The requirement for performing time-resolved FRET is utilizing donors with much longer excited-state lifetimes than the acceptors. It is usually applicable using lanthanide-based donors with millisecond lifetimes and dye or quantum dots with nanosecond lifetime. The large difference of lifetime integrating with a time delay of ca. 50-150 μ s allows for efficient suppression of PL from directly excited acceptors and sample autofluorescence from the media. After a short-pulsed excitation, the excited long-lived donor will transfer

energy non-radiatively to the short-lived acceptor in a close proximity which result in donor quenching and acceptor sensitization. Both signals can be measured by applying a period of time-gated (TG) window after pulsed excitation, so that the signal only participate in FRET will be detected (Figure 2.18). This time-gated window can be varied depending on the experiment to optimize the signal-to-noise ratio.

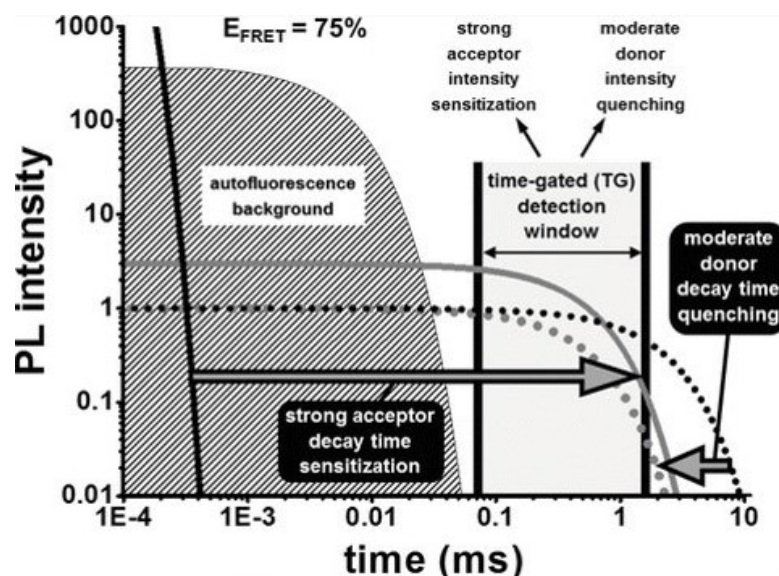


FIGURE 2.18: Principle of time-gated FRET detection. The PL decay curve of long-lived fluorophore (black dotted line, $\tau = 2$ ms) can be efficiently distinguished from those of a short-lived fluorophore (black solid line, $\tau = 20$ ns) and autofluorescence background (filled curve in the background, $\tau = 5$ μ s) by using TG detection window that opens with a delay that is longer than the short-lived PL decays. In the case of FRET from long-lived donor to short-lived acceptor, these fluorophores get quenched and sensitized (indicated by the large arrows), respectively. The resulting PL decay curves (gray) both have the same PL decay time ($\tau = 0.5$ ms in the case of 75 % FRET efficiency) and can both be detected in the TG detection window. (Reprinted from [Zwier and Hildebrandt, 2017])

All PL decay curves were acquired on an EI plate reader (Edinburgh Instruments) integrated with multi-channel scaling (MCS) card functions as photon-counting detectors that can count the photons within a time intervals and store the results in subsequent memory locations of a fast data memory for recording long-lived decay time, using 4000 detection bins of 2 μ s integration time and nitrogen laser (VSL 337 ND, Spectra Physics) excitation (337.1 nm, 20 Hz). Time-gated PL intensity measurements were performed on a KRYPTOR compact plus fluorescence plate reader (Cezanne/BRAHMS/Thermo Fisher Scientific) using 500 detection bins of 2 μ s integration time and nitrogen laser excitation (337.1 nm, 20 Hz, 100 pulses). After sample excitation, emission signals were split in two parallel channels, which were separated by a dichroic mirror (500 nm,

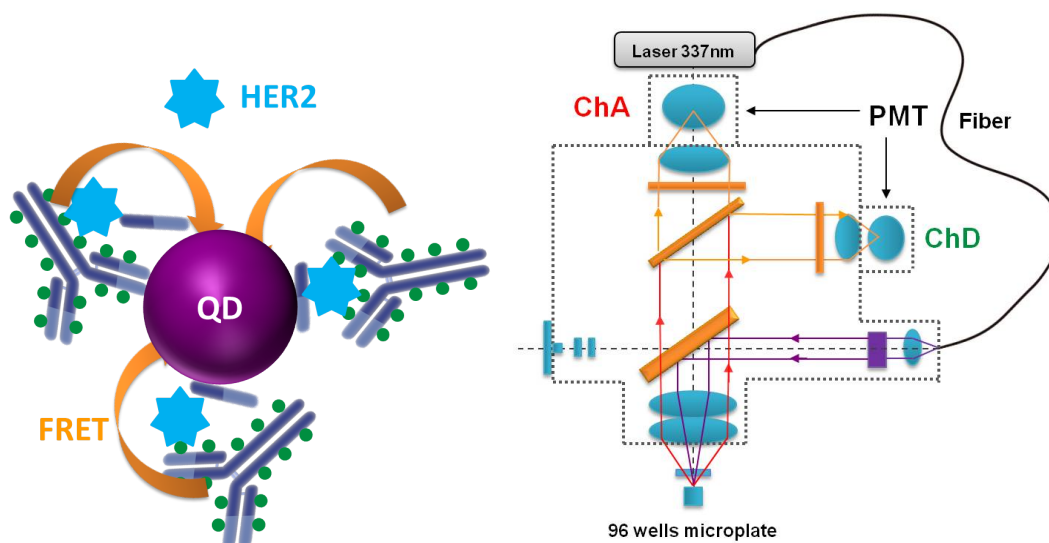


FIGURE 2.19: Left. Principle of homogeneous sandwich immunoassay shows FRET between LTC to QD in the presence of biomarker. Right. Simplified schematic instrumental set up of fluorescence plate reader (Reproduced from Geißler et al., 2010).

Semrock) with bandpass detection filters for donor and acceptor signal using two photomultiplier tubes (PMTs). The simplified schematic instrument set is shown in Figure 2.19 Right. In our case, we will use a lanthanide complex of terbium (LTC) with a decay time of *ca.* 2.6 ms as FRET donor (donor channel, ChD) and quantum dots as FRET acceptor (acceptor channel, ChA) with lifetime ranging from 6 to 90 ns. TG PL intensity of ChA and ChD are measured in a time window from 100 μ s to 900 μ s after excitation. The ratiometric measurement can be obtained by FRET ratio (F_R):

$$F_R = \frac{I(ChA)}{I(ChD)} = \frac{I_{QD}(100 - 900\mu s)}{I_{LTC}(100 - 900\mu s)} \quad (2.15)$$

The calculated FRET ratios for the different concentrations of biomarker in the immunoassay were plotted as a function of the biomarker concentration. The resulting curve is known as calibration curve. The important parameter to characterize the sensitivity and performance of the individual immunoassays were quantified by limit of detection (LOD). LOD is the lowest concentration of the analyte that can be detected in a reasonable range. It can be calculated from the linear part of calibration curve using Equation 2.16. The $3 \times SD$ is equivalent to 99.7% confidence limit. The slope of the calibration curve determines the sensitivity of the immunoassay.

$$LOD = \frac{3 \times (SD)}{slope} \quad (2.16)$$

Chapter 3

ADAPT for HER2 detection

3.1 Introduction

Immunoassays are dominated by the use of antibodies due to their broad accessibility and also since there are fewer restrictions for biosensing in solution regarding size, structure, and environment. However, the large sizes, complex structures, and relatively expensive and laborious production of IgG antibodies have led to the development of alternative affinity proteins [Gilbreth and Koide, 2012]. Small single-domain antibodies (or nanobodies) [Muyldermans, 2013] are naturally produced, but they can also be selected *in vitro*. Similarly, engineered scaffold proteins are selected *in vitro* and can either be produced in bacterial hosts or chemically synthesized. The most common synthetic binding proteins are (in alphabetical order) affibodies [Löfblom et al., 2010], anticalins [Richter, Eggenstein, and Skerra, 2014], designed ankyrin repeat proteins (DARPin) [Plückthun, 2015], and monobodies [Sha et al., 2017]. The main applications of these antibody alternatives are therapy, drug delivery, and *in vivo* and *in vitro* imaging [Schumacher et al., 2018]. However, these much smaller affinity binders would have significant advantages for bioassays based on Förster resonance energy transfer (FRET) and nanoparticles. The limited FRET distance of approximately 10 nm and the requirement of oriented and multivalent conjugation on nanoparticles [Sapsford et al., 2013] in combination with their already relatively large sizes clearly favor the use of small biomolecules for biosensing. Surprisingly, only few studies have reported the combination of synthesized scaffold proteins with FRET [Limsakul et al., 2018, Renberg et al., 2004] or nanoparticles [Gao et al., 2011, Gurunatha et al., 2016]. Semiconductor quantum dots (QDs) are important optical nanomaterials for diagnostics and imaging, and exhibit unique properties for versatile FRET biosensing [Wegner and Hildebrandt, 2015]. Nanobodies have been conjugated to QDs and applied for both FRET immunoassays and FRET imaging in combination with luminescent terbium complexes (LTC) and time-gated (TG) detection [Wegner et al., 2014, Afsari et al., 2016]. The application and performance of even smaller engineered scaffold proteins in such QD-FRET immunosensors remains to be demonstrated.

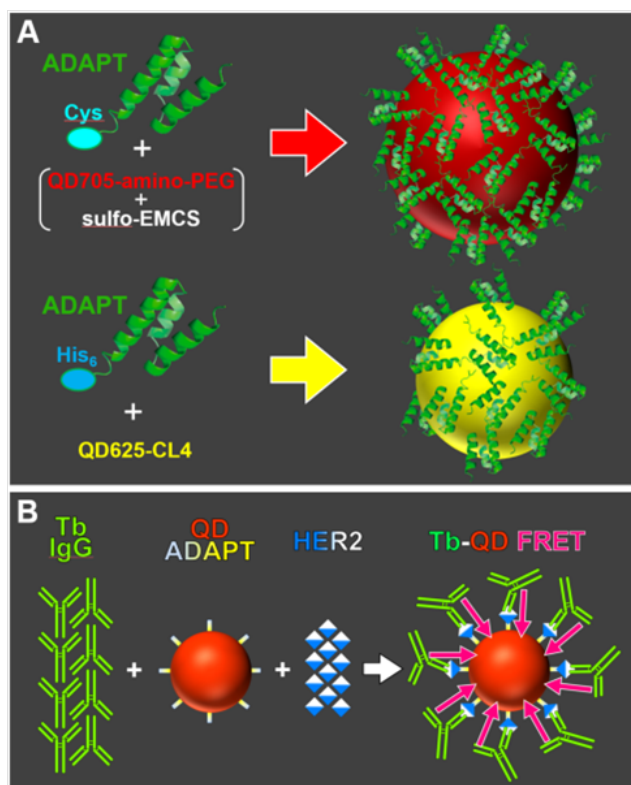


FIGURE 3.1: (A) QD705 was conjugated with ADAPT-Cys via sulfhydryl reaction by adding sulfo-EMCS to introduce maleimide to the amino-PEG QD705. QD625 was conjugated with ADAPT-His₆ via Zn-His₆ self-assembly. (B) Mixing of LTC-conjugated IgG (Pertuzumab), ADAPT-conjugated QDs, and soluble HER2 led to the formation of immunological sandwich complexes and a concomitant close proximity between LTC and QD, which, in turn, resulted in LTC-to-QD FRET for HER2 quantification.

Here, we show that a new class of very small (~ 6.5 kDa, $\sim 1.0 \times 1.5 \times 2.5$ nm³) albumin-binding domain-derived affinity proteins (ADAPTs) against HER2 [Lindbo et al., 2016, Nilvebrant et al., 2014], which have previously been used for *in vivo* radionuclide imaging of HER2 positive tumor xenografts [Garousi et al., 2017, Garousi et al., 2015, Lindbo et al., 2018], can be applied for advanced LTC-to-QD FRET immunoassays against HER2. Specifically engineered anti-HER2-ADAPTs with histidine tags (His₆) or single cysteines (Cys) were used for conjugation to two different QDs emitting at 625 nm and 705 nm, respectively. These ADAPT-QD conjugates are significantly smaller than QD-conjugates based on IgG, Fab', or single-domain antibodies. We demonstrate immediate applicability by the quantification of HER2 in serum-containing samples using time-gated LTC-to-QD FRET detection on the clinical bench-top immunoassay analyzer KRYPTOR. Limits of detection down to 40 pM (~ 8 ng/mL) were in a relevant clinical concentration range and outperformed previously tested assays with antibodies, antibody fragments, and nanobodies.

3.2 Materials and Methods

Recombinant human HER2 Fc chimera (#1129-ER-050) dimers (MW = 196 kDa) were purchased from R&D system. ADAPT variants against HER2 containing the histidine tags (ADAPT-His₆, MW = 6.95 kDa) and a cysteine (ADAPT-Cys, MW = 6.30 kDa) either at the N terminus or the C terminus were produced, purified, and characterized by KTH royal institute of technology (Sweden) [Garousi et al., 2017, Lindbo et al., 2016, Nilvebrant et al., 2014]. Pertuzumab antibody against HER2 was provided by Genentech/Roche Diagnostics GmbH, Penzberg (Germany). 705-nm emitting ITK QDs with amino-PEG (QD705) and 625 nm emitting organic Qdots (QD625) were purchased from Thermo Fisher. Lumi4-LTC complex functionalized with NHS were provided by Lumiphore Inc [Xu et al., 2011].

Trizma hydrochloride, phosphate buffered saline (1xPBS), hydrochloric acid (HCl), sodium hydroxide (NaOH), Tris(2-carboxyethyl) phosphine hydrochloride (TCEP), N,N-dimethylformamide (DMF), Sodium tetraborate decahydrate (Na₂B₄O₇·10H₂O), sodium bicarbonate (NaHCO₃), bovine serum albumin (BSA) and sulfo-EMCS crosslinker were purchased from Sigma-Aldrich. Sodium chloride (NaCl) was purchased from Duchefa. All chemicals were used as received. Newborn calf serum was provided by Thermo Fisher Scientific. High-quality Milli-Q water with a resistivity of 18.2 MΩ.cm was used for preparing solutions.

3.3 QD-antibody conjugation

Conjugation of ADAPTs-Cys to the QD705 was performed using sulfo-EMCS crosslinkers. To receive maleimide-reactive QD705 a >50000-fold molar excess of sulfo-EMCS was mixed with QD for 1 hour at 30 rpm using an ELMI Intelli-Mixer shaker at room temperature. Maleimide-active QD was purified using 100 kDa molecular weight cutoff (MWCO) Amicon spin column from Millipore (Billerica, MA, USA) by washing three times with 1xPBS buffer (pH 7.4) to remove excess crosslinker in a bench-top centrifuge at 4000 g for 3 minutes. Disulfide bonds of ADAPTs were reduced to sulfhydryls with 5 mM TCEP by mixing for 30 minutes at 30 rpm at room temperature without further purification. For final conjugation both solutions (43 μl of 158.9 μM ADAPT + 100 μl of 0.64 μM QD) were mixed and incubated for 6 hours at 30 rpm at room temperature in the dark. Unbounded ADAPTs were separated by 100 kDa MWCO Amicon spin column by washing four times with 100 mM sodium tetraborate buffer (pH 8.4). Purified conjugates were centrifuged at 4000 g and supernatant were taken and stored at 4 °C. QD concentrations were determined by absorbance measurements using molar absorptivity of $8.3 \times 10^6 \text{ M}^{-1} \text{ cm}^{-1}$ (at 405 nm) for QD705 as

provided by manufacturer. ADAPTs were quantified by absorbance measurement at 280 nm using an extinction coefficient $4\,470\text{ M}^{-1}\text{ cm}^{-1}$. The Zn-rich surface of QD625 were functionalized with CL4, a short zwitterionic compact ligand. For conjugation of ADAPTs-His₆ to the QD625 was performed in a molar ratio of 20:1 (ADAPT-His₆ per QD) and mixed for 30 minutes freshly prepared before FRET immunoassays. QD concentrations were determined by the absorbance measurement using a molar extinction coefficient of $9.9 \times 10^6\text{ M}^{-1}\text{ cm}^{-1}$ (at 405 nm) for QD625 as provided by manufacturer. Based on prior work that showed very rapid and stable metal-affinity driven self-assembly between proteins and QDs with an equilibrium constant of 1 nM (Sapsford et al., 2007), we assumed a 100% conjugation efficiency.

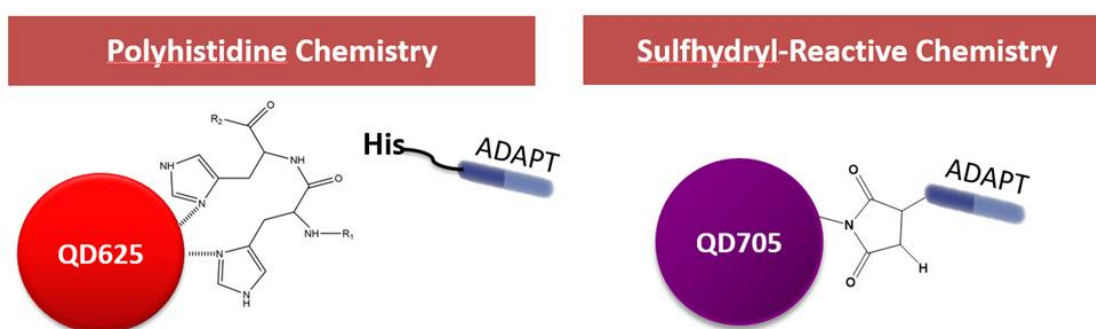


FIGURE 3.2: Schematic presentation of the two ADAPT-QD conjugation strategies

3.4 LTC-antibody conjugation

Lumi4-Tb-NHS (LTC) was dissolved to 8 mM in anhydrous DMF and mixed with the pertuzumab antibody in 100 mM carbonate buffer (pH 9.0). The mixture was incubated for 2 hours at 25 rpm at room temperature. For LTC-conjugate purification, the samples were washed four to six times with 100 mM TRIS-Cl (pH 7.4) using 50 kDa MWCO Amicon spin column in a benchtop centrifuge at 4000 g. LTC concentration was determined by absorbance measurements at 340 nm using a molar absorptivity of $26\,000\text{ M}^{-1}\text{ cm}^{-1}$ as provided by the manufacturer. Antibody was quantified by absorbance measurements at 280 nm using an extinction coefficient of $1.4\text{ g}^{-1}\text{Lcm}^{-1}$ ($207\,200\text{ M}^{-1}\text{cm}^{-1}$) as provided by the manufacturer. The conjugation ratios were determined by a linear combination of the respective absorbance values of LTC and antibody within the LTC-antibody conjugate absorbance.

3.5 Characterization of FRET pairs

Absorption spectra were acquired using a Lambda 35 UV/VIS spectrometer (PerkinElmer). Emission spectra of LTC and QD705 were recorded on a FluoTime 300 fluorescence spectrometer (PicoQuant) using a continuous-wave Xe lamp as excitation source. For QD625 emission spectra were recorded on a Xenius spectrophotometer (SAFAS). LTC-conjugates and QD-conjugates were measured in 100 mM TRIS-Cl buffer (pH7.4) and 100 mM sodium tetraborate buffer (pH 8.4) respectively. Förster distances (R_0) of the FRET pairs were $R_0(\text{LTC}/\text{QD625}) = 9.7$ nm and $R_0(\text{LTC}/\text{QD705}) = 10.4$ nm using the following equations:

$$R_0 = 0.02108(\kappa^2\Phi_D n^{-4}J)^{1/6}(\text{nm}) \quad (3.1)$$

with

$$J = \int \bar{I}_{LTC}\varepsilon_{QD}(\lambda)\lambda^4 d\lambda \quad (3.2)$$

and \bar{I}_D being the area-normalized PL spectrum of LTC (Figure 3.3), $\varepsilon_A(\lambda)$ being molar absorption of QD625 or QD705 (Figure 3.3), κ^2 being the donor-acceptor orientation factor ($\kappa^2=2/3$), Φ_D being the LTC³⁺ PL quantum yield ($\Phi_{LTC} = 0.67$), and n being the refractive index of the surrounding medium ($n = 1.4$).

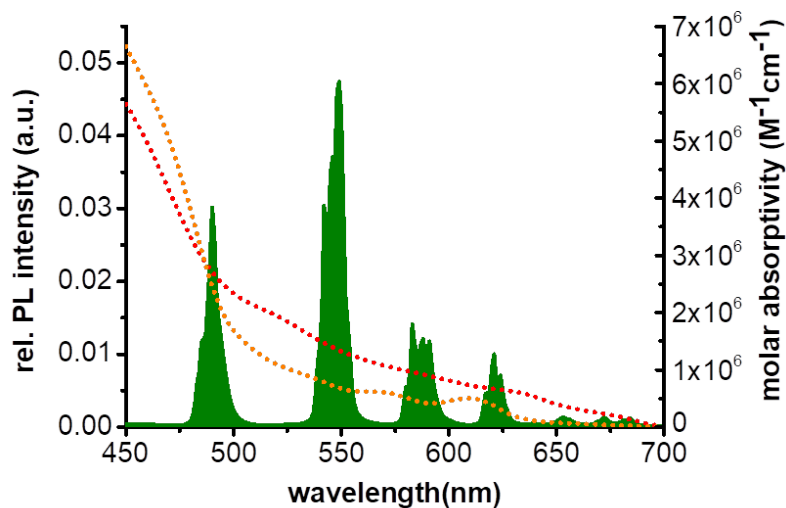


FIGURE 3.3: LTC PL spectrum (green, integral between 450 and 700nm normalized to unity) and QD625 (orange) and QD705 (red) molar absorptivity spectra used for calculating the overlap integral.

3.6 Homogeneous FRET immunoassays

The LTC-Pert and QD-ADAPT conjugates were each dissolved in 50 μL 10 mM TRIS/Cl buffer (pH 7.4) containing 0.5% bovine serum albumin (BSA, Sigma-Aldrich). 50 μL buffer or 10% serum samples with increasing concentration of HER2 were added to the 100 μL of a constant assay solution (50 μL of LTC-Pert conjugate with 3nM Pertuzumab and 50 μL of ADAPT-QD conjugate with 1.5 nM of QD). Optical bandpass filters (Delta and Semrock) for LTC donor and QD acceptor channel were 494 ± 20 nm for LTC and 640 ± 14 nm, and 716 ± 40 nm for QD625 and QD705, respectively. All FRET assays were measured in black 96-well microtiter plates with an optimal working volume of 150 μL . Each sample containing HER2 antigen sample was prepared three times, and the samples without HER2 were prepared 10 times. All samples were measured in triplicates. After sample preparation the microtiter plates were incubated for 180 minutes at 37 °C before measurements on KRYPTOR and EI fluorescence plate readers.

3.7 Results and discussion

3.7.1 Antibody conjugates

To produce ADAPT-QD conjugates, we applied two different approaches (experimental details in the previous section) that we previously used to prepare various QD conjugates with antibodies and nanobodies. The first conjugation strategy attached histidine tag containing ADAPTs by metal-affinity mediated selfassembly to the Zn-rich surface of commercial QDs emitting at 625 nm (Qdot625, Thermo Fisher) coated with compact zwitterionic ligands (CL4). This direct conjugation procedure allowed for a very close proximity between the QD surface and the anti-HER2-ADAPT. The second conjugation technique attached cysteine (Cys) terminated ADAPTs to the amino-PEG coated surfaces of QD705 (Qdot705, Thermo Fisher) via a sulfo-EMCS crosslinker. In contrast to the QD625-ADAPTs, the additional PEG coating on the QD705 placed the ADAPTs significantly further from the QD surface. The more than 1000-fold difference in extinction coefficients at 280 nm between the QDs (~ 30 to $40 \times 10^6 \text{ M}^{-1} \text{ cm}^{-1}$) and ADAPTs ($\sim 4.5 \times 10^3 \text{ M}^{-1} \text{ cm}^{-1}$) did not allow for a quantification of the exact number of ADAPTs per QD, but an excess of ADAPTs per QD could be confirmed by the FRET immunoassays. Taking into account a conjugation efficiency of close to unity for His₆-Zn selfassembly on QD surfaces, we assumed a circa 20:1 ADAPT/QD625 labeling ratio. The large excess of ADAPT-Cys per QD705 (107:1) during conjugation and the larger size compared to the QD625 let us estimate an even higher number of ADAPTs per QD705. As we did not aim at systematically studying the valency of

ADAPT molecules on the QD surfaces, an excess of ADAPTs per QD (without knowing the exact number) was an adequate condition for our FRET immunoassays.

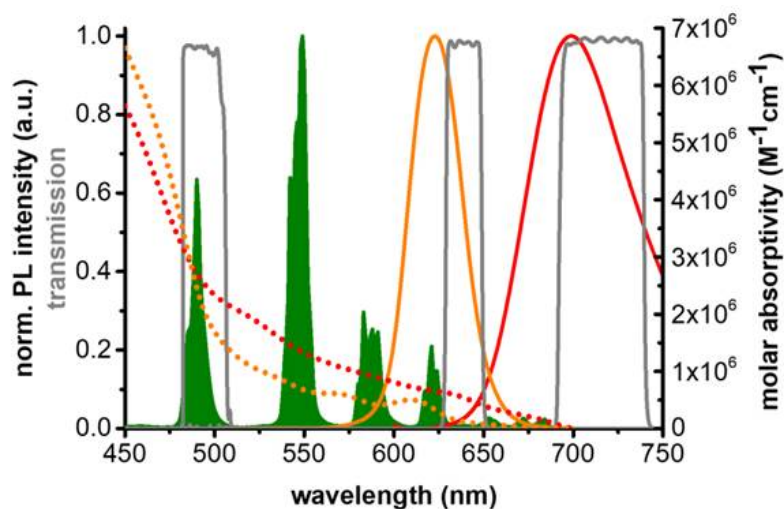


FIGURE 3.4: Absorption (dotted lines) and PL emission spectra of QD625 (orange) and QD705 (red), PL emission spectrum of LTC (green), and transmission spectra of the bandpass filters used for LTC and QD detection (gray). The absorption maximum of LTC is at circa 339 nm (not shown)

As the donor counterpart for the HER2 FRET immunoassays, we used a full length IgG anti-HER2 antibody (Pertuzumab) that was conjugated with Lumi4-LTC. Pertuzumab was used as LTC donor antibody since it recognizes a different epitope on HER2 than anti-HER2 ADAPT. Upon addition of HER2 containing samples to solutions of LTC and QD conjugates, both LTC-Pertuzumab and ADAPT-QD bound to HER2, which brought LTC and QD in close proximity and led to FRET from LTC to QD upon excitation of LTC. As shown in Figure 3.3, the photoluminescence (PL) spectrum of LTC and the absorption spectra of both QDs overlap significantly, which resulted in Förster distances of $R_0(\text{LTC}/\text{QD625}) = 9.7 \text{ nm}$ and $R_0(\text{LTC}/\text{QD705}) = 10.4 \text{ nm}$ (see the previous part for determination). The CL4 coated QD625 allowed for a direct attachment of ADAPT and therefore gave a shorter distance to the QD surface compared to QD705 and thereby also higher FRET efficiency. On the other hand, the larger Förster distance of the LTC-QD705 FRET pair provides a spectrally broader detection of FRET-sensitized QD PL with significantly lower background PL from LTC (Figure 3.4) This usually results in higher sensitivity compared to LTC-QD FRET pairs with shorter QD PL wavelengths.

3.7.2 HER2 sensor development

To evaluate the biosensing performance of the ADAPT-QD conjugates, we studied homogeneous LTC-to-QD FRET immunoassays against HER2 with both conjugates (ADAPT-His₆-QD625 and ADAPT-Cys-QD705). The ADAPT constructs had similar affinities to HER2 than pertuzumab (K_D (ADAPT-His₆) = 1.3 nM; K_D (ADAPT-Cys) = 4 nM; K_D (Pertuzumab) = 1.9 nM), suggesting their suitability for sensitive detection of HER2 in FRET-based assays. The immunoassays were performed both in TRIS buffer containing 0.5% BSA and in samples containing serum and assay calibration curves (Figure 3.7) were acquired on a KRYPTOR compact plus (Thermo Fisher) clinical immunofluorescence plate reader, which simultaneously detected the time-gated (0.1-0.9 ms) PL intensities of LTC donor (I_{LTC}) and QD acceptor (I_{QD}). The FRET ratio $F_R = I_{QD} / I_{LTC}$ was used to determine HER2 concentration. The PL decay curves were measured on a time-resolved fluorescence plate reader (Edinburgh Instruments). A test assay was performed to check the performance of conjugate, the PL decay curves of both QDs at the acceptor channels showed QD significant sensitization via FRET from LTC with increasing concentration of HER2 (Figure.3.5). Then we also tested the FRET assays in the sample containing 10%, 20% and 30% of serum (Figure 3.6) and 10% serum showed the best performance to perform statistical immunoassays.

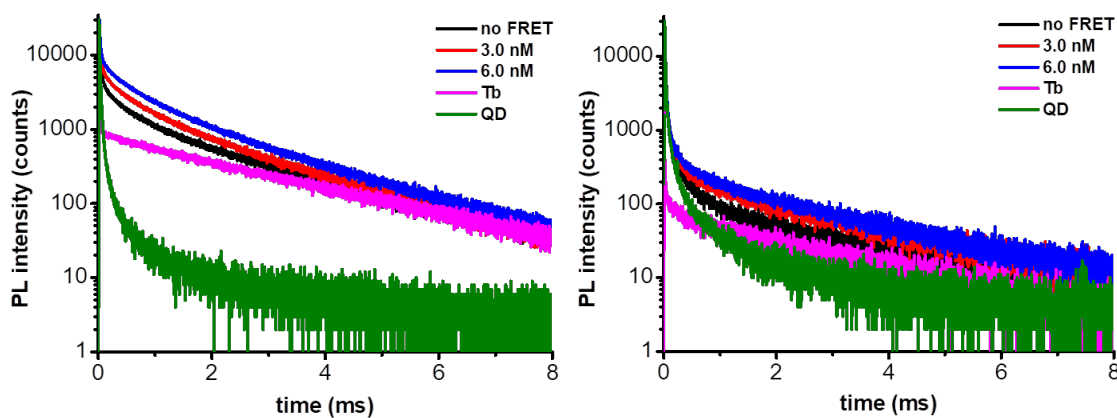


FIGURE 3.5: PL decay curves of FRET immunoassays showing sensitization of the QDs due to FRET. Left. QD625 in buffer Right. QD705 in buffer.

The statistical immunoassays were performed both in TRIS buffer containing 0.5% BSA and in samples containing 10% of serum (Figure 3.7 A). All assay curves showed a strong increase of FRET-ratio with increasing HER2 concentration from 0.075 nM to circa 3 nM, after which the curves start to level off and remains at an approximately constant FRET-ratio between 6 and 12 nM HER2. Such saturation is typical for homogeneous separation-free FRET immunoassays and is caused by the complete binding of one or both affinity binders (ADAPT or antibody) to the HER2 antigens. 50 μ L HER2 sample was added to a 100 μ L solution of 1.5 nM LTC-Pertuzumab and 0.75 nM

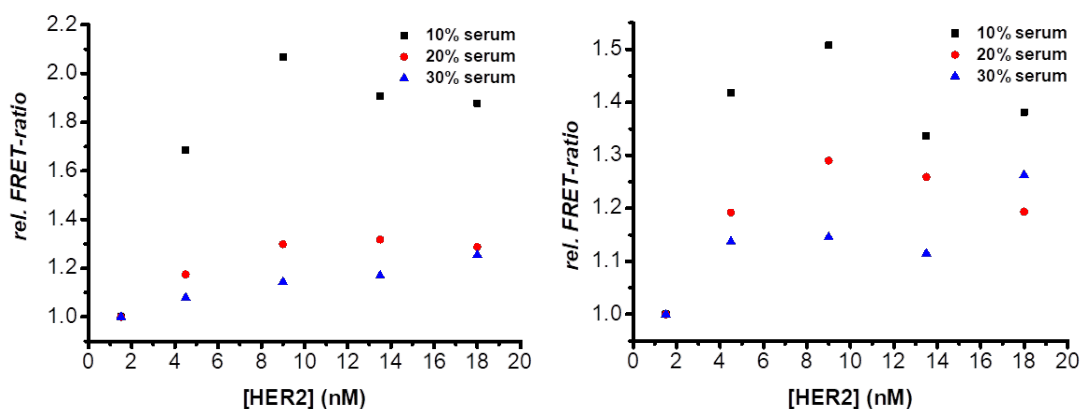


FIGURE 3.6: FRET immunoassay performance in the sample containing 10%, 20% and 30% of serum. Left. ADAPT-His₆-QD625 Right. ADAPT-Cys-QD705

ADAPT-QD (concentrations of Pertuzumab and QD, respectively). 3 nM HER2 corresponded to 1 nM in the measuring volume of 150 μ L, which showed that the saturation was caused by the LTC-Pertuzumab concentration (1 nM in 150 μ L). It also confirmed the excess of ADAPT per QD, because the QD concentration was only 0.5 nM in the 150 μ L assay volume.

Limits of detection (LODs) were determined using the slope of the linear increasing part from 0 to 0.6 nM concentration range (Figure 3.7 B). HER2 detection limits of 39 ± 9 pM (7.8 ± 1.8 ng/mL) in TRIS buffer containing 0.5% BSA and 46 ± 11 pM (9.7 ± 2.2 ng/mL) in samples containing 10% serum using ADAPT-His₆-QD625 conjugates and 260 ± 20 pM (51 ± 4 ng/mL) in TRIS buffer containing 0.5% BSA and 300 ± 30 pM (59 ± 6 ng/mL) in samples containing 10% serum using ADAPT-Cys-QD705 conjugates were in a clinically relevant concentration range of soluble HER2 for breast cancer diagnostics (7 to 3000 ng/mL) and in the case of the ADAPT-His₆-QD625 conjugates even below the clinical cutoff level of 15 ng/mL HER2. The ADAPT-His₆-QD625 also outperformed QD conjugates based on nanobodies, Fab' fragments, and IgG antibodies that were previously used in similar LTC-to-QD FRET immunoassays against HER2.

Although both types of ADAPT-QD assays could distinguish HER2 concentrations in clinically relevant concentrations for breast cancer diagnostics the slopes (sensitivity), the FRET-ratio saturation values of the calibration curves (Figure 3.7A) and the limits of detection (LODs, Figure 3.7B and Table 3.1) clearly show the superior performance of the ADAPT-His₆-QD625. While 10% of serum inside the sample led to slightly higher LODs, they were still below the clinical cutoff level recommended for soluble HER2 (15 ng/mL). The LTC-Pertuzumab-HER2-ADAPT-QD625 FRET assay also outperformed other affinity binder combinations including nanobodies, Fab' fragments, and IgGs (Table 3.1). Only a combination of V_HH nanobodies that were attached to QDs by a terminal cysteine (oriented conjugation) showed similar LODs (Table 3.1).

However, these assays were not performed in serum containing samples. By optimization of the ADAPT-His₆-QD conjugation, e.g., by a detailed investigation of different numbers of ADAPT per QD, or multiplexing with different QDs further improvement of the performance and versatility of the ADAPT-QD conjugates for biosensing should in principle be possible.

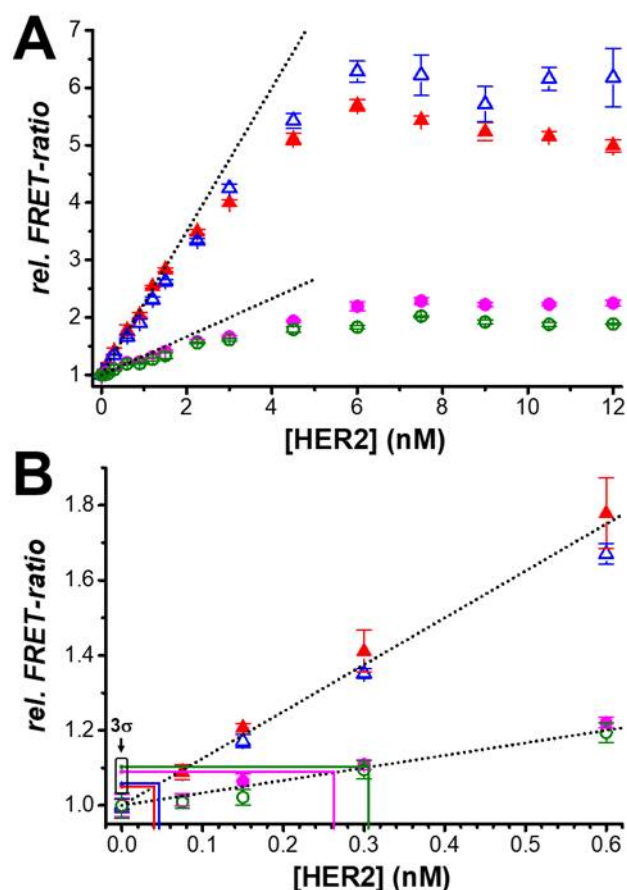


FIGURE 3.7: (A) Calibration curves of LTC-to-QD FRET immunoassay against HER2 using ADAPT-His₆-QD625 (triangles; blue and red) and ADAPT-Cys-QD705 (circles; magenta and green). Concentrations correspond to HER2 in a 50 μ L sample of TRIS buffer with 0.5% BSA (filled symbols; red and magenta) or TRIS buffer with 0.5% BSA and 10% of serum (open symbols; blue and green). Concentration in a pure serum sample (5 μ L within the 50 μ L sample) would be 10-fold higher. Dotted lines present the linearly increasing part of the calibration curves at low concentrations. (B) Lower concentration range of the calibration curves from A, which was used to estimate the LODs (3σ above zero). Error bars correspond to standard deviations (σ) with $n = 3$ for all HER2 containing samples and $n = 30$ for the zero-control (no HER2).

In conclusion, we have demonstrated that small engineered affinity proteins, namely ADAPTs with an approximate molecular weight of 6.5 kDa, can be efficiently self-assembled to 625 nm emitting QDs via histidine tags and that these ADAPT-QD conjugates can be applied for highly sensitive FRET immunoassays against HER2. This new

This work		LOD (nM)	LOD (ng/mL)
LTC-IgG / ADAPT-His ₆ -QD625		0.039±0.009	7.8±1.8
LTC-IgG / ADAPT-His ₆ -QD625 10% serum		0.046±0.011	9.7±2.2
LTC-IgG / ADAPT-Cys-QD705		0.26±0.02	51±4
LTC-IgG / ADAPT-Cys-QD705 10% serum		0.30±0.03	59±6
LODs in previous work (only buffer)			
LTC-IgG / IgG-QD650	0.09 nM	LTC-V _H H-QD650 (O)	0.05 nM
LTC-IgG / IgG-QD605	0.15 nM	LTC-V _H H-QD650 (R)	0.08 nM
LTC-IgG / Fab'-QD650	0.11 nM	LTC-V _H H-QD605 (O)	0.04 nM
LTC-IgG / Fab'-QD605	0.12 nM	LTC-V _H H-QD605 (R)	0.12 nM

TABLE 3.1: Limits of detection (LODs) for HER2 in 50 μ L samples using combinations of different engineered and natural affinity proteins (ADAPT, V_HH nanobodies, Fab' fragments, and IgG). The abbreviation O means oriented labeling, R means random labeling [Qiu et al., 2016]

nanobiomaterial combination showed an improved FRET assay performance compared to QD conjugates with antibodies, antibody fragments, or nanobodies and may become a useful tool for many other optical biosensing and clinical applications in both spectroscopy and imaging. We also showed an alternative conjugation approach of cysteine-terminated ADAPTs through labeling to amino-PEG coated QDs via sulfo-EMCS crosslinkers. Although the detection limits were higher for this strategy, our results demonstrated the versatility of ADAPT conjugation to nanoparticles and the application to another QD color (emitting at 705 nm) showed the general possibility of color multiplexing. Our future efforts will be directed to further sensitivity optimization, the implementation of ADAPT-QD conjugates for different biomarkers, and the multiplexed detection of different analytes from single samples by different QD acceptors. Our proof-of-concept study showed the benefits of combining small affinity binders with QDs for improved FRET biosensing. With the development of ADAPTs against various biomarkers, this nanoaffinity concept can become a very versatile and practical tool for FRET biosensing and other bioanalytical and clinical applications.

Chapter 4

Nanobodies for EGFR detection

4.1 Introduction

Among all the smaller scaffold proteins, single-domain antibodies (sdAb) have emerged as powerful antigen binders next to conventional antibodies and other classes of synthetic binding proteins. This type of antibody is so-called heavy chain antibodies (HcAbs, ~ 95 kDa) naturally produced from animals camelidae, nurse shark and ratfish. To date, they are established functional biomolecules that can be easily selected, produced, and manipulated using standard molecular biology techniques. The variable domain alone of HcAbs (V_{HH}) was proven to have sufficient antigen binding properties with the approximate molecular weight of 15 kDa ($\sim 4 \times 2.5 \times 3 \text{ nm}^3$), which are used in many different antibody based applications [Marco, 2011, Schumacher et al., 2018]. Thus, it can be considered as the smallest naturally derived antigen-binding fragment and the term "nanobodies" was particularly referred to their small size in nanometer range. Despite the many advantages of nanobodies, only few have been applied in the non-competitive FRET immunoassays [Wegner et al., 2014, Qiu et al., 2016]. In our group, Qiu et al. has demonstrated a systematic study of type, orientation, specificity, nonspecific binding, and cross-reactivity of different sizes of antibodies (IgG, $F(\text{ab})_2$, Fab' , V_{HH}). Such as using small antibody fragments or nanobodies as an alternative to conventional antibody, have been proposed for improving the FRET efficiency of donor and acceptor in no-wash immunosensors of protein. In this work, I focus on the three different QD conjugation strategies to study the influence of performance in the detection limit. These nanobodies bind to nonoverlapping epitopes of the human epidermal growth factor receptor 1 (EGFR), noted as EgA1 and EgB4, with three different separation tags (histidine, biotin, cysteine) and without tag (no tag) for several conjugating strategies with FRET pairs. EgA1-no tag and EgA1- His_6 were used for LTC labeling. EgB4- His_6 , EgB4-biotin and EgB4-Cys were used for QD labeling. We first studied the performance of non-competitive immunoassays using two conjugation strategies, biotin-streptavidin recognition and crosslinker covalent attachment.

Biotin-streptavidin showed better sensitivity than the other due to the closer proximity of donor and acceptor. The competitive immunoassays were performed based on metal-polyhistidine coordination. We found out that using only one single type of EGFR-specific sdAb, the EGFR limit of detection can be obtained in sub-nanomolar range, which may be of interest for bioassay applications.

4.2 Materials and Methods

Recombinant human EGFR Fc chimera (#344-ER-050) dimers (MW = 190 KDa) were purchased from R&D system. Nanobodies against EGFR containing biotin, histidine, a single cysteine and without tag (EgA1-no tag, EgA1-His₆, EgB4-His₆-biotin, EgB4-His₆, EgB4-EPEA-Cys, EgB4-no tag) were produced from our collaborator (Utrecht University, Netherlands). 705 nm emitting Qdots ITK Streptavidin Conjugate Kit (sAvQD705), 705 nm emitting ITK Qdots with amino-PEG (QD705) and 625 nm emitting organic Qdots (QD625) were purchased from Thermo Fisher. Lumi4-LTC complexes functionalized with NHS were provided by Lumiphore Inc.

Trizma hydrochloride, phosphate buffered saline (1xPBS), hydrochloric acid (HCl), sodium hydroxide (NaOH), Tris(2-carboxyethyl) phosphine hydrochloride (TCEP), N,N-dimethylformamide (DMF), Sodium tetraborate decahydrate (Na₂B₄O₇·10H₂O), sodium bicarbonate (NaHCO₃), bovine serum albumin (BSA) and sulfo-EMCS crosslinker were purchased from Sigma-Aldrich. Sodium chloride (NaCl) was purchased from Duchefa. All chemicals were used as received. Newborn calf serum was provided by Thermo Fisher Scientific. High-quality Milli-Q water with a resistivity of 18.2 MΩ.cm was used for preparing solutions.

4.3 QD-antibody conjugation

Crosslinker covalent attachment

Conjugation of EgB4-Cys to the QD705 was performed using sulfo-EMCS crosslinkers. To receive maleimide-reactive QD705, a >50000-fold molar excess of sulfo-EMCS was mixed with QD705 for 1 h at 30 rpm at room temperature. Maleimide-activated QDs were purified using 100 kDa MWCO spin column from Millipore (Billerica, MA, USA) by washing three times with 1xPBS buffer (pH 7.4) to remove excess crosslinker. Disulfide bonds of EgB4 were reduced to sulfhydryls with 5 mM TCEP by mixing for 30 minutes at 30 rpm at room temperature without further purification. For final conjugation, both solutions (43 μl of 130.9 μM EgB4 + 100 μl of 0.64 μM QD) were mixed and incubated for 6 h at 30 rpm at room temperature in the dark. Unbound EgB4 were separated by 100 kDa MWCO spin column by washing four times with 100 mM

sodium tetraborate buffer (pH 8.4). Purified conjugates were centrifuged at 4000 g and supernatants were stored at 4°C. QD concentrations were determined by absorbance measurements using a molar extinction coefficient of $8.3 \times 10^6 \text{ M}^{-1} \text{ cm}^{-1}$ (at 405 nm) for QD705 as provided by the manufacturer. EgB4 were quantified by absorbance measurement at 280 nm using an extinction coefficient of $35,535 \text{ M}^{-1} \text{ cm}^{-1}$. The labeling ratios were determined by linear combination of the respective absorbance values of QD705 and EgB4 within the EgB4-Cys-QD705 conjugates.

Metal-polyhistidine self-assembly

The Zn-rich surfaces of QD625 were functionalized with CL4 compact ligands as described previously. Conjugation of EgB4-His₆ to the QD625 was performed in a molar ratio of 20:1 (EgB4-His₆ per QD) and mixed for 30 minutes. The conjugates were freshly prepared before FRET immunoassays. QD concentrations were determined by absorbance measurements using a molar extinction coefficient of $9.9 \times 10^6 \text{ M}^{-1} \text{ cm}^{-1}$ (at 405 nm) for QD625 as provided by the manufacturer. EgB4 was quantified by absorbance measurement at 280 nm using an extinction coefficient of $37,515 \text{ M}^{-1} \text{ cm}^{-1}$.

Biotin-streptavidin self-assembly

For EgB4-His₆-biotin to the sAvQD705 conjugation was performed in a molar ratio of 20:1 (EgB4-biotin per QD) and mixed for 30 minutes. The conjugates were freshly prepared before FRET immunoassays. QD concentrations were determined by absorbance measurements using a molar extinction coefficient of $8.3 \times 10^6 \text{ M}^{-1}$ (at 405 nm) for sAvQD705 as provided by the manufacturer. EgB4 was quantified by absorbance measurement at 280 nm using an extinction coefficient of $38,055 \text{ M}^{-1} \text{ cm}^{-1}$.

4.4 LTC-antibody conjugation

Lumi4-Tb-NHS (LTC) was dissolved to 8 mM in anhydrous DMF and mixed (the reaction ratio of LTC/V_HH = 3) with the nanobodies (EgA1-no tag, EgA1-His₆) in 100 mM carbonate buffer (pH 9.0). The mixture was incubated for 2 hours at 25 rpm at room temperature. For LTC-conjugate purification, the samples were washed four to six times with 100 mM TRIS-Cl (pH 7.4) using 3 kDa MWCO Amicon spin column at 4000 g. LTC concentration was determined by absorbance measurements at 340 nm using a molar absorptivity of $26,000 \text{ M}^{-1} \text{ cm}^{-1}$ as provided by the manufacturer. Nanobodies were quantified by absorbance measurements at 280 nm using an extinction coefficient of $34,505 \text{ M}^{-1} \text{ cm}^{-1}$ (EgA1-no tag) and $38,878 \text{ M}^{-1} \text{ cm}^{-1}$ (EgA1-His₆). The conjugation ratios were determined by a linear combination of the respective absorbance values of LTC and nanobodies within the LTC-nanobody conjugate absorbance.

Conjugation ratios	
LTC conjugate	LTC/V _H H
LTC-EgA1-no tag	2
LTC-EgA1-His ₆	2
QD conjugate	V _H H/QD
EgB4-His ₆ -QD625	20
EgB4-Cys-QD705	28
EgB4-biotin-sAvQD705	20

TABLE 4.1: Labeling ratio of the conjugate in this study.

4.5 Characterization of FRET pairs

LTC-conjugates and QD-conjugates were measured in 100 mM TRIS-Cl buffer (pH7.4) and 100 mM sodium tetraborate buffer (pH 8.4) respectively. Förster distances (R_0) of the FRET pairs were $R_0(\text{LTC}/\text{QD625}) = 9.7$ nm, $R_0(\text{LTC}/\text{QD705}) = 10.4$ nm and $R_0(\text{LTC}/\text{sAvQD705}) = 10.6$ nm.

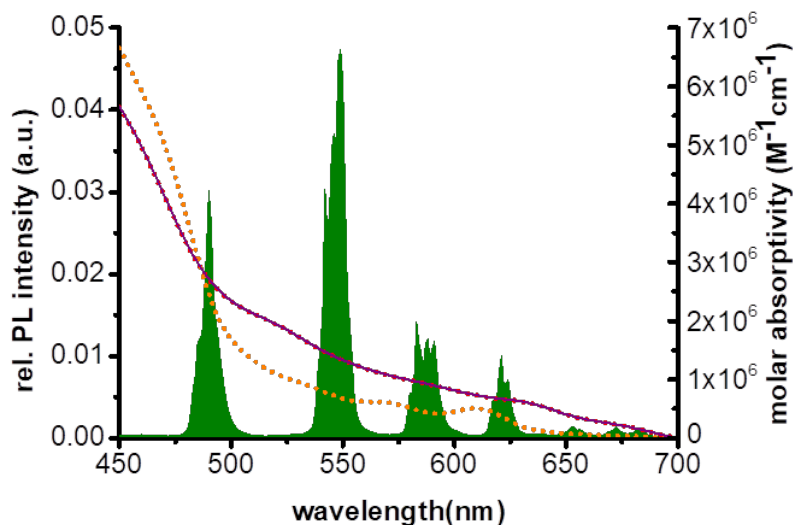


FIGURE 4.1: LTC PL spectrum (green, integral between 450 and 700nm normalized to unity) and QD625 (orange dot), QD705 (red dot) and sAvQD705 (purple line) molar absorptivity spectra used for calculating the overlap integral.

4.6 Homogeneous FRET immunoassay

The LTC-EgA1 and QD-EgB4 conjugates were each dissolved in 50 μL 10 mM TRIS/Cl buffer (pH 7.4) containing 0.5% bovine serum albumin (BSA, Sigma-Aldrich). Homogeneous FRET immunoassay calibration curves against EGFR, where the overall measuring volume of 150 μL contained 100 μL of a constant assay solution (50 μL of LTC-EgA1 with 6 nM EgA1 and 50 μL of EgB4-QD conjugate with 1.5 nM QD705 or 3 nM sAvQD705). Competitive displacement FRET immunoassay calibration curves against EGFR, where the overall measuring volume of 150 μL contained 100 μL of a constant assay solution (50 μL of LTC-EgA1 with 6 nM EgA1 and 50 μL of EgB4-QD conjugate or QD only with 1.5 nM QD625). Optical bandpass filters (Delta and Semrock) for LTC donor and QD acceptor channel were 494 ± 20 nm for LTC and 640 ± 14 nm, and 716 ± 40 nm for QD625 and QD705, respectively. All FRET assays were measured in black 96-well microtiter plates with an optimal working volume of 150 μL . Each sample containing EGFR antigen sample was prepared three times, and the samples without EGFR were prepared 10 times. All samples were measured in triplicates. After sample preparation the microtiter plates were incubated for 180 minutes at 37 $^{\circ}\text{C}$ before measurements on KRYPTOR compact plus (Thermo Fisher) and EI fluorescence plate readers.

4.7 Results and discussion

To evaluate the biosensing performance of the LTC-EgA1-no tag and EgB4-QD conjugate, we studied homogeneous LTC-to-QD FRET immunoassays against EGFR with both conjugation strategies, which are streptavidin-biotin interaction and crosslinker covalent attachment. The immunoassays assay calibration curves (Figure 4.2) were acquired on a KRYPTOR with simultaneous time-gated (0.1-0.9 ms) PL intensities of LTC donor (I_{LTC}) and QD acceptor (I_{QD}). The FRET ratio $F_{\text{R}} = I_{\text{QD}} / I_{\text{LTC}}$ was used to determine EGFR concentration. The PL decay curves were measured on a time-resolved fluorescence plate reader (Edinburgh Instruments). All assays showed an increase of FRET-ratio with increasing EGFR concentration (Figure 4.2). For EgB4-Cys-QD705 the curve showed a saturation at 2 nM EGFR, after which the curves start to level off. For EgB4-biotin-sAvQD705 the FRET ratio increased until *ca.* 6 nM EGFR. The sensitivity of an immunoassay is determined by the slope of its calibration curve. The trend of the curves from Figure 4.2 showed higher sensitivity of EgB4-biotin-sAvQD705 than EgB4-Cys-QD705. EGFR detection limits were 0.48 nM using EgB4-Cys-QD705 conjugate and 0.19 nM using EgB4-biotin-sAv705 in TRIS buffer containing 0.5 % BSA. It can be explained by the average donor-acceptor distance (r_{DA}). The 705 nm emitting

Qdots were coated with streptavidin (sAvQD705, diameter 18.5 nm), where the streptavidin covalently attached to the inner amphiphilic coating without a PEG linker, and therefore provided more freedom for the co-assembly of EgB4-biotin to the QD. The 705 nm emitting Qdots were functionalized with amine-derivatized PEG (QD705, diameter 20.5 nm), which prevented non-specific interactions but also increased the size of QDs. After labeling with crosslinker Sulfo-EMCS (spacer arm length 9.4 Å), the distance of donor and acceptor is even farther away. Thus, the detection limit of EgB4-biotin-sAvQD705 conjugate is lower than EgB4-Cys-QD705 conjugate.

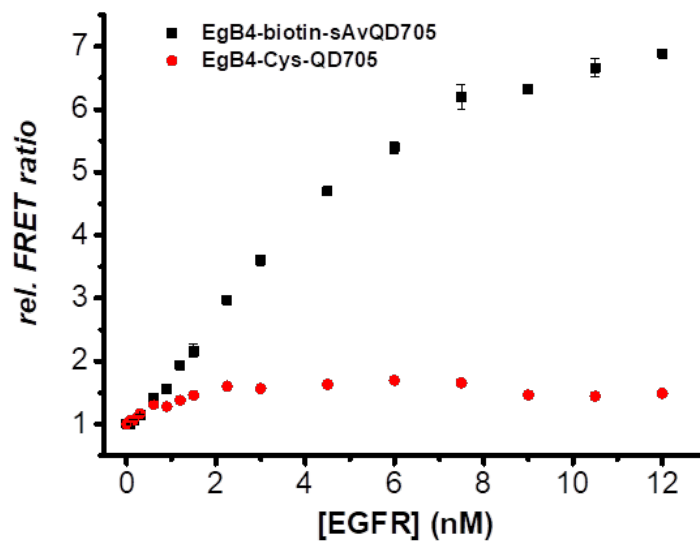


FIGURE 4.2: Homogeneous FRET immunoassay calibration curves against EGFR using LTC-EgA1-no tag/EgB4-biotin-sAvQD705 (black) and LTC-EgA1-no tag/EgB4-Cys-QD705 (red).

To demonstrate the proof of concept, decay time fitting in the two channels were performed to estimate the donor to acceptor distance (r) and FRET efficiency (η_{FRET}). In PL FRET decay curves, for EgB4-biotin-sAvQD705 revealed obvious FRET sensitization in QD channel but for EgB4-Cys-QD705 only a little FRET sensitization. In the LTC channel, both systems showed not significant quenched LTC signals which can be attributed to long distance between donor and acceptor (Figure 4.3). In this case, only EgB4-biotin-sAvQD705 in acceptor channel is applicable for decay time fitting. The pure LTC-EgA1 conjugate exhibit a double-exponential decay resulting in a short τ_{D1} and a long dominant decay time τ_{D2} with amplitude fraction α_{D1} and α_{D2} in the donor channel. Because all decay curves contain a certain amount of unquenched LTC decay, this pure LTC decay time (τ_{D2}) was fixed in the fit functions. FRET-sensitized acceptor decays were fitted with a quadruple-exponential function. Due to sample autofluorescence, direct excitation QD at short time and contribution of LTC donor crosstalk in the QD acceptor channel in the long time range, a time delay starting around 10 μ s to 50 μ s after the excitation pulse was introduced to fit the decay curves. Such fits can be used

when the fitted lifetime is much longer than IRF (instrument response function) and also called tail fitting, which means fit from the different start time t_0 for improving fit quality. All decay curves were fitted using a multiexponential PL intensity decay function:

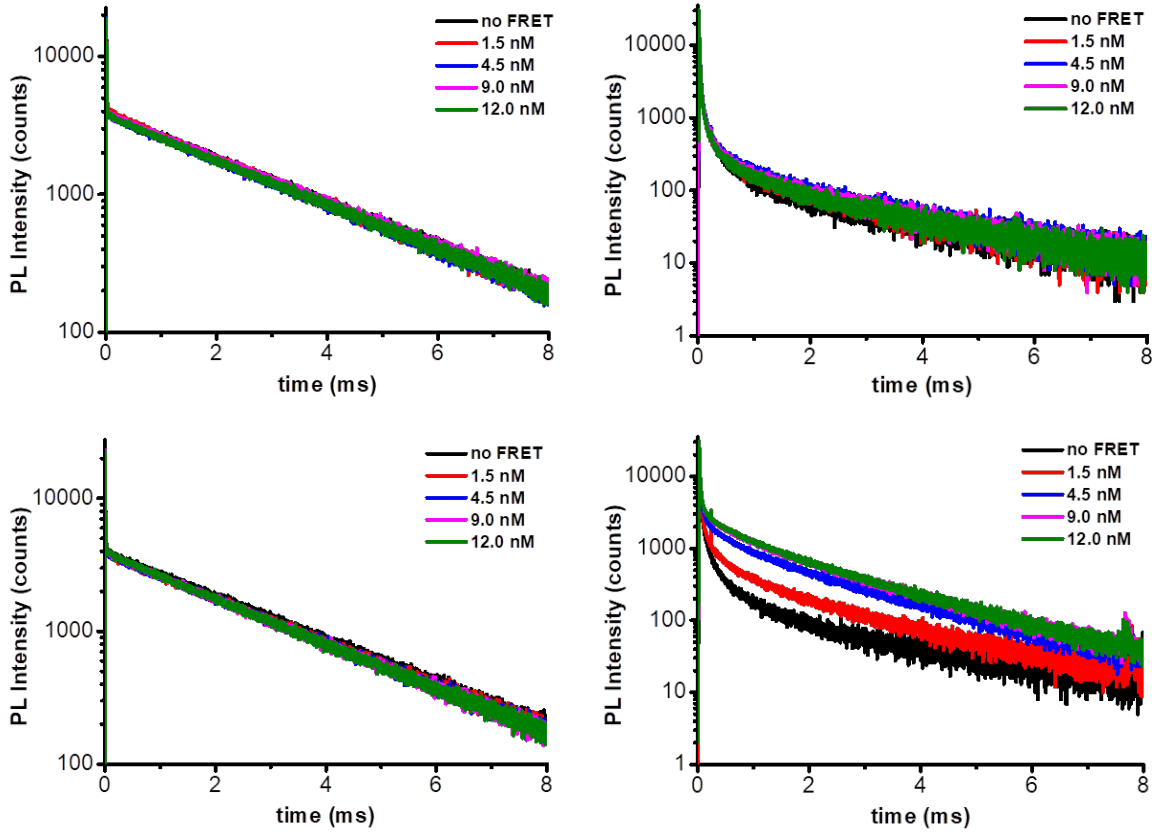


FIGURE 4.3: Representative PL decay curves. Top Left: Donor channel of LTC-EgA1-no tag/EgB4-Cys-QD705. Top Right: Acceptor channel of LTC-EgA1-no tag/EgB4-Cys-QD705. Down Left: Donor channel of LTC-EgA1-no tag/EgB4-biotin-sAvQD705. Down Right: Acceptor channel of LTC-EgA1-no tag/EgB4-biotin-sAvQD705.

$$I = \sum_i A_i \exp\left(-\frac{t}{\tau_i}\right) = A \sum_i \alpha_i \exp\left(-\frac{t}{\tau_i}\right) \quad (4.1)$$

where A is the total amplitude and α_i are the amplitude fractions ($\sum \alpha_i = 1$). All PL lifetime averaging for the dynamic FRET quenching process was performed using amplitude weighted average lifetime. The function after correction of start time :

$$I = A_{i-FIT} \cdot \exp\left(-\frac{t-t_0}{\tau}\right) = A_i \cdot \exp\left(-\frac{t}{\tau}\right) \rightarrow A_i = A_{i-FIT} \cdot \exp\left(\frac{t_0}{\tau}\right) \quad (4.2)$$

Taking the multiexponential PL decay function from Equation 4.1 leads to the following amplitude-averaged decay time:

$$\langle \tau \rangle = \frac{\sum A_i \tau_i}{\sum A_i} = \sum \alpha_i \tau_i \quad (4.3)$$

The FRET-sensitized QD acceptors were fitted with a quadruple-exponential function with amplitude fractions α_{AD*1} , α_{AD*2} , α_{AD*3} and α_{AD*0} and the decay times τ_{AD1} , τ_{AD2} , τ_{AD3} and τ_{AD0} . The fourth decay time has to be fixed to the free and unquenched pure donor $\tau_{AD0} = \tau_{D2}$ due to the crosstalk of LTC in the acceptor channel. The shorter component of pure LTC also has to be corrected using the correction factor z_A although it is almost negligible.

$$z_A = \alpha_{D1} \left(\frac{\alpha_{AD*0}}{\alpha_{D2}} \right) \quad (4.4)$$

To calculate the average FRET-sensitized decay times only the first three components are taken into account. Therefore, the fraction α_{ADi} ($i=1-3$) needs to be corrected by the FRET rate $k_{FRETi} = \tau_{ADi}^{-1} - \langle \tau_D \rangle^{-1}$ by combining Equation 2.7 and 2.8 which considers the dependence of the excitation of the acceptors on the different FRET efficiencies for the different distances, the corrected amplitude fractions is:

$$\alpha_{ADi} = \frac{\alpha_{AD*i}/k_{FRETi}}{(\alpha_{AD*1}/k_{FRET1}) + (\alpha_{AD*2}/k_{FRET2}) + (\alpha_{AD*3}/k_{FRET3})} \quad (4.5)$$

The corrected averaged FRET sensitized decay time is calculated by:

$$\langle \tau_{AD} \rangle = \frac{\alpha_{AD1}\tau_{AD1} + \alpha_{AD2}\tau_{AD2} + \alpha_{AD3}\tau_{AD3} - z_A\tau_{D1}}{1 - z_A} \quad (4.6)$$

and the average FRET-efficiency is

$$\langle \eta_{FRET} \rangle = 1 - \frac{\langle \tau_{AD} \rangle}{\langle \tau_D \rangle} \quad (4.7)$$

The distance of donor and acceptor $\langle r_{AD} \rangle$ can be calculated by:

$$\langle r_{AD} \rangle = R_0 \left\{ \frac{\langle \tau_{AD} \rangle}{\langle \tau_D \rangle - \langle \tau_{AD} \rangle} \right\}^{1/6} \quad (4.8)$$

Using the above correction for taking account the unquenched LTC donor ($\tau_D = 2.61$ ms), the acceptor channel fitting for EgB4-biotin-sAvQD705 resulted in $\langle \tau_{AD} \rangle = 1.00$ ms, FRET-efficiency of 62 % with an estimated donor and acceptor distance of 9.8 nm (a detail decay time fitting data were shown in Appendix). The result is reasonable when we consider the ~ 9.3 nm radius of sAvQD705 with two V_{HH} and EGFR

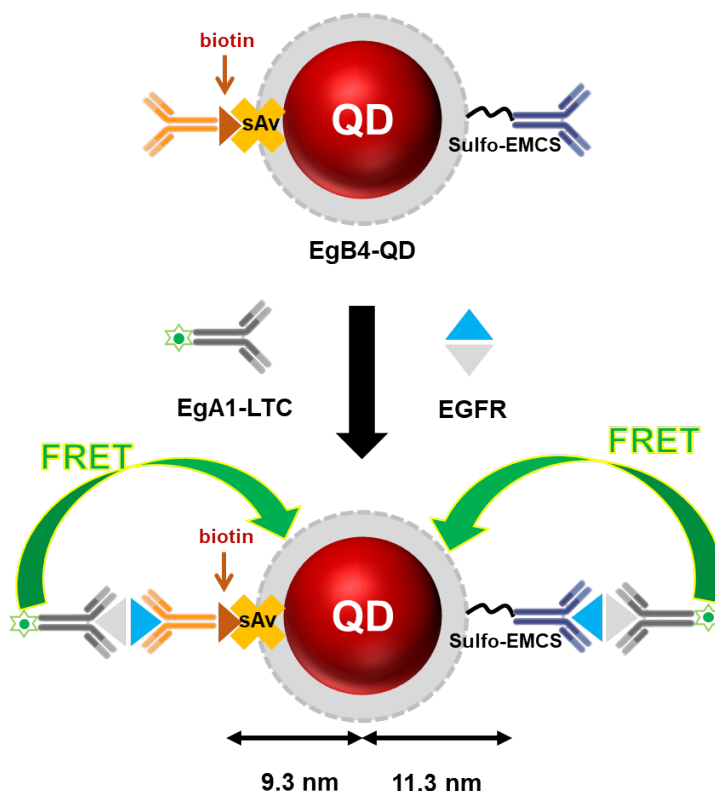


FIGURE 4.4: Schematic of the LTC-QD FRET based on two QD conjugation strategies (Left. streptavidin-biotin interaction. Right. crosslinker covalent attachment.), which composed of 705 nm emitting QD (red), PEG (light gray with dotted line), EgB4-biotin (orange), EgB4-Cys (purple) and LTC-EgA1-no tag (green-gray).

dimer. Due to the four binding site of sAv, EgB4-biotin may bind to the different orientation on the QD surface, it may cause the overall average distance between donor and acceptor closer than expected. Although we could not fit the PL decay curve of EgB4-Cys-QD705, we believe that the ~ 10.3 nm radius of sAvQD705 plus crosslinker Sulfo-EMCS (94 Å) is ~ 11.3 nm (Figure 4.4), which result in longer r_{DA} and decrease QD sensitization therefore assay sensitivity.

Interestingly, another FRET pair of LTC-His₆-EgA1/EgB4-His₆-QD625 showed slightly reduced FRET with increasing concentration of EGFR in both channels, most probably due to the LTC-His₆-EgA1 self-assembled on the QD625 by metal polyhistidine coordination. The EgB4 had similar affinities to EGFR than metal polyhistidine self-assembly (K_D (EgB4-His₆-EGFR) = 0.56 nM; K_D (Zn-His₆) = ~ 1 nM), suggesting that the EgA1-His₆-LTC self-assembled on the QDs and the addition of EGFR replace some of LTC-conjugates resulting in a competitive displacement immunoassay. The QD channel (Figure 4.5 Top Left) showed that the quenching of LTC-His₆-EgA1 by EGFR (Figure 4.5 Top Right) also reduces the QD PL intensity (FRET from LTC). However, the displacement of LTC-His₆-EgA1 from the QD surface to the EgB4-His₆ (binding with EGFR)

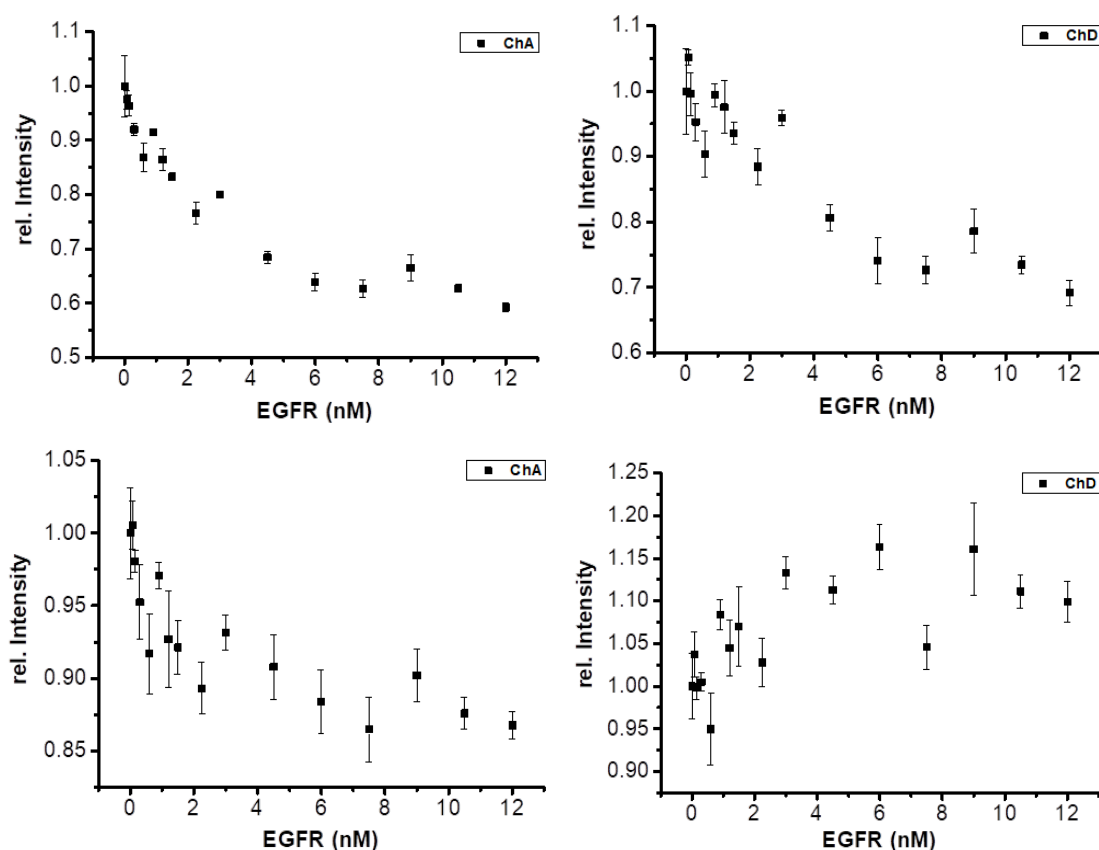


FIGURE 4.5: Time-gated PL intensity (integration from 0.1-0.9 ms). Top Left: Acceptor channel of LTC-EgA1-His₆/EgB4-His₆-QD625. Top Right: Donor channel of LTC-EgA1-His₆/EgB4-His₆-QD625. Down Left: Acceptor channel of LTC-EgA1-His₆/QD625. Down Right: Donor channel of LTC-EgA1-His₆/QD625.

leads to additional QD quenching. In the donor channel (Figure 4.5 Top Right), LTC-His₆-EgA1 is quenched by EGFR almost linearly down to 70%. The QD quenching (Figure 4.5 Top Left) is stronger down to 60 % and the curved form shows a cooperative quenching of the LTC donor by EGFR and reduced FRET due to displacement of LTC-His₆-EgA1 from the QD surface. The concept was confirmed by another experiment, in which the QD FRET acceptor was not conjugated with V_HH. The LTC-His₆-EgA1/QD625 FRET pair showed a "pure" displacement assay (Figure 4.6), LTC-His₆-EgA1 is displaced from QD surface by EGFR, which leads to LTC intensity increase and QD intensity decrease due to reduced FRET (Figure 4.5 Down.). The FRET ratio in both systems are correlates with the EGFR concentration (Figure 4.7), which are capable to detect EGFR at sub-nanomolar concentrations. EGFR detection limits are 0.39 nM using EgB4-His₆-QD625 conjugate and 0.27 nM using QD625 in TRIS buffer containing 0.5 % BSA. Further control experiments need to be done with LTC-EgA1-no tag to study the detailed mechanism of EgB4-His₆-QD625 FRET pair. Although the error bar is quite large compared to the non-competitive immunoassay, this competitive

immunoassay is highly interesting because it requires only one single type of EGFR-specific sdAb, which strongly reduces the antibody development and reagent costs. The performance of assay can be also improved by optimizing assay components (e.g. buffer, probe concentration, incubation time) to accomplish optimized results.

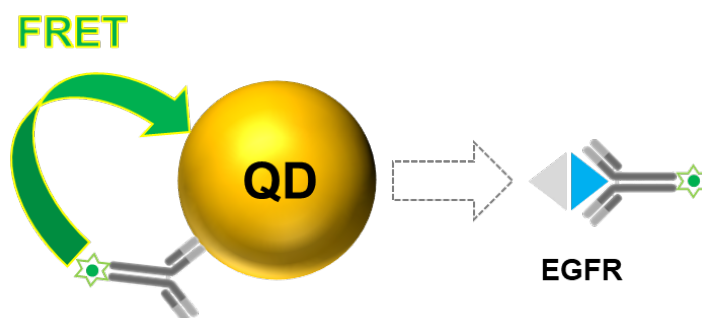


FIGURE 4.6: Schematic of the LTC-to-QD FRET immunoassay against EGFR using QD625 alone. Dotted gray arrow denotes LTC-His₆-EgA1 is displaced from QD surface by EGFR.

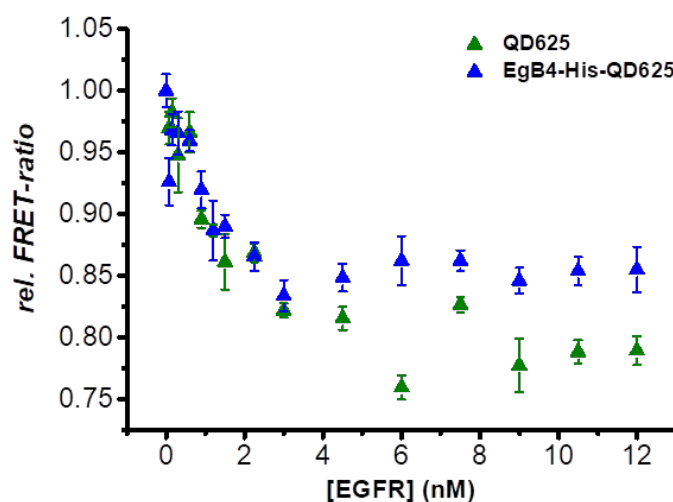


FIGURE 4.7: Calibration curves of LTC-to-QD FRET immunoassay against EGFR using EgB4-His₆-QD625 (blue) and QD625 conjugate (green).

FRET pairs	LOD (nM)	LOD (ng/mL)
LTC-EgA1-no tag/EgB4-Cys-QD705	0.48	91.3
LTC-EgA1-no tag/EgB4-biotin-sAvQD705	0.19	36.1
LTC-EgA1-His ₆ /EgB4-His ₆ -QD625	0.39	74.2
LTC-EgA1-His ₆ /QD625	0.27	51.4

TABLE 4.2: Limit of detection in this study.

Chapter 5

Summary and outlook

The application of LTC-to-QD FRET homogeneous immunoassay using small affinity proteins has demonstrated the versatility for the detection of cancer biomarkers. All FRET immunoassays were based on the time-resolved (TR) measurements in combination with the unique properties of the LTC (e.g. long luminescent decay time, well-separated emission bands) and QD (e.g. multiplexing capability, large surfaces, high extinction coefficient) for binding with different kinds of biomolecules, making TR-FRET advantageous in high-throughput assays.

Small affinity proteins (e.g., ADAPT, sdAb) allow for multivalent QD conjugation, which can increase QD FRET sensitization. ADAPTs-His₆-QD625 conjugate were shown to outperform any other types of antibodies for HER2 immunoassays. SdAbs were used to develop non-competitive immunoassays by using biotin-streptavidin recognition and crosslinker covalent attachment. When comparing these two systems, the smaller distance of donor and acceptor showed better limit of detection. Thus, to increase the FRET may be obtained by using smaller size of QDs or improving QD chemistry: choosing one blue-shifted QDs (QD605 or QD655) or using maleimide-functionalized QDs without crosslinker (e.g. eBioscience/Affymetrix QD), and metal-histidine coordination (QD625) for more compact sandwich immunoassays. For competitive homogeneous immunoassays, we showed that they require only one antibody (instead of two), which can be considered as an useful alternative strategy for EGFR detection.

Both strategies for QD-based homogeneous FRET-immunoassays with small affinity proteins provide a large potential for advanced in vitro diagnostics and other FRET-based biosensing applications, e.g., for imaging analysis of epidermal growth factor receptor dimerization, new approaches for the cellular delivery in live-cell immunolabeling and antigen manipulation.

Chapter 6

Appendix

LTC-Pert-HER2-ADAPT-His₆-QD625 decay curves

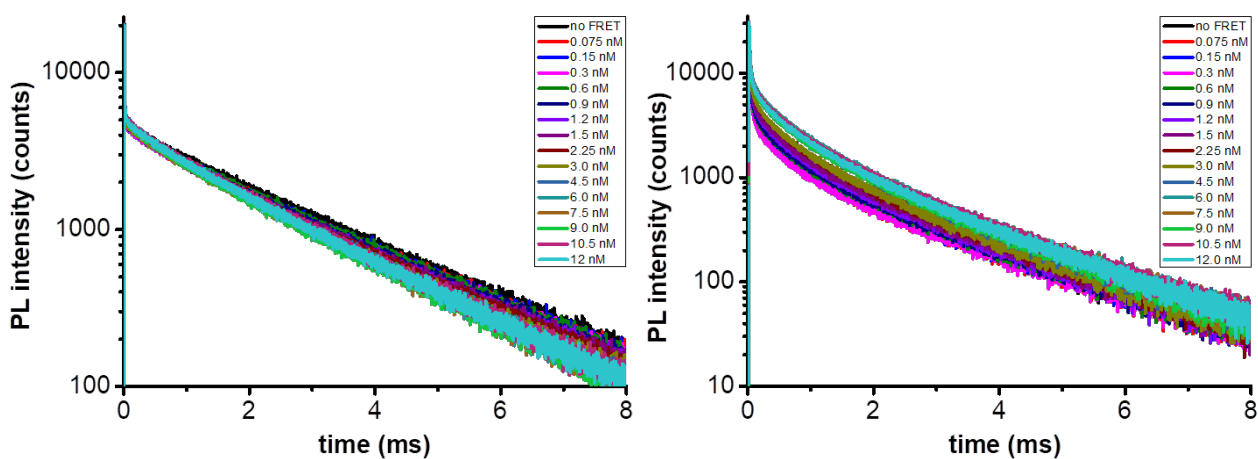


FIGURE 6.1: PL decay curves of LTC ($494\pm 10\text{nm}$, left), and QD625 ($640\pm 7\text{nm}$, right) of LTC-Pert-HER2-ADAPT-His₆-QD625 immunoassays (in buffer)

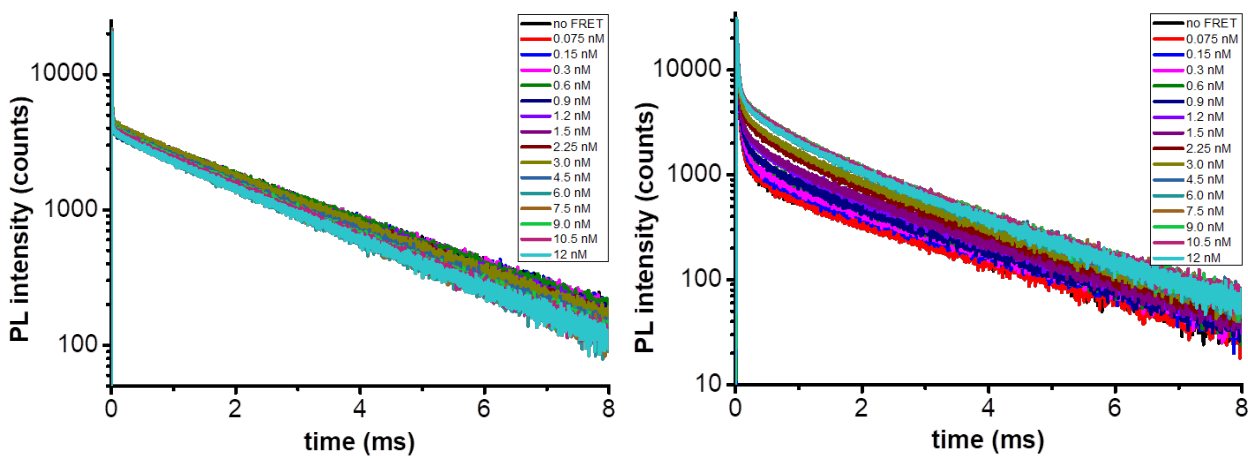


FIGURE 6.2: PL decay curves of LTC ($494\pm 10\text{nm}$, left), and QD625 ($640\pm 7\text{nm}$, right) of LTC-Pert-HER2-ADAPT-His₆-QD625 immunoassays (in serum)

LTC-Pert-HER2-ADAPT-Cys-QD705 decay curves

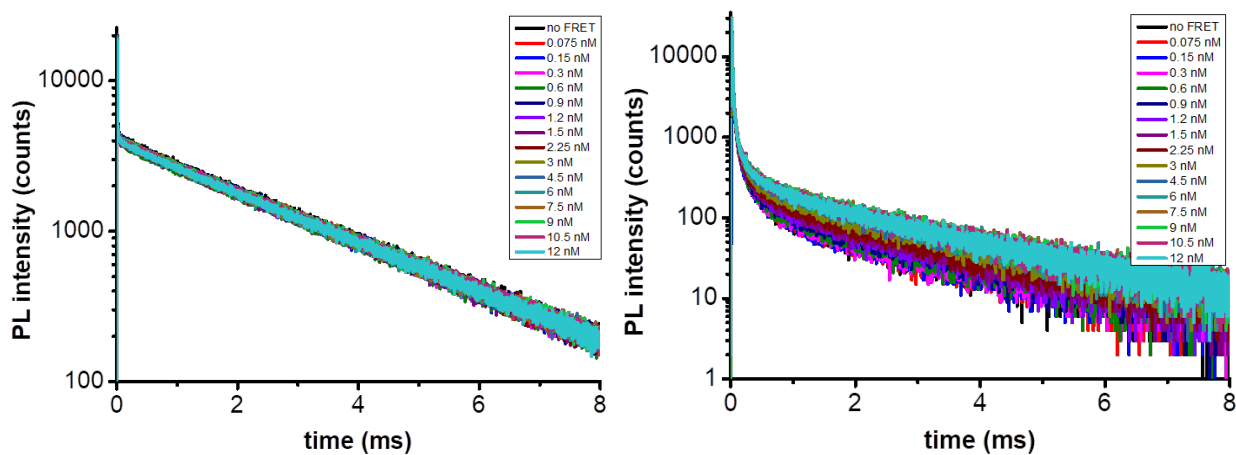


FIGURE 6.3: PL decay curves of LTC ($494\pm 10\text{nm}$, left), and QD705 ($716\pm 20\text{nm}$, right) of LTC-Pert-HER2-ADAPT-Cys-QD705 immunoassays (in buffer)

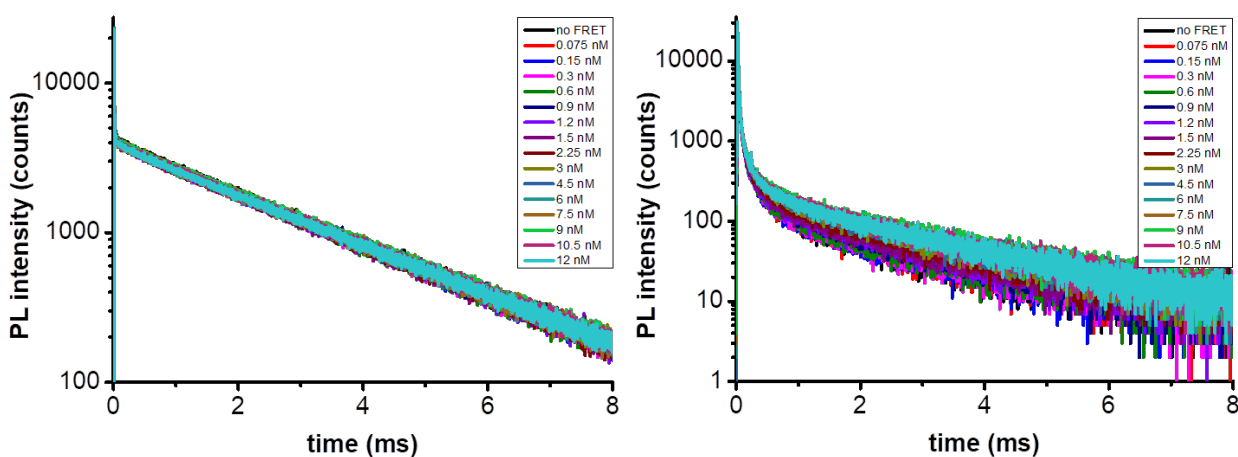


FIGURE 6.4: PL decay curves of LTC ($494\pm 10\text{nm}$, left), and QD705 ($716\pm 20\text{nm}$, right) of LTC-Pert-HER2-ADAPT-Cys-QD705 immunoassays (in serum)

LTC-EgA1-no tag-EGFR-EgB4-Cys-QD705

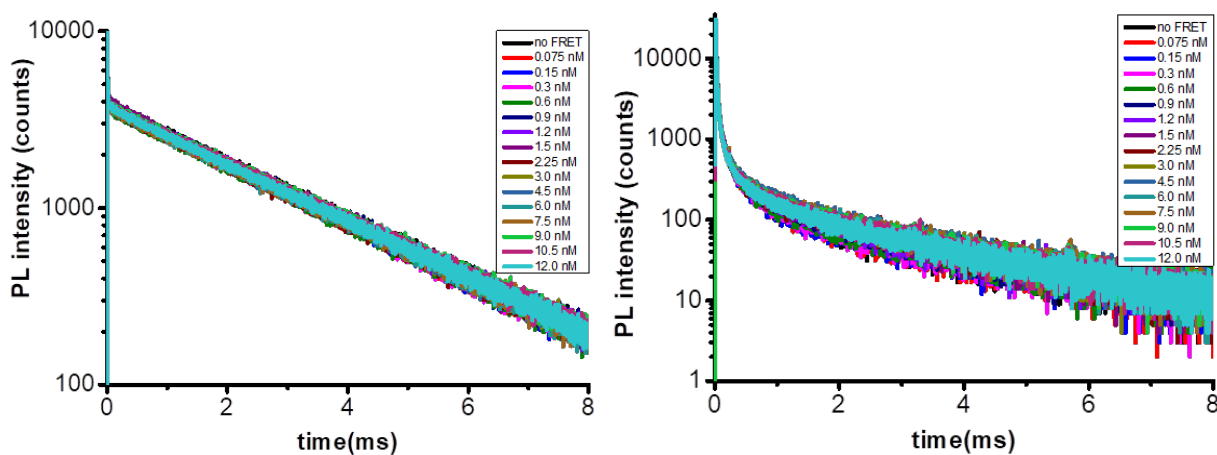


FIGURE 6.5: PL decay curves of LTC ($494\pm 10\text{nm}$, left), and QD705 ($716\pm 20\text{nm}$, right) of LTC-EgA1-no tag-EGFR-EgB4-Cys-QD705

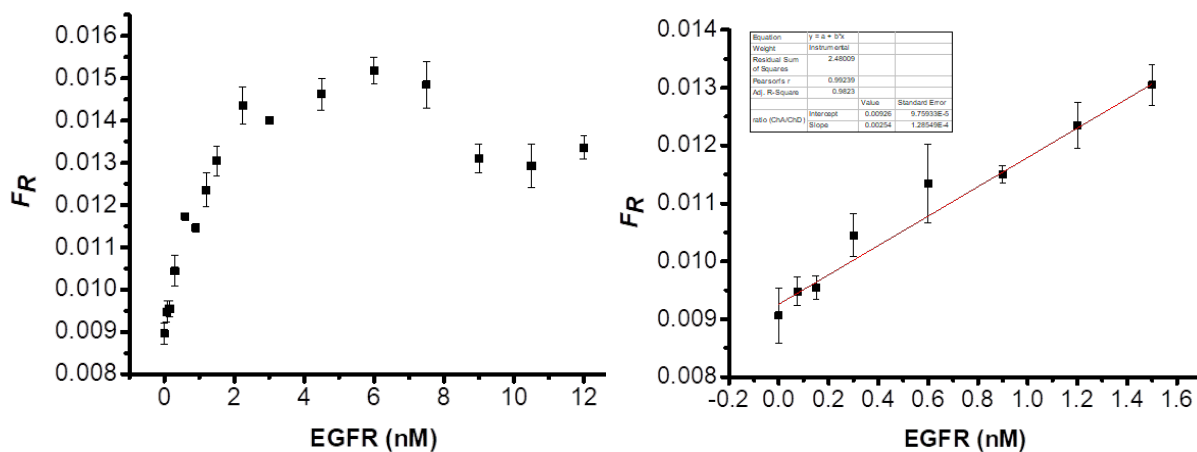


FIGURE 6.6: Left. Calibration curve of LTC-to-QD immunoassay against EGFR using LTC-EgA1-no tag-EGFR-EgB4-Cys-QD705. Right. Lower concentration range was used to estimate LOD.

LTC-EgA1-no tag-EGFR-EgB4-biotin-sAvQD705

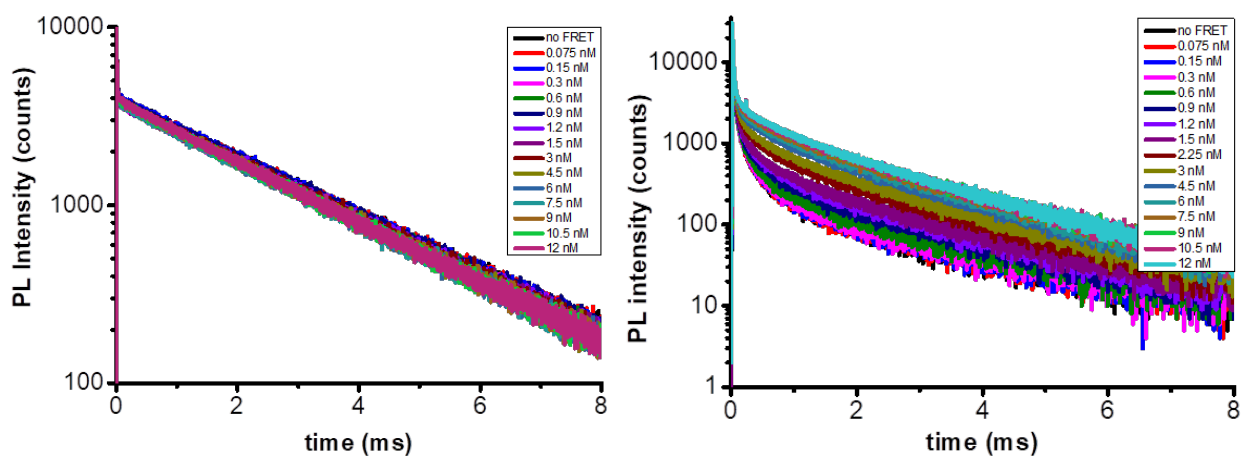


FIGURE 6.7: PL decay curves of LTC ($494\pm 10\text{nm}$, left), and QD705 ($716\pm 20\text{nm}$, right) of LTC-EgA1-no tag-EGFR-EgB4-biotin-sAvQD705

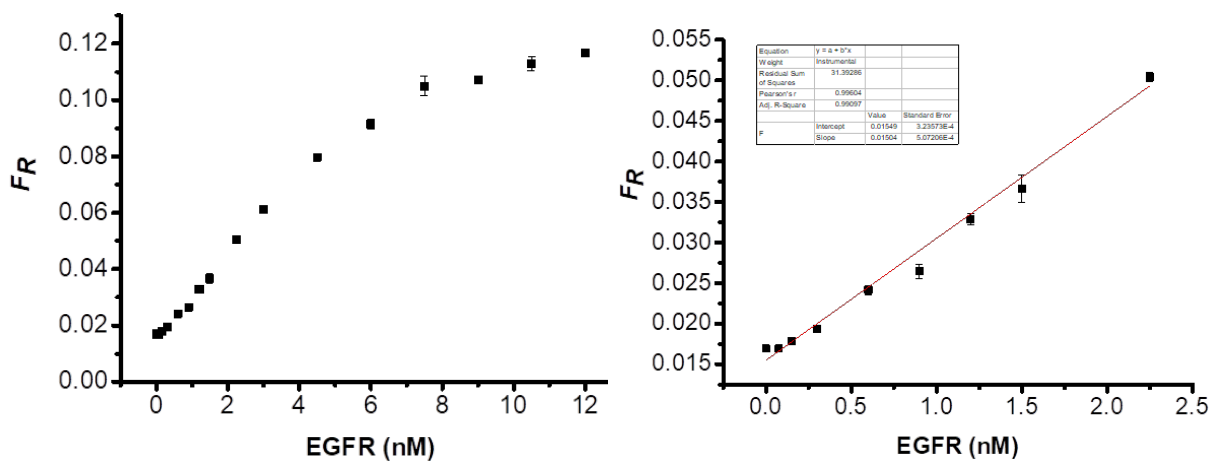


FIGURE 6.8: Left. Calibration curve of LTC-to-QD immunoassay against EGFR using LTC-EgA1-no tag-EGFR-EgB4-biotin-sAvQD705. Right. Lower concentration range was used to estimate LOD.

LTC-EgA1-His₆-EGFR-EgB4-His₆-QD625

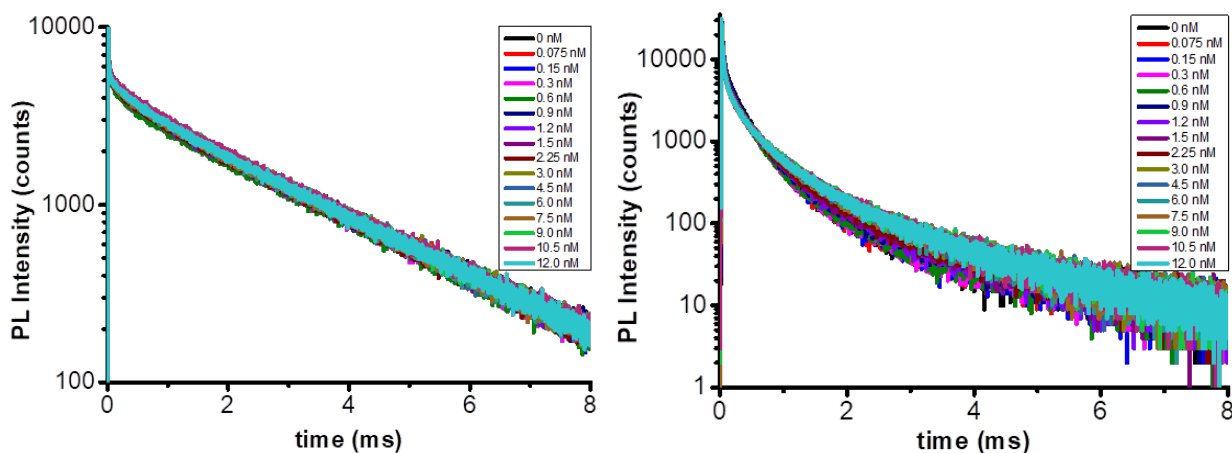


FIGURE 6.9: PL decay curves of LTC ($494\pm 10\text{nm}$, left), and QD625 ($640\pm 7\text{nm}$, right) of LTC-EgA1-His₆-EGFR-EgB4-His₆-QD625

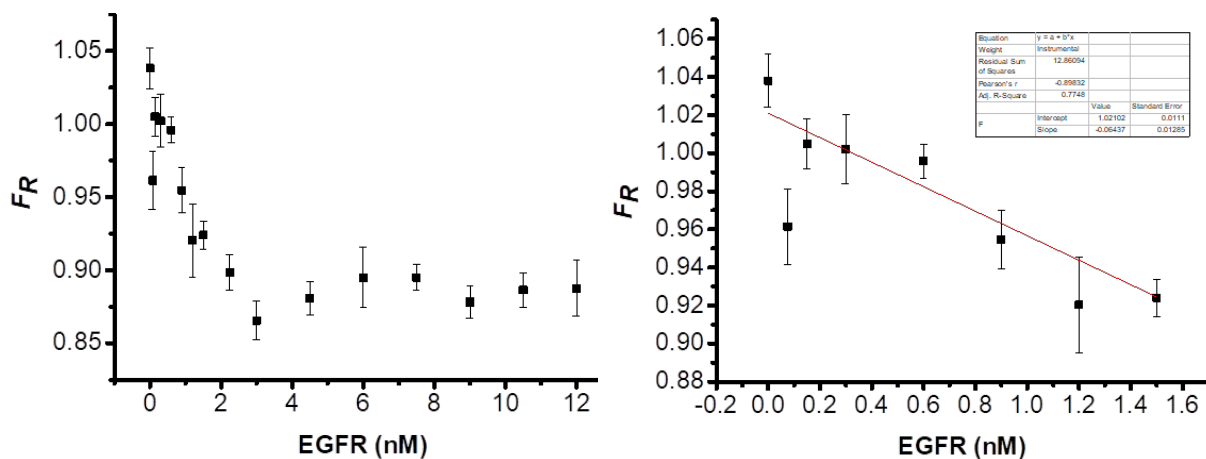


FIGURE 6.10: Left. Calibration curve of LTC-to-QD immunoassay against EGFR using LTC-EgA1-His₆-EGFR-EgB4-His₆-QD625. Right. Lower concentration range was used to estimate LOD.

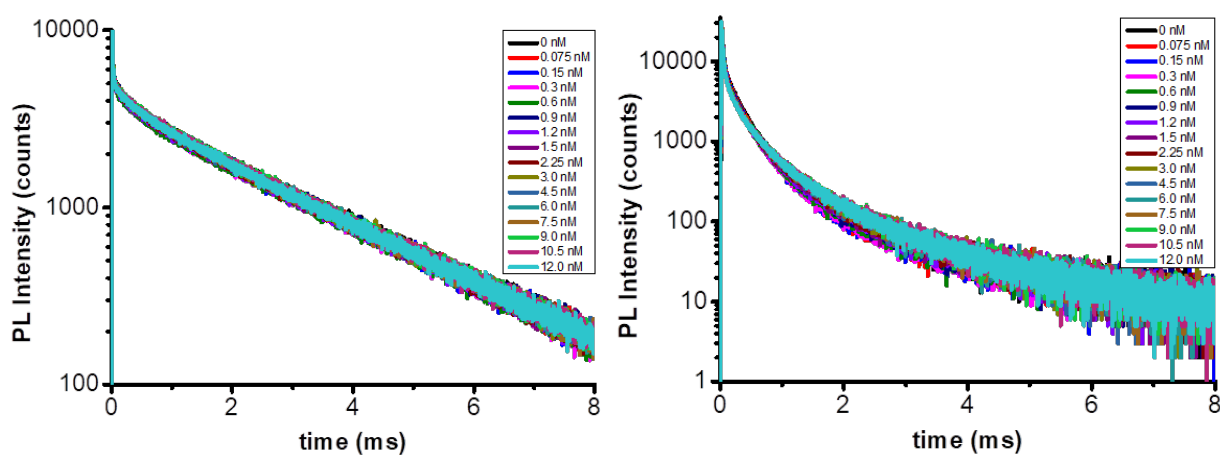
LTC-EgA1-His₆-EGFR-QD625

FIGURE 6.11: PL decay curves of LTC ($494\pm 10\text{nm}$, left), and QD625 ($640\pm 7\text{nm}$, right) of LTC-EgA1-His₆-EGFR-QD625

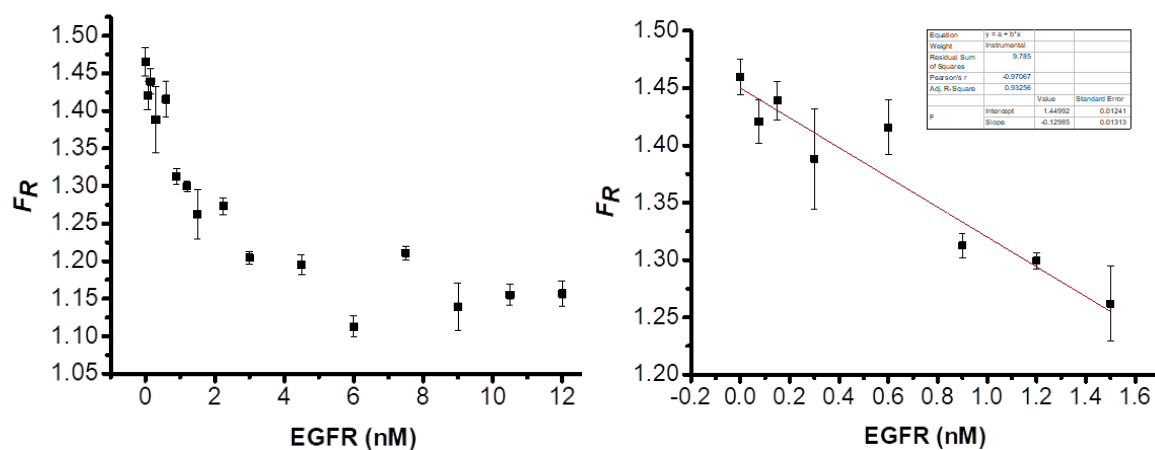


FIGURE 6.12: Left. Calibration curve of LTC-to-QD immunoassay against EGFR using LTC-EgA1-His₆-EGFR-EgB4-QD625. Right. Lower concentration range was used to estimate LOD.

Decay time fitting result for Tb-EgA1-EGFR-EgB4-biot-sAvQD705 (all decay time in μs)

Acceptor Channel $R_0 = 10.6 \text{ nm}$ Fitted from 0.05 to 5 ms (fixed Tb background decay time)

#	AG (nM)
1	1.5
2	3.0
3	4.5
4	6.0
5	9.0
6	12.0
average 3-6	
distance r	

τ_2	$\eta_{\text{FRET}2}$	A_2	α_{AD^*2}	$k_{\text{FRET}2}$	$\alpha_{\text{AD}2}$
140	0.95	2055	0.70	0.00676	0.34
160	0.94	1944	0.58	0.00587	0.20
220	0.92	1507	0.46	0.00416	0.14
200	0.92	1593	0.44	0.00462	0.12
210	0.92	1627	0.40	0.00438	0.11
230	0.91	1554	0.39	0.00396	0.11
215	0.92				0.121
7.1	7.1				12%
fraction: 12%					

6.8% **10.2%**

29.8%

τ_3	$\eta_{\text{FRET}3}$	A_3	α_{AD^*3}	$k_{\text{FRET}3}$	$\alpha_{\text{AD}3}$
730	0.72	593	0.20	0.00099	0.66
910	0.65	936	0.28	0.00072	0.80
1100	0.58	1141	0.35	0.00053	0.86
1100	0.58	1329	0.37	0.00053	0.88
1100	0.58	1607	0.40	0.00053	0.89
1100	0.58	1644	0.41	0.00053	0.89
1100	0.58				0.879
10.0	10.1				88%
fraction: 88%					

5.8% **10.7%**

fixed

#	AG (nM)
1	1.5
2	3.0
3	4.5
4	6.0
5	9.0
6	12.0
average 3-6	
distance r	

τ_0	A_0	α_{AD^*0}
2700	307	0.341
2700	483	0.340
2700	594	0.342
2700	666	0.186
2700	789	0.196
2700	776	0.195
2700		
2700		
>> R_0		

$\langle\tau\rangle$	$z(A)$	$\langle\tau_{\text{DA}}\rangle$	$\langle\eta_{\text{FRET}}\rangle$
1160	0.0128	537	0.80
1260	0.0128	766	0.71
1410	0.0129	985	0.62
1000	0.0070	998	0.62
1050	0.0074	1010	0.61
1070	0.0073	1009	0.61
		1001	0.62
		9.8	9.8

7.9% **10.7%**

Bibliography

- Afsari, Hamid Samareh et al. (2016). "Time-gated FRET nanoassemblies for rapid and sensitive intra-and extracellular fluorescence imaging". *Science advances* 2.6, e1600265.
- Algar, W Russ, Melissa Massey, and Ulrich J Krull (2013). "Semiconductor quantum dots and FRET". *FRET-Förster Resonance Energy Transfer: From Theory to Applications*, pp. 475–605.
- Algar, W Russ et al. (2011a). "Semiconductor quantum dots in bioanalysis: crossing the valley of death". *Analytical chemistry* 83.23, pp. 8826–8837.
- Algar, W Russ et al. (2011b). "The controlled display of biomolecules on nanoparticles: a challenge suited to bioorthogonal chemistry". *Bioconjugate chemistry* 22.5, pp. 825–858.
- Algar, W Russ et al. (2014). "Emerging non-traditional Förster resonance energy transfer configurations with semiconductor quantum dots: Investigations and applications". *Coordination Chemistry Reviews* 263, pp. 65–85.
- Alivisatos, A Paul (1996). "Semiconductor clusters, nanocrystals, and quantum dots". *science* 271.5251, pp. 933–937.
- Aubin-Tam, Marie-Eve and Kimberly Hamad-Schifferli (2008). "Structure and function of nanoparticle–protein conjugates". *Biomedical Materials* 3.3, p. 034001.
- Bazin, H, E Trinquet, and G Mathis (2002). "Time resolved amplification of cryptate emission: a versatile technology to trace biomolecular interactions". *Reviews in Molecular Biotechnology* 82.3, pp. 233–250.
- Becker, W (2012). "Fluorescence lifetime imaging–techniques and applications". *Journal of microscopy* 247.2, pp. 119–136.
- Bergman, Leah and Jeanne L McHale (2011). *Handbook of luminescent semiconductor materials*. CRC Press.
- Bhuckory, Shashi et al. (2016). "Evaluating quantum dot performance in homogeneous FRET immunoassays for prostate specific antigen". *Sensors* 16.2, p. 197.
- Blanco-Canosa, Juan B et al. (2014). "Recent progress in the bioconjugation of quantum dots". *Coordination Chemistry Reviews* 263, pp. 101–137.
- Bruchez, Marcel et al. (1998). "Semiconductor nanocrystals as fluorescent biological labels". *science* 281.5385, pp. 2013–2016.
- Bünzli, Jean-Claude G and Claude Piguet (2005). "Taking advantage of luminescent lanthanide ions". *Chemical Society Reviews* 34.12, pp. 1048–1077.

- Chan, Warren CW and Shuming Nie (1998). "Quantum dot bioconjugates for ultrasensitive nonisotopic detection". *Science* 281.5385, pp. 2016–2018.
- Chen, Mei-Jun et al. (2012). "Quantum-dot-based homogeneous time-resolved fluoroimmunoassay of alpha-fetoprotein". *Analytica chimica acta* 741, pp. 100–105.
- Clapp, Aaron R, Igor L Medintz, and Hedi Mattoussi (2006). "Förster resonance energy transfer investigations using quantum-dot fluorophores". *ChemPhysChem* 7.1, pp. 47–57.
- Clapp, Aaron R et al. (2004). "Fluorescence resonance energy transfer between quantum dot donors and dye-labeled protein acceptors". *Journal of the American Chemical Society* 126.1, pp. 301–310.
- Clapp, Aaron R et al. (2005). "Can luminescent quantum dots be efficient energy acceptors with organic dye donors?" *Journal of the American Chemical Society* 127.4, pp. 1242–1250.
- Clegg, Robert M (1995). "Fluorescence resonance energy transfer". *Current opinion in biotechnology* 6.1, pp. 103–110.
- Dabbousi, Bashir O et al. (1997). "(CdSe) ZnS core-shell quantum dots: synthesis and characterization of a size series of highly luminescent nanocrystallites". *The Journal of Physical Chemistry B* 101.46, pp. 9463–9475.
- Davies, Chris (2013). "Immunoassay performance measures". *The Immunoassay Handbook (4th Edition)*. Elsevier, pp. 11–26.
- Engvall, Eva and Peter Perlmann (1971). "Enzyme-linked immunosorbent assay (ELISA) quantitative assay of immunoglobulin G". *Immunochemistry* 8.9, pp. 871–874.
- Förster, Th (1948). "Zwischenmolekulare energiewanderung und fluoreszenz". *Annalen der physik* 437.1-2, pp. 55–75.
- Gao, Jinhao et al. (2011). "Affibody-based nanoprobe for HER2-expressing cell and tumor imaging". *Biomaterials* 32.8, pp. 2141–2148.
- Garousi, Javad et al. (2015). "ADAPT, a novel scaffold protein-based probe for radionuclide imaging of molecular targets that are expressed in disseminated cancers". *Cancer research* 75.20, pp. 4364–4371.
- Garousi, Javad et al. (2017). "Comparative evaluation of tumor targeting using the anti-HER2 ADAPT scaffold protein labeled at the C-terminus with indium-111 or technetium-99m". *Scientific Reports* 7.1, p. 14780.
- Geißler, Daniel et al. (2010). "Quantum dot biosensors for ultrasensitive multiplexed diagnostics". *Angewandte Chemie International Edition* 49.8, pp. 1396–1401.
- Geißler, Daniel et al. (2013). "Lanthanides and quantum dots as Förster resonance energy transfer agents for diagnostics and cellular imaging". *Inorganic chemistry* 53.4, pp. 1824–1838.

- Gilbreth, Ryan N and Shohei Koide (2012). "Structural insights for engineering binding proteins based on non-antibody scaffolds". *Current opinion in structural biology* 22.4, pp. 413–420.
- Group, Biomarkers Definitions Working et al. (2001). "Biomarkers and surrogate endpoints: preferred definitions and conceptual framework". *Clinical pharmacology & therapeutics* 69.3, pp. 89–95.
- Gschneidner, Karl A, LeRoy Eyring, and Gerry H Lander (2002). *Handbook on the physics and chemistry of rare earths*. Vol. 32. Elsevier.
- Gubala, Vladimir et al. (2011). "Point of care diagnostics: status and future". *Analytical chemistry* 84.2, pp. 487–515.
- Gurunatha, Kargal L et al. (2016). "Nanoparticles self-assembly driven by high affinity repeat protein pairing". *ACS nano* 10.3, pp. 3176–3185.
- Ha, Taekjip (2001). "Single-molecule fluorescence resonance energy transfer". *Methods* 25.1, pp. 78–86.
- Hainfeld, James F et al. (1999). "Ni-NTA-gold clusters target His-tagged proteins". *Journal of structural biology* 127.2, pp. 185–198.
- Han, Sanyang et al. (2014). "Enhancing luminescence in lanthanide-doped upconversion nanoparticles". *Angewandte Chemie International Edition* 53.44, pp. 11702–11715.
- Heffern, Marie C, Lauren M Matosziuk, and Thomas J Meade (2013). "Lanthanide probes for bioresponsive imaging". *Chemical reviews* 114.8, pp. 4496–4539.
- Hemmila, Ilkka (1999). "LANCETTM: homogeneous assay platform for HTS". *Journal of biomolecular screening* 4.6, pp. 303–307.
- Hermanson, Greg T (2013). *Bioconjugate techniques*. Academic press.
- Heyduk, Ewa and Tomasz Heyduk (2010). "Fluorescent homogeneous immunosensors for detecting pathogenic bacteria". *Analytical biochemistry* 396.2, pp. 298–303.
- Hildebrandt, Niko (2013). "How to apply FRET: From experimental design to data analysis". *FRET-Förster Resonance Energy Transfer: From Theory to Applications*. John Wiley & Sons, pp. 105–163.
- Hildebrandt, Niko, K David Wegner, and W Russ Algar (2014). "Luminescent terbium complexes: Superior Förster resonance energy transfer donors for flexible and sensitive multiplexed biosensing". *Coordination Chemistry Reviews* 273, pp. 125–138.
- Hildebrandt, Niko et al. (2016). "Energy transfer with semiconductor quantum dot bioconjugates: A versatile platform for biosensing, energy harvesting, and other developing applications". *Chemical reviews* 117.2, pp. 536–711.
- Hines, Margaret A and Philippe Guyot-Sionnest (1996). "Synthesis and characterization of strongly luminescing ZnS-capped CdSe nanocrystals". *The Journal of Physical Chemistry* 100.2, pp. 468–471.

- Horrocks Jr, William DeW and Daniel R Sudnick (1979). "Lanthanide ion probes of structure in biology. Laser-induced luminescence decay constants provide a direct measure of the number of metal-coordinated water molecules". *Journal of the American Chemical Society* 101.2, pp. 334–340.
- Kupstat, Annette, Michael U Kumke, and Niko Hildebrandt (2011). "Toward sensitive, quantitative point-of-care testing (POCT) of protein markers: miniaturization of a homogeneous time-resolved fluoroimmunoassay for prostate-specific antigen detection". *Analyst* 136.5, pp. 1029–1035.
- Laitala, Ville and Ilkka Hemmilä (2005). "Homogeneous assay based on anti-Stokes' shift time-resolved fluorescence resonance energy-transfer measurement". *Analytical chemistry* 77.5, pp. 1483–1487.
- Lakowicz, Joseph R. (2006). *Principles of fluorescence spectroscopy (3rd Edition)*, pp. 443–445.
- Li, Liang and Peter Reiss (2008). "One-pot synthesis of highly luminescent InP/ZnS nanocrystals without precursor injection". *Journal of the American Chemical Society* 130.35, pp. 11588–11589.
- Limsakul, Praopim et al. (2018). "Directed Evolution to Engineer Monobody for FRET Biosensor Assembly and Imaging at Live-Cell Surface". *Cell chemical biology* 25.4, pp. 370–379.
- Lindbo, Sarah et al. (2016). "Influence of histidine-containing tags on the biodistribution of ADAPT scaffold proteins". *Bioconjugate chemistry* 27.3, pp. 716–726.
- Lindbo, Sarah et al. (2018). "Radionuclide Tumor Targeting Using ADAPT Scaffold Proteins: Aspects of Label Positioning and Residualizing Properties of the Label." *Journal of nuclear medicine: official publication, Society of Nuclear Medicine* 59.1, pp. 93–99.
- Löfblom, John et al. (2010). "Affibody molecules: engineered proteins for therapeutic, diagnostic and biotechnological applications". *FEBS letters* 584.12, pp. 2670–2680.
- Marco, Ario de (2011). "Biotechnological applications of recombinant single-domain antibody fragments". *Microbial cell factories* 10.1, p. 44.
- Mathis, Gérard (1999). "HTRF® technology". *Journal of biomolecular screening* 4.6, pp. 309–313.
- Mattoussi, Hedi et al. (2000). "Self-assembly of CdSe- ZnS quantum dot bioconjugates using an engineered recombinant protein". *Journal of the American Chemical Society* 122.49, pp. 12142–12150.
- Medintz, Igor (2006). "Universal tools for biomolecular attachment to surfaces". *Nature materials* 5.11, p. 842.
- Medintz, Igor L et al. (2005). "Quantum dot bioconjugates for imaging, labelling and sensing". *Nature materials* 4.6, p. 435.

- Meer, B Wieb van der (2013). "Förster theory". *FRET-Förster Resonance Energy Transfer: From Theory to Applications*. John Wiley & Sons, pp. 23–62.
- Morgner, Frank et al. (2010). "A Quantum-Dot-Based Molecular Ruler for Multiplexed Optical Analysis". *Angewandte Chemie International Edition* 49.41, pp. 7570–7574.
- Murray, CBea, David J Norris, and Mounji G Bawendi (1993). "Synthesis and characterization of nearly monodisperse CdE (E= sulfur, selenium, tellurium) semiconductor nanocrystallites". *Journal of the American Chemical Society* 115.19, pp. 8706–8715.
- Muyldermans, Serge (2013). "Nanobodies: natural single-domain antibodies". *Annual review of biochemistry* 82, pp. 775–797.
- Nilvebrant, Johan et al. (2014). "Engineering of bispecific affinity proteins with high affinity for ERBB2 and adaptable binding to albumin". *PloS one* 9.8, e103094.
- Ohno, Yoshiyuki et al. (2007). "Enhanced fluorescence resonance energy transfer immunoassay with improved sensitivity based on the Fab'-based immunoconjugates". *Analytical biochemistry* 360.2, pp. 266–272.
- Plückthun, Andreas (2015). "Designed ankyrin repeat proteins (DARPs): binding proteins for research, diagnostics, and therapy". *Annual review of pharmacology and toxicology* 55, pp. 489–511.
- Prevo, Bram and Erwin JG Peterman (2014). "Förster resonance energy transfer and kinesin motor proteins". *Chemical Society Reviews* 43.4, pp. 1144–1155.
- Qiu, Xue et al. (2016). "Nanobodies and antibodies for duplexed EGFR/HER2 immunoassays using terbium-to-quantum dot FRET". *Chemistry of Materials* 28.22, pp. 8256–8267.
- Renberg, Björn et al. (2004). "Fluorescence resonance energy transfer-based detection of analytes using antiidiotypic affinity protein pairs". *Analytical biochemistry* 334.1, pp. 72–80.
- Resch-Genger, Ute et al. (2008). "Quantum dots versus organic dyes as fluorescent labels". *Nature methods* 5.9, p. 763.
- Richter, A, E Eggenstein, and A Skerra (2014). "Anticalins: exploiting a non-Ig scaffold with hypervariable loops for the engineering of binding proteins". *FEBS letters* 588.2, pp. 213–218.
- Robers, Matthew B et al. (2008). "Cellular LanthaScreen and β -lactamase reporter assays for high-throughput screening of JAK2 inhibitors". *Assay and drug development technologies* 6.4, pp. 519–529.
- Rosenthal, Sandra J et al. (2011). "Biocompatible quantum dots for biological applications". *Chemistry & biology* 18.1, pp. 10–24.
- Rusling, James F et al. (2010). "Measurement of biomarker proteins for point-of-care early detection and monitoring of cancer". *Analyst* 135.10, pp. 2496–2511.

- Sapsford, Kim E et al. (2007). "Kinetics of metal-affinity driven self-assembly between proteins or peptides and CdSe- ZnS quantum dots". *The Journal of Physical Chemistry C* 111.31, pp. 11528–11538.
- Sapsford, Kim E et al. (2010). "Biomarkers to improve the benefit/risk balance for approved therapeutics: a US FDA perspective on personalized medicine". *Therapeutic delivery* 1.5, pp. 631–641.
- Sapsford, Kim E et al. (2013). "Functionalizing nanoparticles with biological molecules: developing chemistries that facilitate nanotechnology". *Chemical reviews* 113.3, pp. 1904–2074.
- Sasajima, Yoshiyuki et al. (2006). "Detection of protein tyrosine phosphorylation by open sandwich fluoroimmunoassay". *Biotechnology progress* 22.4, pp. 968–973.
- Schuler, Benjamin and William A Eaton (2008). "Protein folding studied by single-molecule FRET". *Current opinion in structural biology* 18.1, pp. 16–26.
- Schumacher, Dominik et al. (2018). "Nanobodies: Chemical Functionalization Strategies and Intracellular Applications". *Angewandte Chemie International Edition* 57.9, pp. 2314–2333.
- Sekar, Rajesh Babu and Ammasi Periasamy (2003). "Fluorescence resonance energy transfer (FRET) microscopy imaging of live cell protein localizations". *The Journal of cell biology* 160.5, pp. 629–633.
- Selvin, Paul R (1995). "[13] Fluorescence resonance energy transfer". *Methods in enzymology*. Vol. 246. Elsevier, pp. 300–334.
- Sha, Fern et al. (2017). "Monobodies and other synthetic binding proteins for expanding protein science". *Protein Science*.
- Susumu, Kimihiro et al. (2007). "Enhancing the stability and biological functionalities of quantum dots via compact multifunctional ligands". *Journal of the American Chemical Society* 129.45, pp. 13987–13996.
- Susumu, Kimihiro et al. (2011). "Multifunctional compact zwitterionic ligands for preparing robust biocompatible semiconductor quantum dots and gold nanoparticles". *Journal of the American Chemical Society* 133.24, pp. 9480–9496.
- Tyler, Germund (2004). "Rare earth elements in soil and plant systems-A review". *Plant and soil* 267.1-2, pp. 191–206.
- Ullman, Edwin F, Moshe Schwarzberg, and Kenneth E Rubenstein (1976). "Fluorescent excitation transfer immunoassay. A general method for determination of antigens." *Journal of Biological Chemistry* 251.14, pp. 4172–4178.
- Valeur, Bernard (2001). "Effects of intermolecular photophysical processes on fluorescence emission". *Molecular fluorescence: principles and applications*, pp. 72–124.
- Van Weemen, BK and AHWM Schuurs (1971). "Immunoassay using antigen—enzyme conjugates". *FEBS letters* 15.3, pp. 232–236.

- Wang, Rongsheng E, Ling Tian, and Yie-Hwa Chang (2012). "A homogeneous fluorescent sensor for human serum albumin". *Journal of pharmaceutical and biomedical analysis* 63, pp. 165–169.
- Wegner, K David and Niko Hildebrandt (2015). "Quantum dots: bright and versatile in vitro and in vivo fluorescence imaging biosensors". *Chemical Society Reviews* 44.14, pp. 4792–4834.
- Wegner, K David et al. (2013). "Quantum-dot-based forster resonance energy transfer immunoassay for sensitive clinical diagnostics of low-volume serum samples". *Acs Nano* 7.8, pp. 7411–7419.
- Wegner, K David et al. (2014). "Nanobodies and Nanocrystals: Highly Sensitive Quantum Dot-Based Homogeneous FRET Immunoassay for Serum-Based EGFR Detection". *Small* 10.4, pp. 734–740.
- Wei, Quande et al. (2006). "Development of an open sandwich fluoroimmunoassay based on fluorescence resonance energy transfer". *Analytical biochemistry* 358.1, pp. 31–37.
- Weissman, SI (1942). "Intramolecular energy transfer the fluorescence of complexes of europium". *The Journal of Chemical Physics* 10.4, pp. 214–217.
- Werts, Martinus HV (2005). "Making sense of lanthanide luminescence". *Science progress* 88.2, pp. 101–131.
- Wild, David (2013). "Immunoassay for beginners". *The Immunoassay Handbook (4th Edition)*. Elsevier, pp. 7–10.
- Willard, Dale M et al. (2001). "CdSe- ZnS quantum dots as resonance energy transfer donors in a model protein- protein binding assay". *Nano Letters* 1.9, pp. 469–474.
- Xu, Jide et al. (2011). "Octadentate cages of Tb (III) 2-hydroxyisophthalamides: a new standard for luminescent lanthanide labels". *Journal of the American Chemical Society* 133.49, pp. 19900–19910.
- Zeug, André et al. (2012). "Quantitative intensity-based FRET approaches—a comparative snapshot". *Biophysical journal* 103.9, pp. 1821–1827.
- Zwier, Jurriaan M and Niko Hildebrandt (2017). "Time-Gated FRET Detection for Multiplexed Biosensing". *Reviews in Fluorescence 2016*. Springer, pp. 17–43.

Synthèse en français

Le diagnostic précoce du cancer est crucial pour un traitement performant. Comme l'analyse diagnostique en laboratoire peut être un processus long et compliqué, des immunodosages rapides, sensibles et spécifiques de biomarqueurs protéiques dans le sérum, le sang total ou le plasma peuvent améliorer significativement le diagnostic précoce de cancer et son traitement ultérieur. Par conséquent, il existe une demande croissante pour la mise au point de biocapteurs permettant de détecter les biomarqueurs du cancer à des concentrations très basses au cours des stades précoces, ainsi que pour la surveillance de la progression de la maladie. Les biocapteurs basés sur le transfert d'énergie par résonance de type Förster (FRET) ont démontré de nombreux avantages pour des diagnostics simples, rapides, sensibles et multiplexés. Le FRET est un transfert d'énergie non radiatif entre une molécule donneur excitée (donneur FRET) et une molécule accepteur dans l'état fondamental (accepteur de FRET), qui doit être proche et en résonance énergétique comme prévu par le recouvrement spectral. En raison de la dépendance de l'efficacité de ce transfert d'énergie en fonction de la distance du donneur et de l'accepteur (en r^{-6}), également appelée efficacité du FRET, cette technique est polyvalente et sensible pour l'analyse qualitative et quantitative des interactions biologiques et des processus dans une gamme nanométrique d'environ 1-20 nm. Pour la détection de la cible d'intérêt, il existe de nombreuses stratégies de transduction du signal en fonction de sa variation, qui est médiée par les biomolécules auxquelles le donneur et l'accepteur sont conjugués. Pour les immunodosages en sandwich à base de FRET, le donneur et l'accepteur sont conjugués avec deux biomolécules qui reconnaîtront la molécule d'intérêt (biomarqueur) sur deux sites (épitopes) distincts. La présence du biomarqueur entraîne la liaison d'un donneur et d'un accepteur de FRET à celui-ci. Le donneur et l'accepteur se retrouveront ainsi proches, induisant un changement mesurable des signaux FRET. La capacité unique du FRET à sonder les concentrations de biomarqueurs et les distances de séparation inter et intramoléculaires a conduit à une augmentation rapide des études FRET dans la détection diagnostique des biomarqueurs.

Divers matériaux sont actuellement utilisés pour le FRET, comme les colorants organiques, les protéines fluorescentes, les boîtes quantiques semiconducteurs (QDs), les chélates métalliques, les métaux nobles et d'autres nanoparticules. Parmi ceux-ci, la combinaison de complexes de lanthanides luminescents (LLC) en tant que donneurs et des QDs en tant qu'accepteurs est l'une

des paires de FRET les plus prometteuses. De plus, les LLC possèdent de longues durées de vie à l'état excité, allant jusqu'à quelques millisecondes, ce qui permet des mesures résolues dans le temps et offre un grand potentiel pour le multiplexage temporel.

Les QD sont des nanocristaux semiconducteurs qui présentent plusieurs avantages par rapport aux colorants organiques conventionnels, notamment des coefficients d'extinction molaires élevés, des bandes d'émission étroites et symétriques de largeur maximale à mi-hauteur (FWHM) ~ 25-40 nm allant de l'UV au proche infrarouge. Ils possèdent aussi un déplacement de Stokes et une photo stabilité remarquable. En particulier, une caractéristique tout à fait unique des QDs est leurs bandes d'émission dépendantes de leur taille en raison des effets de confinement quantique. Lorsque le matériau semi-conducteur est réduit à l'échelle nanométrique, les bandes d'énergie continue se divisent en états excitoniques discrets (interaction trou-électron). A cause d'excitons confinés à des dimensions plus petites que le rayon de Bohr (distance électron-trou), l'énergie de la bande interdite augmente avec la diminution de taille du QD, ce qui engendre un décalage vers le bleu des longueurs d'onde d'absorption et d'émission. Les stratégies bien établies de synthèse et de fonctionnalisation de surface rendent les QDs biocompatibles et permettent la conjugaison avec des biomolécules en solution aqueuse. Dans la plupart des applications du FRET, les QDs sont généralement utilisés comme donneurs du FRET. Les principaux problèmes de l'utilisation des QDs en tant qu'accepteurs sont leur spectre large d'absorption et leur coefficient d'extinction élevé, qui conduisent à une excitation directe des QDs à quasiment n'importe quelle longueur d'onde utilisée pour l'excitation du donneur. Par conséquent, seule une fraction mineure des QDs étant dans l'état fondamental participe au FRET. Les solutions à ce problème sont l'utilisation de matériaux ayant de longues durées de vie à l'état excité en tant que donneur de FRET tels que les LLC (durée de vie jusqu'à plusieurs millisecondes) et l'excitation pulsée. La combinaison des LLC et des QDs permet le multiplexage spectral des QDs de différentes couleurs pour un même donneur avec une séparation facile des différentes bandes d'émission grâce à une diaphonie optique fortement réduite. De plus, leurs absorptivités molaires larges (coefficients d'extinction) entraînent de grandes intégrales de recouvrement spectral et donc de longues distances de Förster.

En raison des avantages précités des LLC et des QDs en tant que paires de FRET, celui-ci devient une technique très prometteuse pour les mesures de photoluminescence (PL) à résolution

temporelle (TR) permettant une suppression efficace de l'intensité PL due aux accepteurs directement excités et à l'autofluorescence. Par conséquent, de telles paires de FRET ont été utilisées dans des diagnostics cliniques pour la détection de différents biomarqueurs. L'approche la plus populaire pour cibler ces biomarqueurs consiste à utiliser des anticorps dans un immunodosage homogène, ce qui simplifie la procédure de préparation des échantillons sans plusieurs étapes d'incubation, de lavage et de séparation, mais seulement une procédure de mélange et de mesure très simple. La distance à l'intérieur des immunodosages peut être adaptée à la taille des matériaux photoluminescents et des anticorps. Ainsi, en diminuant la taille d'anticorps tout en gardant la même spécificité ou en utilisant des matériaux luminescents plus compacts, le FRET peut encore être amélioré.

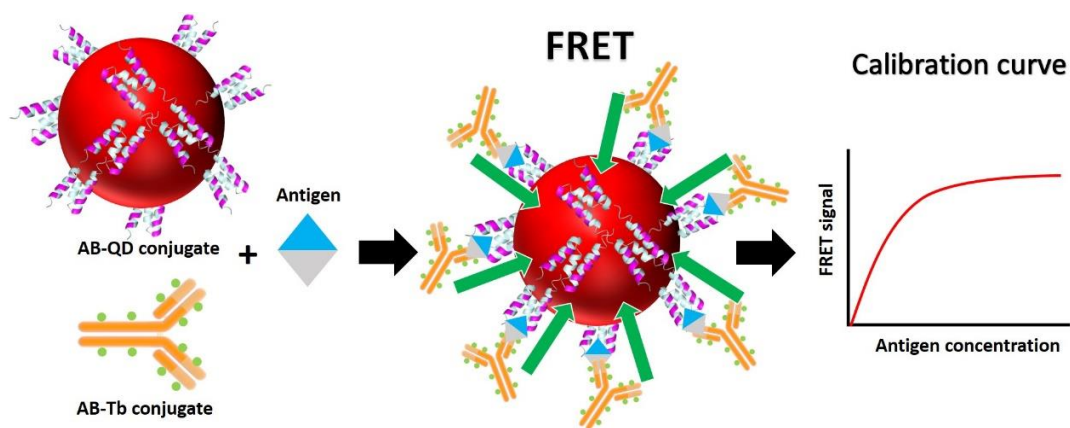


Figure 1.1 Principe de l'immunosage homogène. La conjugaison d'anticorps (AB) liés à un LLC (comprenant par exemple du Terbium, Tb) et d'un QD permet la formation de complexes en sandwich Tb-AB-antigène-AB-QD lors de l'addition d'antigène, ce qui entraîne le FRET de plusieurs molécules de Tb vers le QD. La mesure résolue dans le temps de la photoluminescence des QDs excités par le FRET est utilisé pour une quantification précise de la concentration de l'antigène. Le test conduit à une courbe d'étalonnage d'immunosage typique, pour laquelle le signal FRET augmente avec l'augmentation de la concentration d'antigène jusqu'à un plateau de saturation lorsque la concentration d'antigène est égale à la concentration de Tb-AB ou QD-AB.

Le but de ce travail est d'utiliser les propriétés photophysiques exceptionnelles des complexes Lumi4-Tb (LTC) et QD pour le TR-FRET et d'étudier l'influence des tailles d'anticorps sur la sensibilité du dosage immunologique pour la détection des biomarqueurs des protéines cancéreuses. Pour les immunodosages en sandwich étudiés par TR-FRET (Figure 1.1), des LTC et différents QDs sont marqués respectivement par deux anticorps qui se lient à différents épitopes de l'antigène (biomarqueur). Une caractérisation photophysique détaillée des paires de FRET (conjugués LTC et QD) a été réalisée et les ratios de marquage ont été estimés en utilisant la spectroscopie d'absorption UV / Vis. La première étude (**Chapitre 4**) présente des protéines d'affinité dérivé du domaine de liaison à l'albumine (ADAPTs, ~ 6,5 kDa, ~ 1,0 x 1,5 x 2,5 nm) pour la quantification du récepteur du facteur de croissance épidermique humain 2 (HER2). Ces petites protéines d'affinité sont bénéfiques pour la conjugaison de nanoparticules multivalentes et pour un FRET efficace. Des variantes d'ADAPT spécifique d'HER2 contenant l'étiquette histidine (ADAPT-His₆) et une cystéine (ADAPT-Cys) soit à l'extrémité N-terminale, soit à l'extrémité C-terminale, ont été produites par nos collaborateurs du KTH - Royal Institute of Technology (Stockholm, Suède). L'anticorps anti-HER2 pertuzumab (Roche Genentech) a été utilisé pour le marquage du LTC-NHS par les amines primaires du résidu lysine. Deux méthodes différentes de conjugaison des QDs ont également été comparés. ADAPT-His₆ peut se lier efficacement par coordination d'affinité métallique aux surfaces riches en Zn des QD émettant à 625 nm (QD625, Thermo Fisher) revêtues de ligands zwitterioniques. Cet assemblage direct sur la surface du QD fournit un FRET efficace. Une autre façon est d'utiliser un ADAPT-Cys, qui peut marquer les QD ITK avec des PEG-aminés émettant à 705 nm (QD705, Thermo Fisher) par la chimie sulfhydrique. Les QD réactifs à l'amine ont été convertis en QD réactifs au maléimide en utilisant l'agent de réticulation hétérobifonctionnel sulfo-EMCS qui a des groupes réactifs NHS ester et maléimide. Les QD activés par le maléimide ont ensuite été conjugués à l'ADAPT-Cys via des groupes sulfhydryl libres, qui ont été réduits par le TCEP. Les ratios de marquage de QD / ADAPT sont très difficiles à quantifier en raison de la grande différence de coefficient d'extinction des QD et des ADAPT à 280 nm, mais le grand excès d'ADAPT par rapport aux QD et la fonctionnalité des tests FRET ont fourni de très bonnes preuves d'une conjugaison ADAPT-QD. Des immunodosages par TR-FRET ont permis de quantifier HER2 à la fois dans 50 µL de tampon et dans des échantillons contenant du sérum avec des limites de détection sub-nanomolaires, en utilisant un instrument d'immunoanalyse clinique (KRYPTOR

compact plus). La limite de détection (LOD) a été acquise à partir de la partie linéaire de la courbe d'étalonnage. La LOD du conjugué QD625 a surpassé les précédents tests effectués avec des anticorps, des fragments d'anticorps ou des nanocorps. Bien que le conjugué QD705 ait montré des LOD plus élevées que le conjugué QD625, les résultats ont fourni des informations importantes concernant la possibilité de multiplexer différentes longueurs d'ondes et la polyvalence de la conjugaison d'ADAPT à d'autres nanoparticules.

La deuxième étude (**Chapitre 5**) se concentre sur les anticorps monocaténaux (sdAb), des fragments d'anticorps constitués d'un seul monomère à domaine variable avec un poids moléculaire de seulement 15 kDa qui sont utilisés dans de nombreuses applications immunologiques. Pour la réalisation des immunodosages en sandwich, les deux types de sdAb ont été fournis par nos collaborateurs à l'Université d'Utrecht (Pays-Bas). Ces nanocorps se lient à des épitopes distincts du récepteur du facteur de croissance épidermique humain 1 (EGFR), notés EgA1 et EgB4. Quatre systèmes de liaison différents (histidine, biotine, cystéine, pas de marqueur) ont été utilisés pour tester plusieurs stratégies de conjugaison des nanocorps avec des paires de FRET. EgA1-no tag et EgA1-His₆ ont été utilisés pour le marquage de LTC. EgB4-His₆, EgB4-biotine et EgB4-Cys ont été utilisés pour trois stratégies de conjugaison différentes. Les QD utilisés dans ces systèmes étaient les mêmes QD625 et QD705 que ceux employés dans l'étude précédente. De plus, un autre QD commercial émettant à 705 nm (sAvQD705, 705 ITK Streptavidin Conjugate Kits) a été introduit ici pour la reconnaissance de la biotine-streptavidine, où la streptavidine est fixée de manière covalente au revêtement amphiphile interne du QD sans un lieu PEG, permettant un co-assemblage plus aisé d'autres biomolécules au QD. Ainsi, la limite de détection du conjugué EgB4-biotine-sAvQD705 est supérieure à celle du conjugué EgB4-Cys-QD705. Fait intéressant, une autre paire de FRET EgA1-His₆-LTC et EgB4-His₆-QD625 a montré un FRET légèrement réduit avec des concentrations croissantes d'EGFR en raison de la liaison de l'étiquette polyhistidine de EgA1-His₆-LTC sur le QD625. L'addition d'EGFR remplace certains des conjugués LTC, ce qui résulte en un immunodosage par déplacement compétitif. Le concept a été confirmé par une autre expérience, dans laquelle le QD, l'accepteur FRET, sans sdAb conjugué, c'est-à-dire EgA1-His₆-LTC et QD625, présentait toujours le même résultat compétitif, qui était applicable pour détecter l'EGFR aux concentrations sub-nanomolaires. Ce test compétitif est très intéressant car il ne nécessite qu'un

seul type de sdAb spécifique de l'EGFR, ce qui réduit fortement le coût du développement de l'anticorps et du réactif.

En résumé, les résultats de cette thèse montrent que des petites protéines d'affinité se sont révélées très utiles pour les immunodosages à base de QDs. De telles protéines de petite taille (par exemple ADAPT, sdAb) permettent une conjugaison de QDs multivalente pour augmenter la sensibilisation des QDs au FRET. Il a été montré que les ADAPT surpassaient tous les autres types d'anticorps pour les immunodosages HER2. Les sdAbs ont été utilisés pour développer un immunodosage homogène compétitif qui ne nécessite qu'un seul anticorps (au lieu de deux), ce qui peut être considéré comme une stratégie alternative utile pour la détection de l'EGFR. Les deux stratégies pour des immunodosages FRET homogènes à base de QDs avec de petites protéines d'affinité fournissent un potentiel important pour des diagnostics *in vitro* avancés et d'autres applications de biocapteurs à base de FRET, par exemple pour l'imagerie de la dimérisation du récepteur du facteur de croissance épidermique.

Titre : Tests immunologiques par transfert d'énergie par résonance de Förster en utilisant des protéines modifiées pour la détection de biomarqueurs du cancer du sein

Mots clés FRET, boîtes quantiques, complexe de lanthanides, bioconjugaison, spectroscopie résolue en temps

Les protéines modifiées ont suscité un grand intérêt en raison de leur taille extrêmement petite par rapport à l'anticorps entier. Ces petites protéines de liaison ont démontré de nombreux avantages tels qu'une biodistribution rapide, une bonne pénétration dans le tissu tumoral et une élimination rapide du sérum et des tissus non-infectés. Ainsi, ces protéines devraient être d'excellentes alternatives aux anticorps pour les applications cliniques. Cette thèse présente le développement de biocapteurs basés sur des anticorps synthétiques et le transfert d'énergie par résonance de type Förster (FRET) résolu en temps par la détection de biomarqueurs.

Les tests immunologiques à base de FRET sont établis en utilisant des complexes de terbium (Tb) comme donneurs de FRET et des boîtes quantiques semi-conducteurs (QDs) comme accepteurs de FRET. Les propriétés photophysiques exceptionnelles de ce couple de FRET Tb-QD permettent une détection quantitative ultrasensible. Des anticorps monocaténaux (single-domain antibody, sdAb) et des petites protéines d'affinité synthétiques (albumin-binding domain-derived affinity protein, ADAPT) sont utilisées pour étudier différentes stratégies de conjugaison d'anticorps, et quantifier des biomarqueurs cliniques (EGFR, HER2). Ce travail peut être considéré comme une condition préalable à l'utilisation des QDs en diagnostic clinique.

Title : Förster resonance energy transfer immunoassays using engineered proteins for breast cancer biomarker detection

Keywords : FRET, quantum dots, lanthanide complex, bioconjugation, time-resolved spectroscopy

Abstract : Engineered affinity proteins have raised great interest due to their extremely small size compared to full length antibodies. Such small binding proteins have demonstrated many advantages such as quick biodistribution, good penetration into tumor tissue, and fast elimination from serum and nondiseased tissues. Thus, they are expected to be excellent alternatives to antibodies for clinical applications. This thesis focuses on the development of biosensors based on engineered antibodies and time-resolved Förster resonance energy transfer (FRET) through biological recognition of biomarkers.

FRET-based immunoassays are established using terbium complexes (Tb) as FRET donors and semiconductor quantum dots (QDs) as FRET acceptors. The exceptional photophysical properties of the Tb-QD FRET pair allow for ultrasensitive quantitative biosensing. Single-domain antibodies (sdAb) and small engineered scaffold antibodies (ADAPT) are used to investigate different antibody-conjugation strategies for quantifying human epidermal growth factor receptors (EGFR, HER2) as clinical biomarkers. This work can be considered as a prerequisite to implementing QDs into applied clinical diagnostics.

